# RESEARCH & REVIEWS IN ENGINEERING

MAY,2021

VOLUME I


**EDİTÖRLER**

**ASSOC. PROF. DR. BELMA HASDEMİR**
**DR. MAHMUT TURHAN**
**DR. CEREN KARAMAN**

AUTHORS

AHMET B. DEMİRPOLAT
ERCAN AYDOĞMUŞ
MERİÇ CAN ÖZYURT
ÜMİT ÖZER
ABDULKADİR KARADOĞAN
MEHMET GÜLER
EGEMEN ÖZSARIKAMIŞ
ALİ NOORULDEEN ISMAEL
AHMET ARİF ULUSLU
YAVUZ SÜMER
CEREN KARAMAN
BİLGE ÇELİK
NİL ACARALI
MELİH ONAY
ELİF ÇAĞDA KANDEMİR
SERHAT KÜÇÜKDERMENCİ



gece kitaplığı

**İmtiyaz Sahibi / Publisher** • Yaşar Hız
**Genel Yayın Yönetmeni / Editor in Chief** • Eda Altunel
**Kapak & İç T asarım / Cover & Interior Design** • Gece Kitaplığı
**Editörler / Editors** • Assoc. Prof. Dr. Belma Hasdemir
Dr. Mahmut Turhan
Dr. Ceren Karaman
**Birinci Basım / First Edition** • © Mayıs 2021
**ISBN** • 978-625-7411-78-3



**Gece Kitaplığı / Gece Publishing**
**Türkiye Adres / Turkey Address:** Kızılay Mah. Fevzi Çakmak 1. Sokak Ümit Apt. No: 22/A Çankaya / Ankara / TR
**Telefon / Phone:** +90 312 384 80 40
**web**: www.gecekitapligi.com
**e-mail:** gecekitapligi@gmail.com

**Baskı & Cilt / Printing & Volume**
**Sertifika / Certificate No: 47083**

# RESEARCH & REVIEWS IN ENGINEERING

## Volume I

EDITOR
ASSOC. PROF. DR. BELMA HASDEMİR
DR. MAHMUT TURHAN
DR. CEREN KARAMAN

gece kitaplığı

# İÇİNDEKİLER

# Chapter 1

# THE HYBRID-NANOFLUIDS REINFORCED WITH ZIRCONIUM DIOXIDE AND ALUMINA

*Ahmet B. DEMİRPOLAT*[1]
*Ercan AYDOĞMUŞ*[2]

1 Turgut Özal University, Arapgir Vocational School, Electronics and Automation, Malatya, Turkey. E-mail: ahmetb.demirpolat@ozal.edu.tr, (Orcid: https://orcid.org/0000-0003-2533-3381)
2 Fırat University, Faculty of Engineering, Chemical Engineering, Elazığ, Turkey. Corresponding Author: ercanaydogmus@firat.edu.tr. (Orcid: https://orcid.org/0000-0002-1643-2487)

## 1. INTRODUCTION

In this research, the change of thermal conductivity coefficient with temperature and concentration of the hybrid nano-fluids obtained by using zirconium oxide ($ZrO_2$) and alumina ($Al_2O_3$) nanoparticles have been investigated. Hybrid-nanofluids have been produced $ZrO_2$ and $Al_2O_3$ nano-powders at different concentrations (0.1wt%, 0.2wt%, 0.3wt%, 0.4wt%, and 0.5wt%). Besides, hybrid-nanofluids have been prepared at a mixture ratio of 0.3% by weight (equilibrium saturation with water), and the $ZrO_2/Al_2O_3$ ratios were studied as 4/1, 3/1, 2/1, 1/1, 1/2, 1/3, and 1/4. It was evaluated that the hybrid-nanofluids have a higher thermal conductivity coefficient compared to water, and the thermal conductivity goes up with the increase in concentration. The thermal conductivity coefficients of the nano-fluids were measured and compared at 20°C, 30°C, 40°C, 50°C, 60°Cand 70°C temperatures. It has been observed that thermal conductivity is directly proportional to temperature. Also, the increase of nano-particle concentration went up the viscosity, while the increase in temperature decreased the viscosity of the hybrid-nanofluids.

It has been determined that the hybrid-nanofluids exhibit non-Newtonian behavior especially at high concentrations and low temperatures. It has been found that these nanofluids, which can be used in the heating of houses or workplaces, go up the thermal conductivity coefficient approximately 1.20 times. However, in high concentrations (above 0.3wt%), it has been observed that the hybrid-nanoparticles in the fluid cause precipitation at the bottom of the water. Besides, the thermal conductivity coefficient determined from the experimental data was modeled with the help of statistical analysis using theoretical models. The most compatible results were found with the models with high $R^2$ values and low error values.

In recent studies, it has been observed that the use of hybrid nano-powder improves many properties of the nano-fluids. According to the intended use, specific properties of nano-fluids such as viscosity, surface tension, thermal conductivity, and magnetic field effect need to be improved. With the methods developed in the literature, the use of nano-fluids has become widespread and various researches have been made for different sectors.

In an experimental study investigating the thermal conductivity of water-based zirconium oxide nano-fluid, a new correlation was proposed using an artificial neural network. Thermal conductivity measurements were made by preparing $ZrO_2$/Water nano-fluid in different volumetric concentrations in the temperature range of 10 °C to 65 °C. The thermal conductivity coefficients of five different water-based $ZrO_2$ nano-fluids in volumetric concentrations of 0.0125%, 0.025%, 0.05%, 0.1% and 0.2% were measured in the temperature ranges. It was observed that the $ZrO_2$/Water nano-fluids have higher thermal conductivity compared to water and the thermal conductivity goes up with the increase in temperature and concentration [1]. On the paper studying alumina, copper oxide, and zirconium oxide, the thermal efficiencies of nano-fluids in different weight fractions were compared. The efficiencies calculated using 0.4wt.% nanoparticle in the solar collector was respectively $Al_2O_3$ (55%), CuO (51%), $ZrO_2$ (47%), and water (38%). Experimental results have shown that nanoparticle rates go up the heat transfer coefficient of the nano-fluids, thus increasing the heat collection efficiency in the collector [2].

In research where heat transfer analysis of zirconium oxide reinforced nano-fluid has been performed, the ratios of 0.025%, 0.05%, 0.075%, and 0.1% by volume have been studied. It has been observed that the higher the particle concentration in the water-ethylene glycol mixture (1:1), the higher the thermal conductivity. With boiling experiments, it has been found that the thermal conductivity of zirconium oxide increased by 18% [3]. The viscosity of the zirconium oxide nano-fluids has been modeled by artificial neural network and examined both experimentally and theoretically at volumetric ratios of 0.0125%, 0.025%, 0.05%, 0.1%, and 0.2%. A multi-layer perceptron feed-forward back-propagation artificial neural network has been developed to estimate the viscosity of the ZrO2/water nano-fluids. Viscosity changed inversely with temperature and directly proportional to concentration. With the developed artificial neural network, it has shown that the viscosity of ZrO2/water nano-fluid can be predicted with an average error rate of 0.11% [4]. Aluminum oxide and zirconium oxide nanoparticles can be used as hybrids in many surfactant interactions. These nanoparticles can affect the surface tension of the fluid by increasing the surface energy. Especially in adsorption applications, they can provide an electrostatic interaction between molecules by increasing the wettability alteration [5].

In another study where $ZrO_2$ nanoparticle, Ag (30nm), and distilled water were used together, the efficiency of the solar collector at different flow rates and concentrations was investigated. The effects of volume concentrations (0%, 1%, 3%, and 5%) and flow rates (30, 60 and 90 $L/h \cdot m^2$) on total yield were compared. It has been determined that the nano-fluid mixture goes up the heat transfer and improves the solar collector performance [6]. The convective heat transfer behavior of aluminum oxide/water and zirconium oxide/water nanoparticle's colloids have been examined in an article investigating the effect of temperature, concentration, flow rate, and hybrid mixture. $Al_2O_3$ and $ZrO_2$ were mixed at the ratios of 0.9–3.6% and 0.2–0.9%, respectively, by volume [7].

Liquids such as water, ethylene glycol, and motor oil have low thermal conductivity. Improvement is achieved by using nano-sized particles to increase the thermal conductivity of these liquids. It has been shown that nano-particles without surfactant exhibit better stability to produce stable nano-liquids [8].

In an experimental study investigating the thermal performance of nano-liquids, the effective thermal conductivity and thermal dispersion of $Al_2O_3$/water, $ZrO_2$/water, $TiO_2$/water, and CuO/water nanofluids have been measured. The effects of the thermal conductivity of the volume fractions and temperature of $Al_2O_3$ (20 nm), $ZrO_2$ (20 nm), $TiO_2$ (40 nm), and CuO (33 nm) nanoparticles with different particle diameters have been compared. The thermal conductivity performance was found according to the order of $Al_2O_3$, CuO, $ZrO_2$, and $TiO_2$ nanoparticles [9]. In another article, the effective thermal conductivity and thermal diffusivity of nano-fluids containing spherical and cylindrical nanoparticles were investigated, and the effects of particle concentration, particle diameter, and shape on thermal conductivity were compared. In this study, the highest performance has been observed in the carbon nanotube. It has been determined that as the concentration, diameter, and length of the carbon nanotubes increase, the thermal conductivity also goes up [10].

The hybrid use of nanoparticles can provide many advantages. The combination of aluminum oxide and zirconium oxide in water can provide both more stable viscosity and effective thermal conductivity. The colloidal particle balance in the water can be reduced with the use of a single nanoparticle. The effective thermal conductivity coefficient shows a stable state with the homogeneous distribution of this colloid balance. In this study, different combinations have been developed for hybrid nano-particle mixtures that can keep the water in maximum balance.

## 2. MATERIALS AND METHODS

### 2.1 Materials

Nano-alumina, nano-zirconium oxide, triglyceride, and acetic acid have been supplied. Nanofluids in different concentrations were prepared using distilled water. The total mixture amount was 1 kg and the concentrations were prepared in 0.1wt%, 0.2wt%, 0.3wt%, 0.4wt%, and 0.5wt%. For the hybrid mixtures, alumina (0.3wt%) and zirconium oxide (0.3wt%) components were mixed in proportions of 4/1, 3/1, 2/1, 1/1, 1/2, 1/3, and 1/4 by mass. Appropriate mixing ratios were determined by measuring thermal conductivity and viscosity.

## 2.2. Methods

By mixing alumina and zirconium oxide by mass in different proportions, the maximum amount of nanoparticles that the water can carry was determined as 0.3wt%. In experimental studies, when higher ratios of nanoparticles were used, precipitation increased in the bottom of the water even at the 1000 rpm rotation speed of the fluid. To increase the stability of the nanofluid, 95 mL of triglyceride, and 5 mL of acetic acid were added to 1 L of the total mix. These additives provide a homogeneous suspension of the hybrid-nanofluid as colloidal. In experimental studies, the thermal conductivity coefficient was made with the Thermtest TLS device. Measurements were made according to the correlation developed using pure liquids with a known heat conduction coefficient. Viscosity measurements were made with the vibration viscometer, and density measurements were made with the help of a pycnometer.

## 3. RESULTS AND DISCUSSIONS

The values in Table 1 are the values of hybrid and nanoparticles measured according to the heating water at an average temperature of 60°C. Alumina (0.3wt%) and zirconium oxide (0.3wt%) mixtures reached the highest heat conduction coefficient in the 7th experiment.

**Table 1.** *The mixing ratio of nanoparticles with each other by mass*

| Experiments | $ZrO_2$ (wt.%) | $Al_2O_3$ (wt.%) |
|---|---|---|
| 1 | 4: (80%) | 1: (20%) |
| 2 | 3: (75%) | 1: (25%) |
| 3 | 2: (67%) | 1: (33%) |
| 4 | 1: (50%) | 1: (50%) |
| 5 | 1: (33%) | 2: (67%) |
| 6 | 1: (25%) | 3: (75%) |
| 7 | 1: (20%) | 4: (80%) |
| 8 | 0: (0%) | 1: (100%) |
| 9 | 1: (100%) | 0: (0%) |

The relative thermal conductivity measurements of the hybrids and nanofluids prepared according to the optimum mixing ratio are seen in Fig. 1.

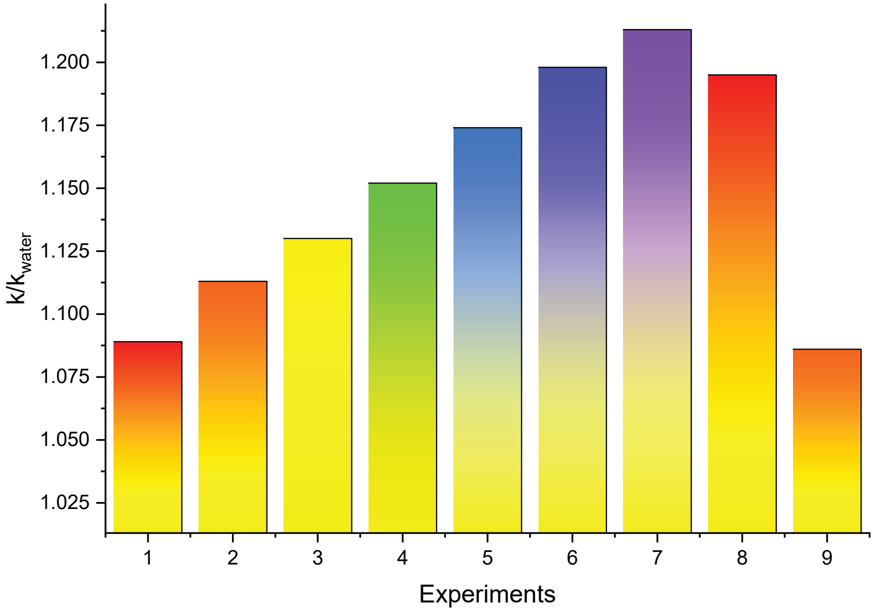


**Fig. 1.** *Relative thermal conductivity coefficients of nanofluids concerning water at 60 ℃*

According to Fig. 2, it is seen that the heat transfer coefficient of hybrid and nanofluids increases as the temperature increases.

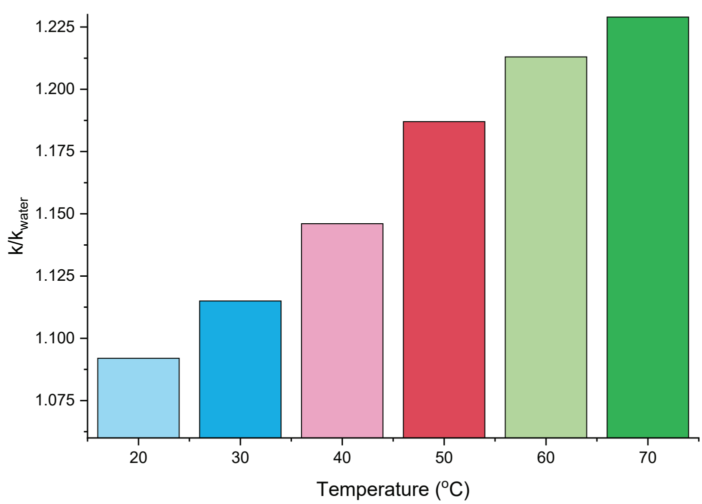


**Fig. 2.** *The variation of the relative thermal conductivity coefficient with temperature*

In Fig. 1, the variation of the thermal conductivity coefficient of hybrid-nanofluid at different concentrations and densities at room temperature is modeled according to the Response Surface Methodology (RSM).

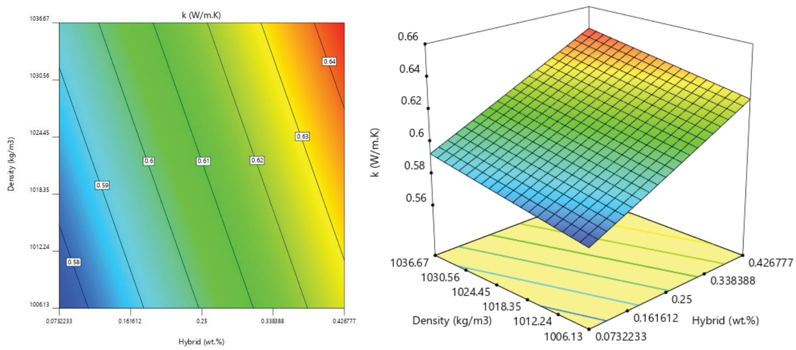


**Fig. 1.** *Variation of the hybrid's thermal conductivity coefficient with density and concentration according to the RSM method.*

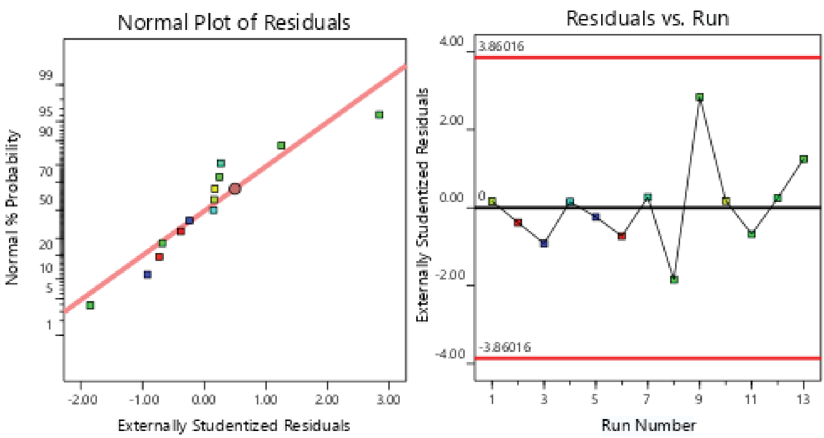


**Fig. 2.** *The compatibility of experimental data with model results and the appearance of error distributions*

Eq. 1 shows the equation of thermal conductivity coefficient (k) depending on density (ρ) and hybrid concentration (C) by mass.

$$\sqrt{k} = +0.362026 + 0.094955 \times C + 0.000387 \times \rho \qquad (1)$$

The curve of the viscosity of hybrid nanofluid with temperature is shown in Fig. 3. Although the viscosity decreased with the effect of temperature, it showed a more stable state even at higher temperatures than water.

**Table 2.** *Density and concentration dependent RSM statistical analysis of hybrid nanofluids*

| Source | SST | P | $R^2$ | Std. D. | Mean | C.V. % |
|---|---|---|---|---|---|---|
| Linear Mean | 0.00253 | 0.0001 | 0.9975 | 0.0070 | 0.7809 | 0.0891 |

Nanoparticles increased the viscosity of the water and made it stable up to high temperatures [11]. The change of temperature and viscosity of the hybrid (experiment 7) mixture obtained from alumina and zirconium oxide is shown in Fig.3.

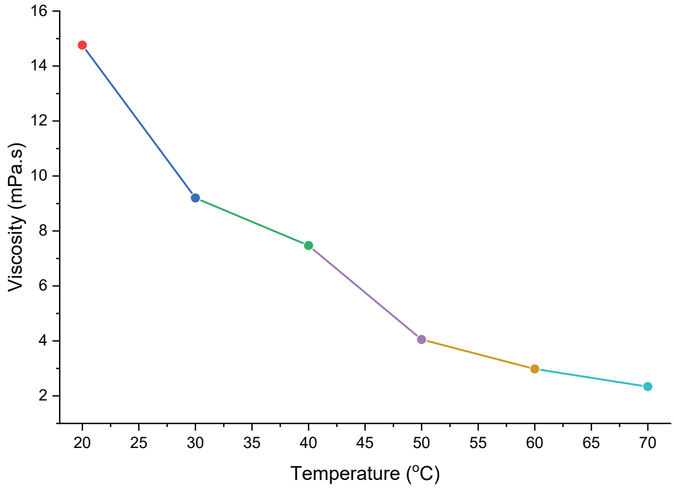


**Fig. 3**. *Variation of absolute viscosity of hybrid with temperature*

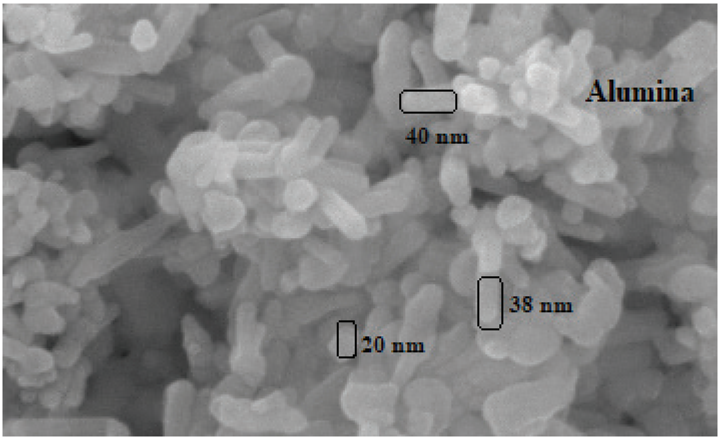


**Fig. 4.** *SEM image of alumina nanoparticles for experiment 8*

Fig. 4 shows SEM images of alumina particles below 50 nm particle size. The FTIR spectrum of the nanofluid in Experiment 7 is shown in Fig. 5.

Due to hydrogen bonding between hydroxyl groups (O-H) in the nanofluid, there is a strong peak of 3200 - 3450 $cm^{-1}$. The vibration band formed between Al-O is in the range of 400 to 900 $cm^{-1}$ wavelength.

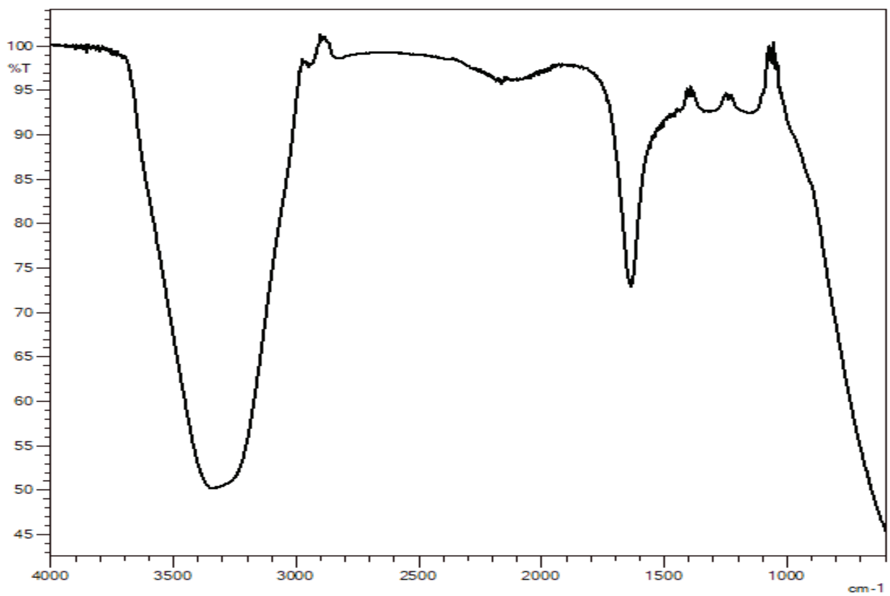


**Fig. 5.** *FTIR spectrum of the hybrid-nanofluid for experiment 7*

## 4. CONCLUSIONS

According to the results obtained:

(i) Hybrid use of nanoparticles has shown more thermal conductivity performance than the use alone.

(ii) The viscosity of both nanofluids and hybrid-nanofluids decreased with temperature.

(iii) Temperature increased the thermal conductivity coefficient of nanoparticle reinforced nanofluids.

(iii) Alumina gave the nanofluid a higher thermal conductivity effect than zirconium oxide.

(iv) The viscosity and thermal conductivity properties of nanofluids have always performed better than water.

(v) As the concentration of nanoparticles in water increased, the density of the nanofluid increased.

(vi) It was determined by statistical analysis that the model equality obtained in the RSM results and the experimental results were compatible.

It has been evaluated that the results found in the literature and the results of this article are consistent with both theoretical and experimental considerations [12].

## 5. REFERENCES

[1] Çolak, A. B. (2021). Experimental study for thermal conductivity of water-based zirconium oxide nanofluid: Developing optimal artificial neural network and proposing new correlation. International Journal of Energy Research, 45(2), 2912–2930.

[2] Devarajan, Y., & Munuswamy, D. B. (2016). Analysis on the Influence of Nanoparticles of Alumina, Copper Oxide, and Zirconium Oxide on the Performance of a Flat-Plate Solar Water Heater. Energy and Fuels, 30(11), 9908–9913.

[3] Sarafraz, M. M., Kiani, T., & Hormozi, F. (2016). Critical heat flux and pool boiling heat transfer analysis of synthesized zirconia aqueous nano-fluids. International Communications in Heat and Mass Transfer, 70, 75–83.

[4] Çolak, A. B. (2021). A novel comparative analysis between the experimental and numeric methods on the viscosity of zirconium oxide nanofluid: Developing optimal artificial neural network and new mathematical model. Powder Technology, 381, 338–351.

[5] Moslan, M. S., Sulaiman, W. R. W., Ismail, A. R., & Jaafar, M. Z. (2017). Applications of aluminum oxide and zirconium oxide nanoparticles in altering dolomite rock wettability using different dispersing medium. Chemical Engineering Transactions, 56(April), 1339–1344.

[6] Hussain, H. A., Jawad, Q., & Sultan, K. F. (2015). International Journal of Sustainable and Green Energy. Special Issue: Engineering Solution for High Performance of Solar Energy System, 4(1), 19–28.

[7] Williams, W., Buogiorno, J., & Hu, L. W. (2008). Experimental investigation of turbulent convective heat transfer and pressure loss of alumina/water and zirconia/water nanoparticle colloids (nanofluids) in horizontal tubes. Journal of Heat Transfer, 130(4).

[8] Fadhillahanafi, N. M., Leong, K. Y., & Risby M. S. (2013). Stability and Thermal Conductivity Characteristics of Carbon Nanotube-Based Nanofluids. International Journal of Automotive and Mechanical Engineering, 8, 1376–1384.

[9] Zhang, X., Gu, H., & Fujii, M. (2006). Experimental study on the effective thermal conductivity and thermal diffusivity of nanofluids. International Journal of Thermophysics, 27(2), 569–580.

[10] Zhang, X., Gu, H., & Fujii, M. (2006). Effective thermal conductivity and thermal diffusivity of nanofluids containing spherical and cylindrical nanoparticles. Journal of Applied Physics, 100(4).

[11] Shanker, N., Reddy, M., & Rao, V. (2012). On prediction of viscosity of nanofluids for low volume fractions of nanoparticles. International Journal of Engineering, 1(8), 1–10.

[12] Senthilraja, S., Vijayakumar, K., & Gangadevi, R. (2015). A comparative study on thermal conductivity of $Al_2O_3$/water, CuO/water, and $Al_2O_3$–CuO/water nanofluids. Digest Journal of Nanomaterials and Biostructures, 10(4), 1449–1458.

# Chapter 2

## INVESTIGATION AND DEVELOPMENT OF CONTROLLED BLASTING DESIGNS FOR DEMOLITION OF 75 GRAIN SILOS IN AQABA, JORDAN


*Meriç Can ÖZYURT*[1]

*Ümit ÖZER*[2]

*Abdulkadir KARADOĞAN*[3]

*Mehmet GÜLER*[4]

*Egemen ÖZSARIKAMIŞ*[5]

*Ali Nooruldeen ISMAEL*[6]

---

1 Dr. Corresponding Author. Istanbul University-Cerrahpasa, Engineering Faculty, Mining Eng. Dept., Buyukcekmece, Istanbul/TURKEY. E-mail: meric.ozyurt@iuc.edu.tr, ORCID ID: 0000-0002-7545-7756

2 Assoc. Prof., Istanbul University-Cerrahpasa, Engineering Faculty, Mining Eng. Dept., Buyukcekmece, Istanbul/TURKEY. E-mail: uozer@iuc.edu.tr, ORCID ID: 0000-0001-5930-0321

3 Dr., Istanbul University-Cerrahpasa, Engineering Faculty, Mining Eng. Dept., Buyukcekmece, Istanbul/TURKEY. E-mail: akadir@iuc.edu.tr, ORCID ID: 0000-0001-7321-3320

4 Ege Nitro Explosives Co.Ltd., İzmir/Turkey. E-mail: mehmet@egenitro.com.tr

5 Ege Nitro Explosives Co.Ltd., İzmir/Turkey. E-mail: e.sarikamis@hotmail.com

6 Ege Nitro Explosives Co.Ltd., İzmir/Turkey. E-mail: ali_tuz@yahoo.com

## 1. INTRODUCTION

Demolition of structures as a project is the implementation of procedures that involve the breaking down of man-made structures by taking necessary and sufficient security measures, using appropriate techniques, and removing the resulting debris (Güven, 2019).

Demolition varies according to the properties of the structure material. While wooden structures can be disassembled and reused very easily, steel structures are more difficult to disassemble and collapse due to their weight. In masonry structures, there are difficulties in demolition depending on the horizontal and vertical carrier system materials' characteristics. However, it can be stated that the dismantling and demolition of reinforced concrete structures are the most difficult because of the reinforced concrete materials (Güven, 2019). For this reason, more accidents have occurred during the demolition of reinforced concrete structures (Osha, 2020).

A demolition project should ensure that the structure is demolished in a planned and controlled manner and that the debris is removed correctly. To achieve successful results, issues such as sustainability, removal, and transportation of demolition waste, disputes between building owners, risk factors, and environmental factors should be considered in the demolition method selection process. Since no return is possible in a demolition activity, to prevent extra time and cost losses that may be experienced, demolition methods should be examined by considering the following points.

a. Legislation, specifications, and regulations involving demolition techniques,

b. Occupational health and safety regulations and environmental conditions,

c. Various workforce needs such as personnel, machinery, and equipment,

d. The type, age, condition of the structure,

e. Cost and commercial benefits (Özyurt, 2013; Güven, 2019).

As a result of the evaluations made on the issues mentioned above, a demolition method suitable for the purpose should be determined. Demolition techniques in their most general form;

a. Demolition with hand tools,

b. Mechanical demolition (use of machines and robots),

c. Chemical destruction,

d. Demolition with controlled blasting

## 2. DEMOLITION WITH CONTROLLED BLASTING TECHNIQUE

Many reseachers, such as Stevenston (1972), Olofsson (1980), Gustafsson (1981), Thomas (1985), Jimeno et al. (1994), Dowding (1996), Özyurt (2013) and Güven (2019), have studied the demolition with controlled blasting technique. using explosives.

The demolition with controlled blasting is based on breaking down the carrier elements on the lower floors by using explosives. As a result of the explosion, the structure's load has to be carried by the remaining carrier elements. In a short time, like seconds, these elements are also defeated by the increasing pressure and moment loads, and then the structure begins to demolish (Özyurt et al., 2016).

The structures differ in terms of geometric and material properties. In addition to these, it is possible to encounter millions of different possibilities when considering the location of the structures and environmental conditions. This diversity causes not a general design proposal for the demolition of the buildings by controlled blasting and the necessity of evaluating each project separately (Ozyurt, 2013).

The methods applied for the demolition with the controlled blasting technique can be divided into two main groups. The first is tilting the structure due to changing its gravity center, and the other is collapsing the structure within its boundaries as a result of the exploding of some carrier elements and the deformation of the remainings in the face of increasing loads. There are also applications where both methods have been used together.

In the tilting method, a wedge is created that rises in the direction of destruction behind the projection of the center of gravity of the structure. Wedge geometry varies depending on the structural and geometric features of the structure. The carrier elements remaining in the specified wedge (if necessary, floors should be added) are exploded sequentially from the edge of the structure to the interior. A presentation of the tilting method is shown in Figure 1.

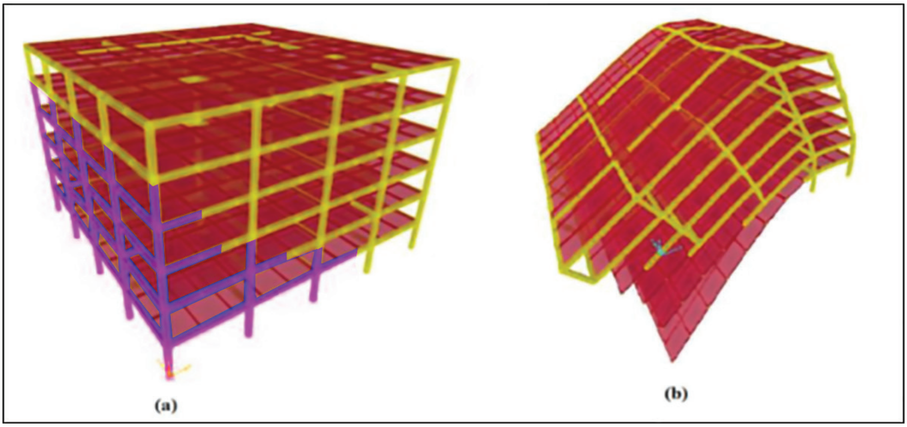


*Figure 1. A presentation of the tilting method*

In the collapsing within the boundaries method, the carrier elements located in the structure's center are primarily blasted. Thus, the perimeter carrier elements of the structure begin to lean towards the structure's center. After the central columns on the floors are blasted, the braces are blasted. A presentation of the collapsing within the boundaries method is given in Figure 2.

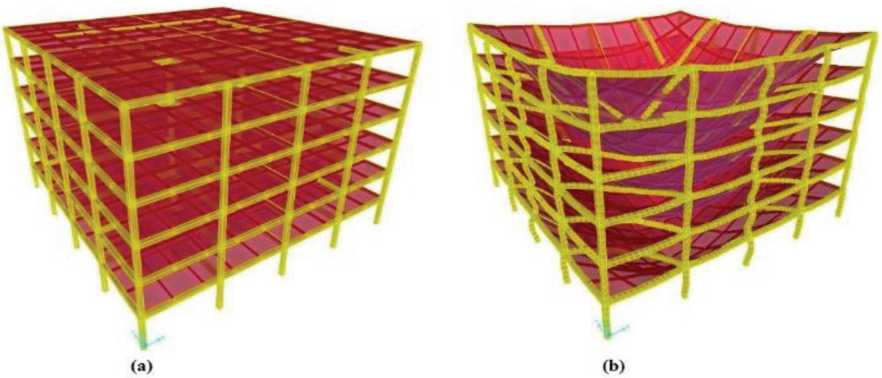


*Figure 2. A presentation of the collapsing within the boundaries method*

Another necessary process is determining the amount of explosives. The structural element's geometry and material properties are two parameters that directly affect the amount of explosives with sufficient detonation power to lose the bearing properties of the structural elements. Although there are approaches for determining the amount of charge in the literature, all of these approaches are based on ratio-proportion. The charge is calculated by multiplying the structural element's volume with a coefficient, which represents the structural properties of the material and calls the experience coefficient. Thomas (1985) determined the experience coefficients for the elements with different properties by doing experiments on various samples. However, these experience coefficients do not represent many of the examples encountered in practice. For this reason, it is important to take samples from the structure, make trial shots on these samples and determine the experience coefficient (Özyurt, 2013).

Another critical design parameter is the timings. The applied timings must be sufficient to meet the reinforced concrete material's reaction and failure time. Otherwise, predicted fragmentation and sufficient deformation might not be achieved. Özyurt et al. (2016) argued that the loads affecting the columns during the firing are not enough to deform the column alone and that the firing time must be at a level to meet the building's failure time. As stated in the literature, "Concrete breaks when it reaches a certain deformation, not when the maximum stress is reached (Türk, 2011)." and "As the speed of the load applied to the concrete sample decreases, the sample breaks under a smaller load and under a larger load as the loading speed increases (Felekoğlu and Türkel, 2004) confirms this result. Besides, the accuracy of the information above has been practically supported by the study titled "Demolition of Tüm Emek İş Site Buildings Using Explosives (Özer et al., 2015)". There is no approach in the literature to determine the timings, and the project team's experience determines it.

## 3. SILO BUILDINGS

The silo buildings are located in Aqaba, Jordan. Seventy-five silos with a diameter of 9 meters and a height of 45 meters, which are connected to each other, are positioned as a whole. It is a huge structure with a total wheat storage capacity of 200 thousand tons (Figure 3). Geometrical properties of silo buildings are given in Table 1.


*Figure 3. Silo Buildings*

*Table 1. Geometrical properties of silo buildings (Anon, 2018).*

| | |
|---|---|
| Heigth | 45 m |
| Diameter | 8.67 m |
| Wall Thickness | 18-20 cm |

The silos are connected in series with each other in groups such as "2 rows x 3 units" and "3 rows x 3 units". Within the scope of the study, 10 silo buildings groups, 5 of each groups, in other words, 75 silo buildings are planned to be demolished by controlled blasting techniques. The plan views and side views of the groups are given in Figure 4 and 5.

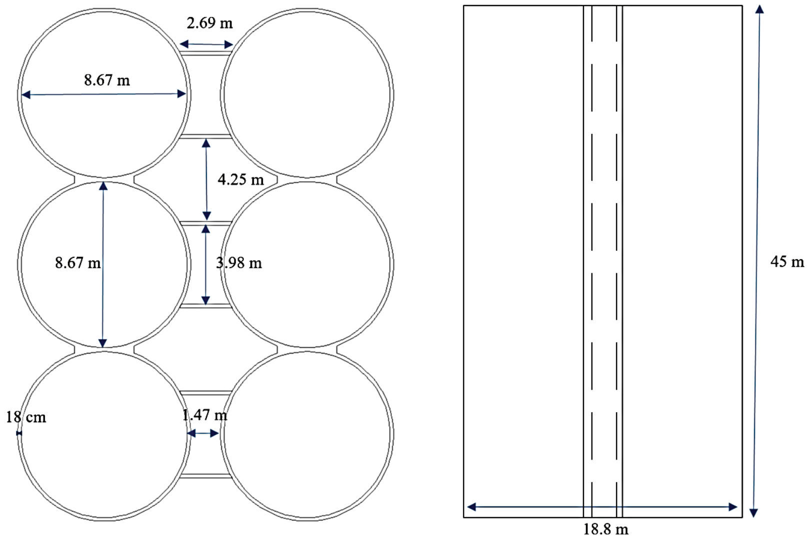


(a) (b)

*Figure 4. (a) Plan View and (b) Side View of "2 rows x 3 units" Silo Buildings Group*

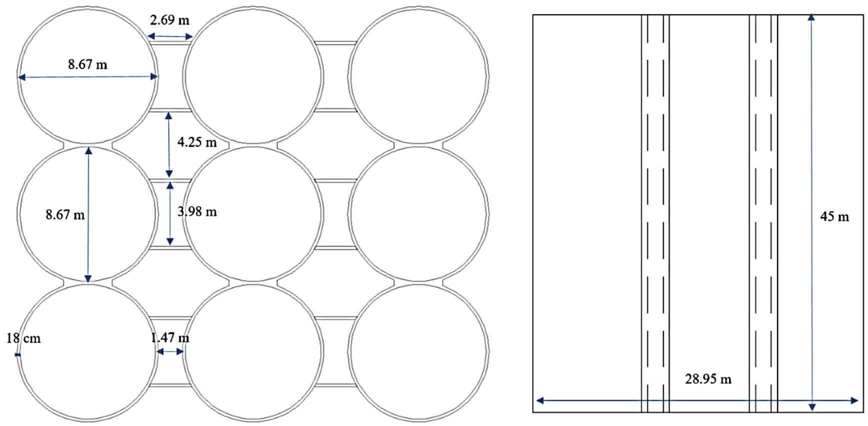


*(a)* *(b)*

*Figure 5. (a) Plan View and (b) Side View of "3 rows x 3 units" Silo Buildings Group*

## 3.1. Reinforced Concrete Material Properties

The silos are made of reinforced concrete. The reinforced concrete material properties obtained as a result of the test performed on the samples taken from the silos are given in Table 2.

*Table 2. The characteristics of reinforced concrete materials (Güner, 2018).*

| | | |
|---|---|---|
| Concrete | Weight per Unit Volume | 2500 kgf/m$^3$ |
| | Modulus of Elasticity, Ec | 240000 kgf/cm$^2$ |
| | Characteristic Concrete Compressive Strength, fck | 150 kgf/cm$^2$ |
| Reinforcement | Modulus of Elasticity, Ec | 2000000 kgf/cm$^2$ |
| | Minimum Yield Strength, fyk | 3500 kgf/cm$^2$ |
| | Minimum Tensile Strength, fu | 5200 kgf/cm$^2$ |
| | Expected Yield Strength, fye | 5980 kgf/cm$^2$ |

Considering the medium-level characteristics of the concrete and the frequently located reinforcement materials, it was understood that the structure is not in a collapsing state. Therefore, it can be said that the structure can only be defeated and collapsed due to high level of destruction. This will be possible by blasting a large part of the structure. However, considering that 75 large-sized silos are integrated as a whole, there will be a need for excessive amounts of explosives. This is also harmful in terms of environmental effects.

*Figure 6. A photograph of silo buildings after demolishing parts of concrete walls*

In order to weaken the structure before blasting, parts of concrete walls were demolished to a certain height (3.8 m for 2 rows x 3 units" Silo Buildings Group and 5.75 m for 3 rows x 3 units" Silo Buildings Group) by machines (Figure 6). In addition, a 20 cm deep cutting process at the determined elevations (3.8 m for 2 rows x 3 units" Silo Buildings Group and 5.75 m for 3 rows x 3 units" Silo Buildings Group) was done on the concrete walls in the rearmost row in order to help the concrete walls overcome the tensile and compressive strengths.

## 4. DETERMINATION OF CONTROLLED BLASTING DESIGN PARAMETERS

As a result of in-situ examinations-observations and static analysis, it was understood that tilting was the appropriate method for demolition due to the geometry of the silos and the absence of risk factors in and around the study area.

A several of trial shots were made to determine the experience coefficient, which is an important parameter in determining the amount of charge. As a result of trial shots, it was calculated that the experience coefficient was varies between 0.6 and 0.7 kg/m$^3$.

### 4.1. Blasting Design For Demolition Silo Building

In order to tilt "2 rows x 3 units" silo buildings group, a wedge cutting application was designed (Figure 7 and 8).

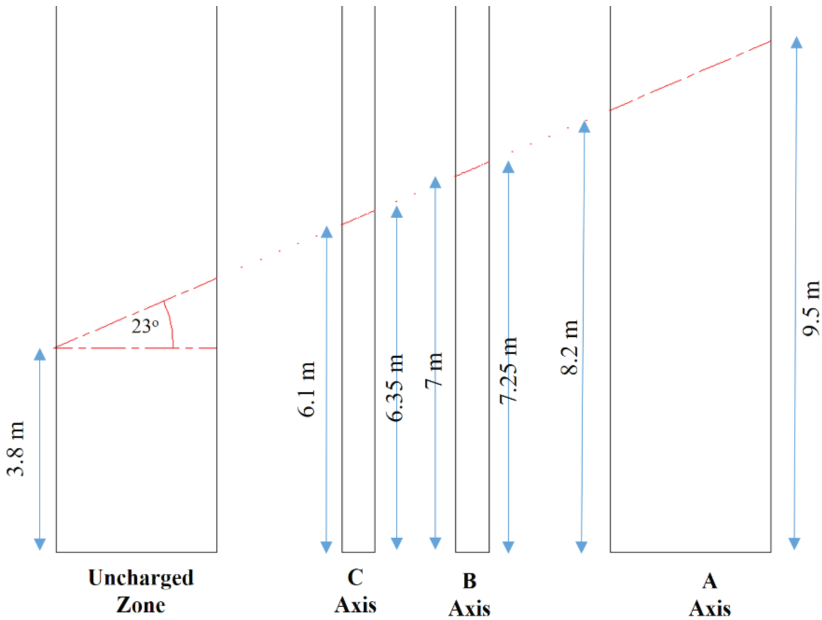


*Figure 7. Suggested Wedge Cutting Application for "2 rows x 3 units" silo buildings group*

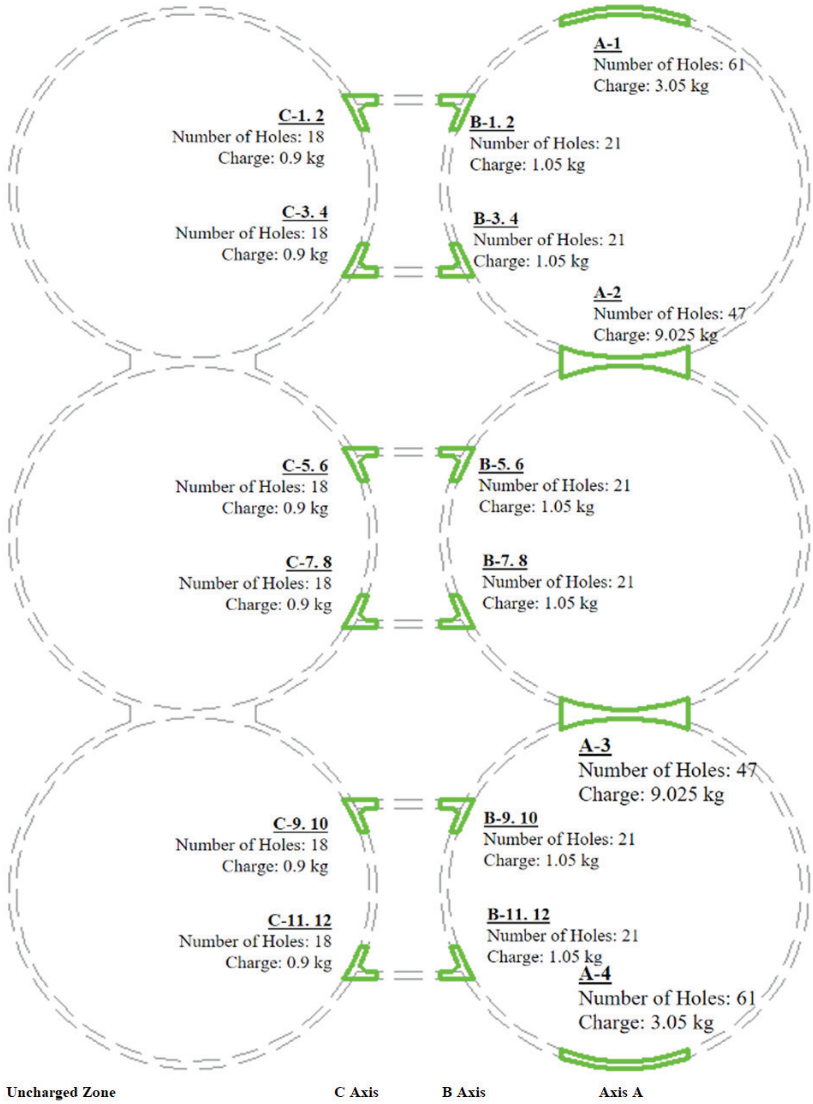


*Figure 8. Summary of Blasting Designs of "2 Rows X 3 Units" Silo Buildings Group*

In order to tilt "3 rows x 3 units" silo buildings group, a wedge cutting application was designed (Figure 9 and 10).

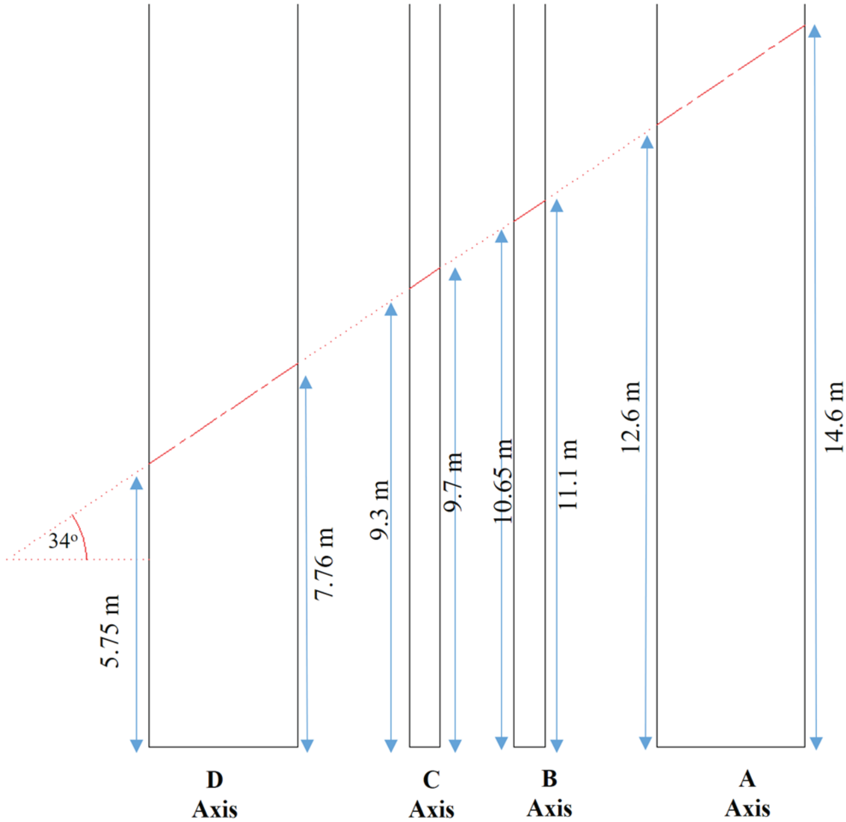


*Figure 9. Suggested Wedge Cutting Application for "3 rows x 3 units" silo buildings group*

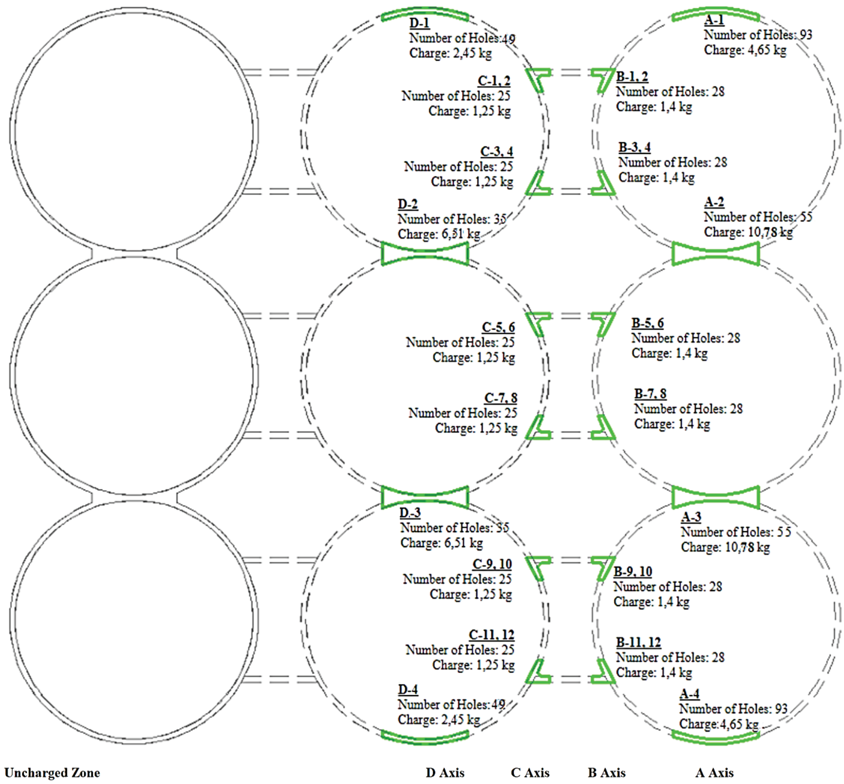


*Figure 10. Summary of Blasting Designs of "3 Rows X 3 Units" Silo Buildings Group*

## 4.2. Initiation Systems And Explosives Used Suggested Blasting Design

Information of total capsules, explosives, and other materials recommended for use within the scope of the project are given in Table 3. Accordingly, it was planned to drill a total of 6160 blast holes, use 520.65 kg dynamite and 6226 capsules to demolish 75 silos. Use of capsules were shown in Figure 11.

During the pre-blasting phase, missing connectors were encountered in most of the 6226 capsules ordered months ago. The fact that the capsules with missing connectors would be used at the critical points of the structures, the completion of the contractual demolition and the approaching time of the delivery of the field, the time to bring the capsules again abroad, and the very long procedures made the situation even more critical. Considering the high number of defective capsules, the search for the most practical method applicable was launched.

In this context, various connection methods were selected for capsules with missing connectors, and their applicability was tested with a test shot. In this shot, the ignition capsules were connected in three directions, which were vertical to the detonating cord, parallel to the direction of the shot, and opposite to the shot's direction. Insulating tape and plastic velcro clamps were used to act as connectors. As a result of the trial shot, all the capsules were fired and exploded without error.

*Table 3. Information of total capsules, explosives and other materials (Ozer et al., 2018).*

| Parameters | | 2 ROWS X 3 UNITS | | 3 ROWS X 3 UNITS | | Between Groups | TOTAL |
|---|---|---|---|---|---|---|---|
| | | 1 Group | 5 Group | 1 Group | 5 Group | | |
| Number of Holes | | 450 | 2250 | 782 | 3910 | - | **6160** |
| Explosive Charge (kg) | | 65,8 | 179,25 | 64,68 | 323.4 | - | **502.65** |
| Number of Capsules | LP500 | 216 | 1080 | 296 | 1480 | - | **2560** |
| | LP1000 | 126 | 630 | 168 | 840 | - | **1470** |
| | LP1400 | 108 | 540 | 150 | 750 | - | **1290** |
| | LP2000 | - | - | 168 | 840 | - | **840** |
| | LP200 | - | - | - | - | 56 | **56** |
| | Electrical Capsules | - | - | - | - | - | **10** |
| 5 gr Detonating Cord (m) | | - | - | - | - | - | **3000** |
| Number of Stemming Cartridges (400 $cm^3$) | | 59 | 294 | 109 | 544 | - | **838** |

The fired capsules' shock tubes were examined, and the occurred damages were examined. As can be understood from the destruction types, the isolated band and plastic velcro clamp worked well, and the other connection types were found to be unsafe and risky because the damages were in the form of stripping despite firing. As a result of the trial firing, plastic velcro camps in terms of practical applicability and vertical connection form were adopted and applied to reduce the risks in terms of firing health.

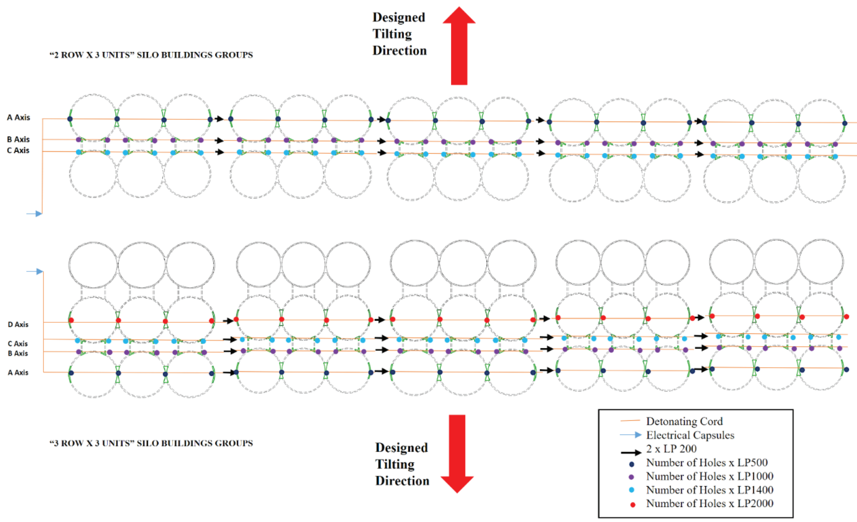


*Figure 11. Use of initation systems*

## 5. STATICAL ANALYSIS OF TILTING OPERATION

The structural behavior of the structure according to the scenario is considered in this part. The structure is modeled by using SAP 2000 structural analysis software (Figure 12). In order to provide a sufficient tilting moment, enough mass must be activated. Blasting would activate the tilting. The structure would be deformed partially, rotation of silos together will be started. When enough rotation occurs, tilting moments will win resisting moments (Figure 13) (Güner, 2018).

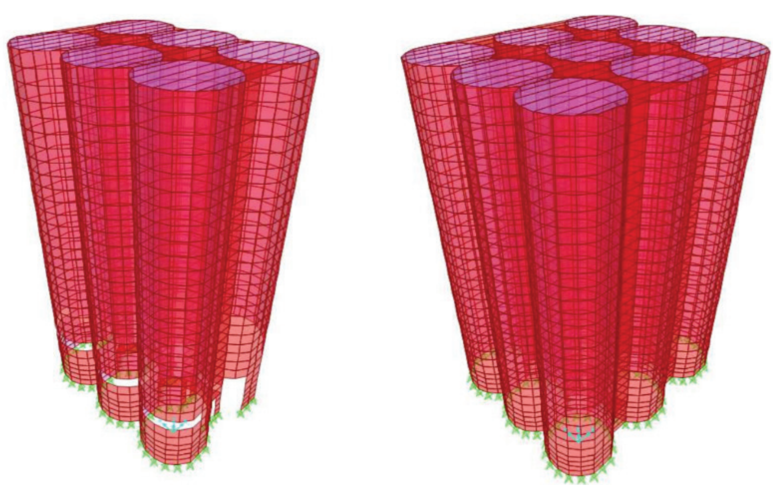

*Figure 12. Statical models of "2 Rows X 3 Units" Silo Groups (left) and "3 Rows X 3 Units" Silo Groups (right)*

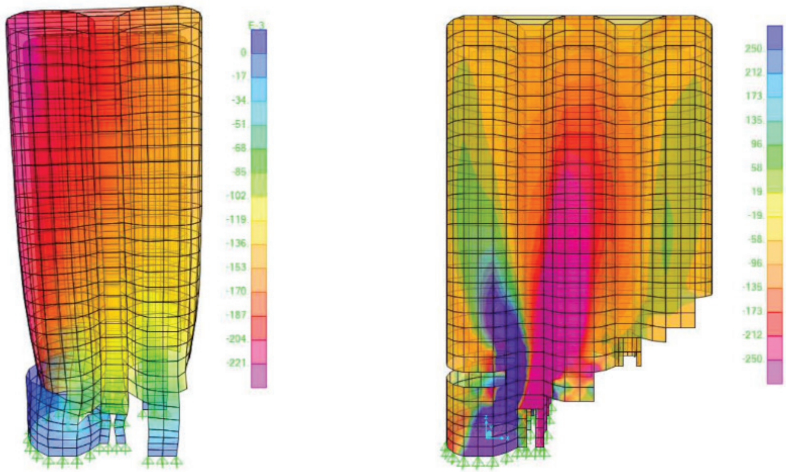


*Figure 13. Total Displacement in cm unit of "2 Rows X 3 Units" Silo Groups (left) and "3 Rows X 3 Units" Silo Groups (right)*

## 6. ENVIRONMENTAL RISK ANALYSIS

In the demolition of a structure by controlled blasting, the risky processes must be carried out appropriately and sequentially. These operations must be applied precisely before, during, and after demolition. However, with the plans made in this way, the impact on the detonator's environment can be reduced to a minimum by destroying it in the desired manner. Therefore, besides the studies carried out for the proper design of blasting in the planning of detonation explosions by controlled blasting, studies should be carried out in order to take measures to minimize the potential environmental effects from blasting.

### 6.1. Determination of Forbidden Zone

To prevent the possible environmental effects that may occur during the demolition of 75 silo buildings, the process of forming a **"Forbidden Zone"** including the blasting area before and after blasting. The main purpose of the building of the prohibited zone is to monitor the destruction during the blasting and isolate the potential mass of the audience and residents living in the vicinity of the blast and ensure the safety of the structures and possible blasting effects. The extent and limit of the prohibited zone, which effectively reduces environmental impacts in the area of demolition, is shown in Figure 14.

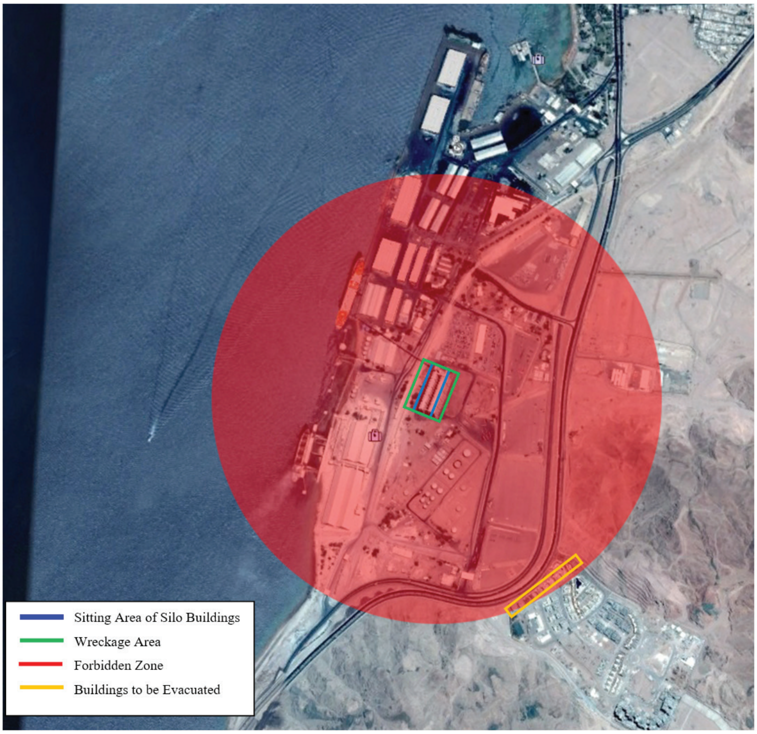


*Figure 14. Forbidden Zone*

## 6.2. Environmental Effects of Controlled Blasting Techniques

It was necessary to control the flying objects' dynamic movements, damaging the residents and the surrounding buildings during the destruction studies with a controlled explosion. This control was achieved using protective materials such as heavy braided mats, tarpaulins, conveyor belts on construction elements such as columns and curtain walls where the explosives will be placed. The use of such cover materials significantly reduced the shattering of the parts.

Two different precautions were taken in work to be done after blasting to prevent dust formation. The first of these was irrigated by the fountain from the water tankers, where appropriate spotting was to be carried out before blasting so that even a small amount of dust can be suppressed. In the second method that was applied, 1 m3 water tanks were placed at specific points of the silos to be exploded, and immediately after they exploded, they could be kept in a specific area by dusting the dust with explosion fog.

Infrastructure transmission lines such as electricity and natural gas connection within the forbidden area were cut off. Risky structures in the forbidden area were evacuated, and pedestrian, vehicle, and marine traffic were cut off in the forbidden area.

## 7. RESULTS

After the preparations were completed by charging the blast holes and connecting capsules, it was aimed to demolish the silos on January 9, 2019. However, the demolition of 75 silos resulted in failure due to the fact that the blasting power of the explosives was not high as stated, and therefore it did not provide sufficient pressure to break up the hole walls. As seen in Figure 13, explosives caused only micro cracks on the structure elements.

*Figure 13. Blast-induced damage in/around the blastholes in January 9, 2019*

A second implementation was carried out on January 15, 2019 with the supply of new explosives, where the demolition was completed as planned (Figure 14). In the controls carried out in the area after demolition, it was observed that the silos collapsed with the estimated wreckage area.

*Figure 15. Demolition of the 75 silo buildings*

## REFERENCES


Dowding, H.C., 1996, Construction Vibration, pp. 265-283, Prentice Hail, Upper Saddle River, NJ, U.K.

Felekoğlu B, Türkel S (2004) The Effects of Loading Rate on Compressive Strength and Modulus of Elasticity of Concrete, DEÜ Mühendislik Fakültesi Fen ve Mühendislik Dergisi, Volume 6 No 1 sh.65-75.

Jimeno, C.L., Jimeno, E.L., Curceda R.J.A, 1995, "Drilling and Blasting of Rocks", A.A. Balkemo, Rotherdam, pp. 312-322.

Gustaffson, R., 1981, Blasting Technique, Dynamit Noben Wien, Vienna, 327 s.

Jimeno, C.L., Jimeno, E.L., Curceda R.J.A, 1995, "Drilling and Blasting of Rocks", A.A. Balkemo, Rotherdam, pp. 312-322.

Güner Ş (2018) Silo Buildings Demolition Akabe-Jordan Structural Report. Izmir, Turkey.

Güven F (2019) Demolition of Concrete Structure and Examination of Demolition Techniques From Applicability, Time and Cost. Master Thesis, Bursa Uludag University, Graduate School of Natural and Applied Sciences Department of Civil Engineering.

Oloffson, S.O., 1980, Applied Explosives Technology for Construction and Mining, ISBN 91-7970-634-7, pp. 268-277.

Özyurt MC (2013) Controlled Demolıtıon Of Structures By Usıng Explosıves And Examınatıon Of Its Effıcıency. Master Thesis, Istanbul University.

Özer Ü, Karadoğan A, Özyurt MC, Kalayci Şahinoğlu Ü, Tutar U, Demir B, Toprak F (2015) Demolition of the Tüm Emek İş Buildings by Using Explosives. The Publication of the Chamber of Mining Engineers of Turkey, Volume 54, No 3-4, pages 11-24.

Özer Ü, Karadoğan A, Sertabipoğlu Z, Özyurt MC (2018) Investigation and Development of Controlled Blasting Designs for Demolition of Grain Silo Buildings in AKABE_JORDAN. Istanbul University, Engineering Faculty, Project Code: 26/07/2018-33298.

Özyurt MC, Özer Ü, Karadoğan A, Kalaycı Şahinoğlu U (2016) The Demolition of a Reinforced Concrete Building by Using Explosives and Examination of It's Efficiency. Uludağ University Journal of The Faculty of Engineering, Volume 21, No 2. DOI: 10.17482/uujfe.77635

Stevenston, A., 1972, Blasting Practice, Nobel's Explosives Company Limited, Scotland,284 p.

Thomas K (1985) Formeln zur landemengenberechnung für das sprengen von bauwerken und bauvverkteilen, Nobel Hefte, April-Juni: 83-90

Türk K (2011) Reinforced Concrete I Notes, Harran University, Civil Engineering Department.

United States Department of Labor (OSHA) (2020) Demolition Accident Search Results. https://www.osha.gov/pls/imis/AccidentSearch.search?acc_keyword=%22Demolition%22&keyword_list=on

# Chapter 3

## MICROSTRIP LOW PASS FILTER ANALYSIS AND DESIGN

*Ahmet Arif ULUSLU*[1]

1 Öğr. Gör. Dr., İstanbul Üniversitesi-Cerrahpaşa, ORCID ID: 0000-0002-5580-1687

## 1- INTRODUCTION

Signs are called functions with one or more variables that carry information about a physical state. Unwanted noise components that occur on the signals due to the structure of the transmission medium or environmental factors disrupt its structure and limit the signal carrying information [1]. Filters are used to pass some signals, stop some signals, separate multiple signals in the same environment, and reduce or eliminate undesirable effects such as noise [2]. Filters are divided into two as analog and digital. There are two types of analog filters, active and passive filters. Passive filters are structures that contain circuit elements (passive circuit elements) such as resistors, capacitors and coils (inductors). These passive elements can pass certain frequencies and damp certain frequencies according to their connection type. In addition to passive circuit elements, the active filter circuit can contain circuit elements such as transistors, coils or microprocessors. It is the passive circuit elements that filter in such circuits [3].

Digital filters can be divided into two main groups: finite impulse response (FIR) and infinite impulse response (IIR) digital filters. In FIR filters, output is only a function of inputs (without recursion), while in IIR filters output is defined as a function of past outputs (recursively) [3]. Figure 1 shows the recursive and non-recursive structure of the digital filters for the input $(n)$ input signal versus the $y(n)$ exit signal.

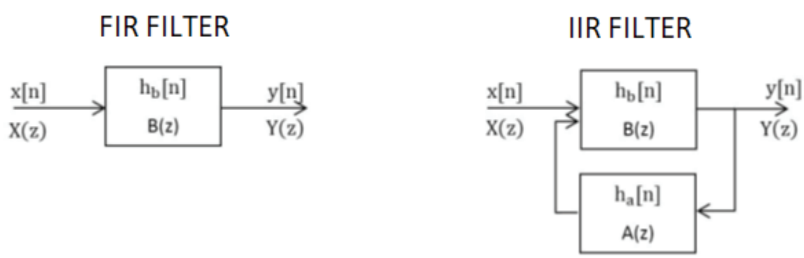


**Figure 1** *Digital filter structures*

FIR filters are completely stable and show linear phase shift. Such filters use only past and current inputs and have no counterparts in the analog world. Since the error surfaces of these filters are convex according to the transfer function (single mode), they contain a single point that represents the best solution. IIR filters produce better performance with a lower number of coefficients, but FIR filters do not always have some advantages such as being stable and linear phase. On the other hand, depending on the filter coefficients, points or points representing the local minimum as well as the solution representing the global minimum can be found on the error surfaces of the IIR filters (multi-mode). For this reason, it is more difficult to accurately calculate the coefficients of the design of IIR filters compared to FIR filters [4]. The main purpose in digital filter design is to calculate the optimal numerator and denominator coefficients depending on the transfer function of the filter [5].

Evolutionary algorithms are one of the most frequently used methods when classical calculation methods are insufficient or when different solutions are needed. There are many studies in the literature on analog and digital filter designs using evolutionary algorithms.

## 2- FILTERS

Filters allow some signs to pass and some signals to be stopped. It allows the signal frequencies applied to the input to pass over the output with little or no reduction. Some terms used in filters are summarized below.

- Passband: It is the name given to the frequency region in which the signal applied to the filter input is passed exactly.
- Passband Ripple: It is the unwanted fluctuations in the passband of the filter.
- Stopband: It is the name given to the frequency region in which the signal applied to the filter input is not advanced but stopped.
- Stopband Attenuation: It is the attenuation of the signal applied to the filter input.
- Cutoff Frequency: It is defined as the point or points where the voltage gain is weakened by 3 dB.

### 2.1- Low Pass Filter

Low-pass filters are filters that pass the signal below a certain frequency value and do not pass the signals above this frequency value. This type of filter is used in cases where high frequency components need to be filtered [6]. The ideal low pass filter can be mathematically defined as in Equation (1).

$$G = \begin{cases} 0 & f > f_h \quad \text{Stop-band} \\ 1 & 0 \le f \le f_h \quad \text{pass-band} \end{cases} \tag{1}$$

Here, $G$ is the gain of the filter and $F_H$ is the cutoff frequency of the filter. In Figure 2, the frequency characteristic graph of the ideal low-pass filter is given. As can be seen from the graph, the frequencies within the cut-off frequency are defined as the pass band, while the frequencies above this frequency are called the stop (quenching) band.

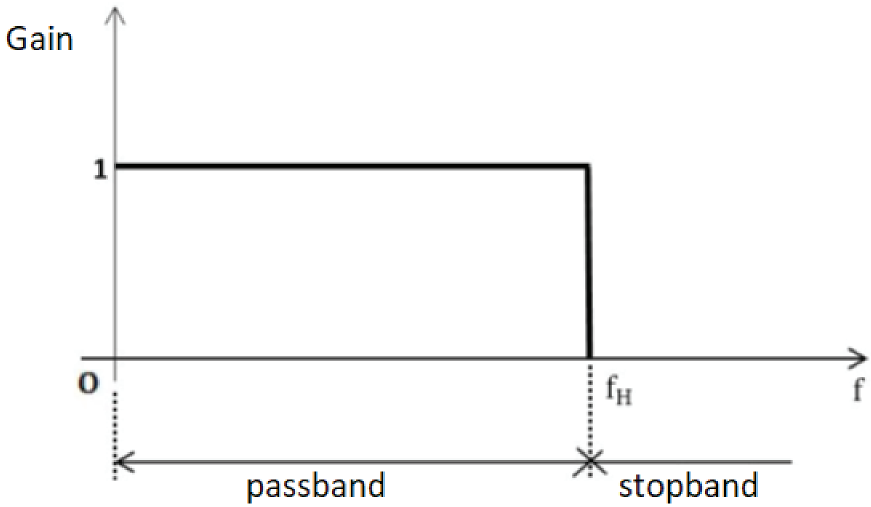


**Figure 2** *Ideal low pass filter*

### 2.2- High Pass Filter

High-pass filters are filters that pass signals above a certain frequency and do not pass signals below this frequency. It is used in applications where the low frequency components of the signals must be filtered [6]. The ideal high pass filter can be mathematically defined as in Equation (2).

$$G = \begin{cases} 0 & 0 < f < fL \quad \text{stop-band} \\ 1 & f \geq fL \quad \text{pass-band} \end{cases} \tag{2}$$

In Equation (2), indicates the gain of the filter and the cutoff frequency of the $F_L$ filter. In Figure 3, the frequency characteristic graph of the ideal high-pass filter is given. As can be seen from the graph, the signal is damped at frequencies below the cutoff frequency, while the signal is allowed to pass at frequencies above this frequency.

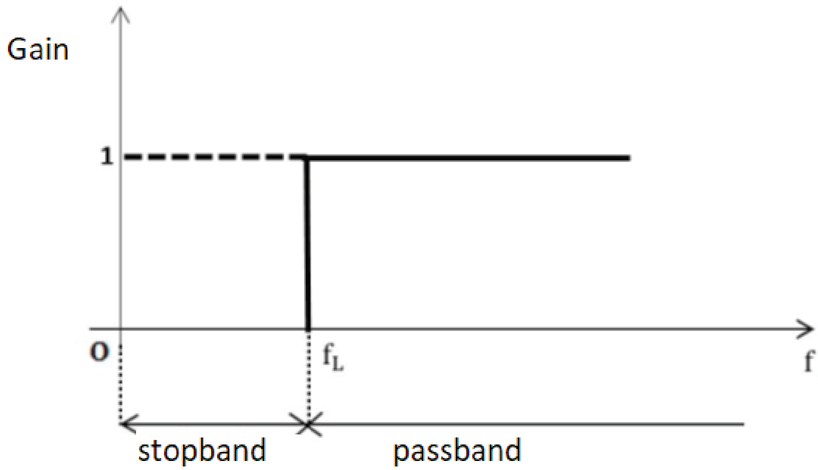


**Figure 3** *Ideal high pass filter*

## 2.3- Band Pass Filter

Band-pass filters are filters that pass signals with frequencies in the specified frequency range and do not pass signals outside of this frequency range. They can be used to separate signals in a certain frequency or to separate signals in one frequency band from signals on other frequencies [6]. The ideal bandpass filter can be defined mathematically as in Equation (3).

$$G = \begin{cases} 0 & \text{In other case} \quad \text{stop-band} \\ 1 & fL \le f \le fH \quad \text{pass-band} \end{cases} \tag{3}$$

In the above equation, $G$ is the gain of the filter, $F_L$ and $F_H$ denote the lower and upper cutoff frequencies of the filter. In Figure 4, the frequency characteristic graph of the ideal bandpass filter is given. In this filter type, the frequencies between the lower and upper cut frequencies are called the pass band, and the frequencies outside this frequency are called the stop band.

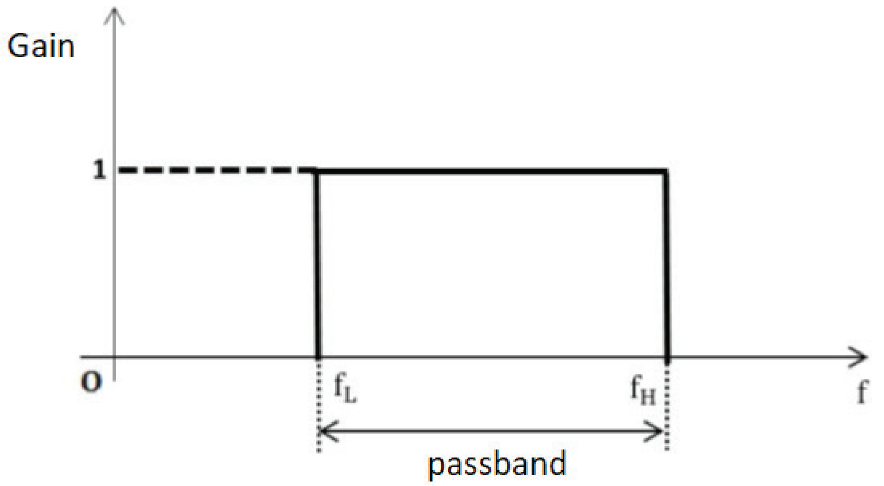


**Figure 4** *Ideal band-pass filter*

### 2.4- Band Stop Filter

Band-stopping filters are filters that do not pass signals between the specified frequency range, but pass signals at frequencies below and above this frequency range. It can be used to filter unwanted frequencies in a signal so as to affect the signal's components at other frequencies as little as possible [6]. The ideal band stopping filter can be defined as in Equation (4).

$$G = \begin{cases} 0 & fL < f < fH \quad \text{stop-band} \\ 1 & \text{In other case} \quad \text{pass-band} \end{cases} \tag{4}$$

In Equation (4), indicates the gain of the filter, $F_L$ and $F_H$ indicate the lower and upper cut frequencies of the filter. In Figure 5, the frequency characteristic graph of the ideal band stopping filter is given. While the signal is damped between the lower and upper cutoff frequencies of the band-stop filter, it is allowed to pass at frequencies outside this frequency range.

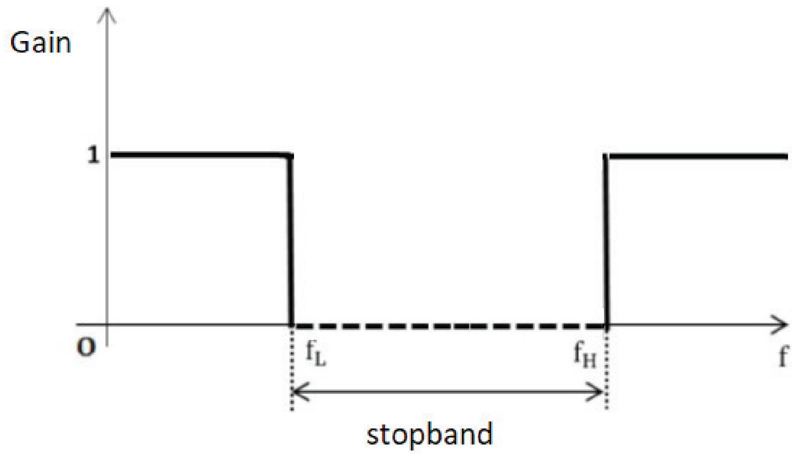


**Figure 5** *Ideal band-stopping filter*

## 3- MICROSTRIP FILTERS

Microstrips are the most widely used type of planar transmission path from radio frequency and microwave frequencies. The origin of microstrips is based on the transition from coaxial lines with central circular conductors to rectangular coaxial lines with the contributions of Rumsey and Jammison in the 1940s. Strip lines were discovered in 1949 with the idea that the thick center conductor of the rectangular coaxial transmission line could be designed thinner. But even though strip lines have many advantages compared to coax lines, their integration with circuit elements was difficult. With the removal of one of the substrates of the strip line by Grieg and Engelmann in 1952, the microstrip lines that form the basis of many microwave printing circuits today were born [7].

### 3.1- Microstrip Structure

The structures obtained by forming w-width and t-thickness transmission paths on an insulating substrate with dielectric constant and thickness h are called microstrip transmission line. Figure 6 shows the structure of a standard microstrip line. Microstrip transmission lines are one of the most popular planar transmission paths because; It can be easily produced by photolithographic method and can be easily integrated into miniature active / passive microwave filters [8]. Microstrip lines are a suitable transmission path for frequency applications in the range of 1 GHz and 110 GHz. The structure of the microstrip transmission path is as follows:

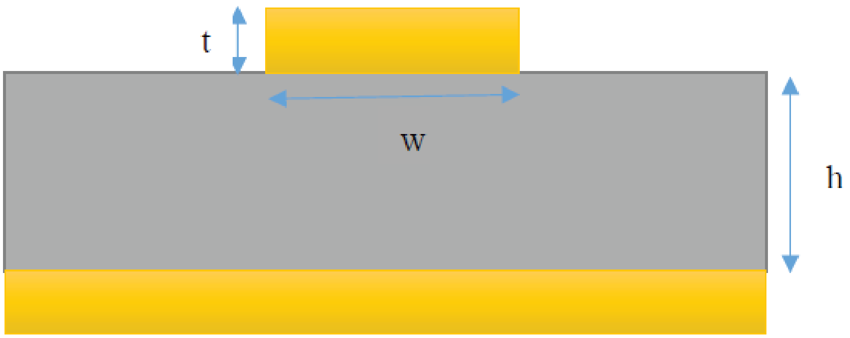


**Figure 6** *Microstrip structure*

Microstrip structures can transmit both AC and DC signals. Active devices, diodes, and transistors can be easily incorporated, and shunt connections are also fairly straightforward. In addition, the structure is very robust and can withstand moderately high voltages and power levels [7].

## 4- STUDY CASE

In this section, optimum width and length values of a broadband microstrip filter have been obtained by using genetic algorithms. This process is done for different stepped microstrip filters. In this design, for the sake of low cost, low size and easy manufacturability, 7, 8 and 9 transmission lines were individually optimized and FR4 material was selected. The parameter values of the genetic algorithm used in the design of the microstrip filter are given in Table 1. In addition, the target criteria of the ultra-wide band microstrip filter are presented in Table 2. Depending on the criteria and cost functions in Table 2, 7,8 and 9-step microstrip structures were obtained.

**Table 1** *Parameters of the algorithm*

| | |
|---|---|
| **Maximum iteration** | 30 |
| **Population** | 80 |

**Table 2** *Performance criteria of the multi-broadband filter*

| **Band** | **Transmission band** | | **Pass band** | |
|---|---|---|---|---|
| **Frequency (GHz)** | 0 | 2.4 | 2.4 | 5 |
| **$S_{11}$ (dB)** | f < -10 | | f = 0 | |
| **$S_{21}$ (dB)** | f = 0 | | f < -10 | |

### 4.1- 7 Step Microstrip Filter Design

The microstrip structure in figure 7 has been obtained depending on the criteria and cost functions in Table 2. The change of cost and function evaluation of the algorithm according to iteration while obtaining these results is shown in Figure 8. Among the results obtained, the result values with the lowest cost value are shown in Table 3. The $S_{11}$ and $S_{21}$ graphics obtained using the results in Table 3 are shown in Figure 9 and Figure 10, respectively.

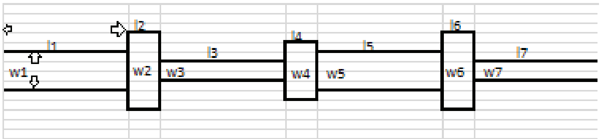


**Figure 7** *Schematic view of ultra-wideband 7-element microstrip filter*

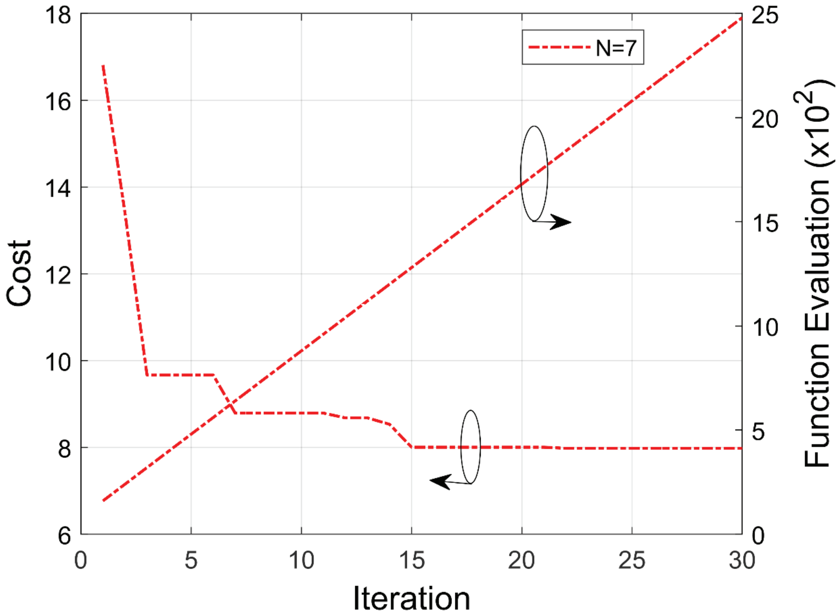


**Figure 8** *Cost-iteration performance of the GA*

**Table 3** *Dimensions of the stepped impedance low pass filter (N=7)*

| Section | $Z_i$=$Z_L$ or $Z_H$ (Ω) | $\beta l_i$ (degree) | $w_i$ (mm) | $l_i$ (mm) |
|---|---|---|---|---|
| **1** | 20 | 26.5695 | 11.1056 | 4.7773 |
| **2** | 120 | 39.8224 | 0.4084 | 8.0568 |
| **3** | 20 | 42.0901 | 11.1056 | 7.5680 |

| | | | | |
|---|---|---|---|---|
| **4** | 120 | 47.1077 | 0.4084 | 9.5308 |
| **5** | 20 | 36.5141 | 11.1056 | 6.5654 |
| **6** | 120 | 29.8965 | 0.4084 | 6.0486 |
| **7** | 50 | 22.9183 | 3.0589 | 4.3606 |

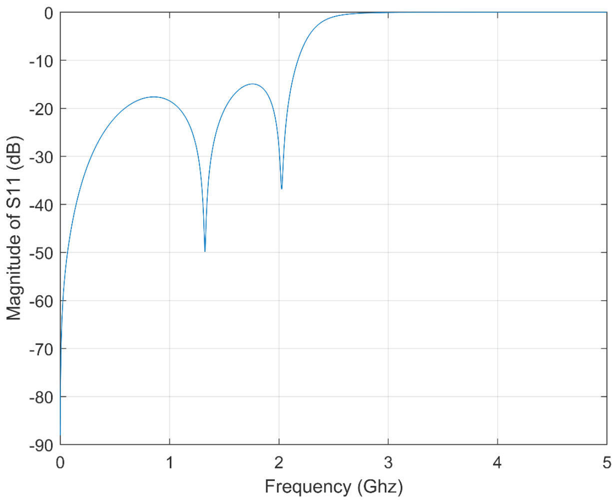


**Figure 9** *$S_{11}$ simulation results*

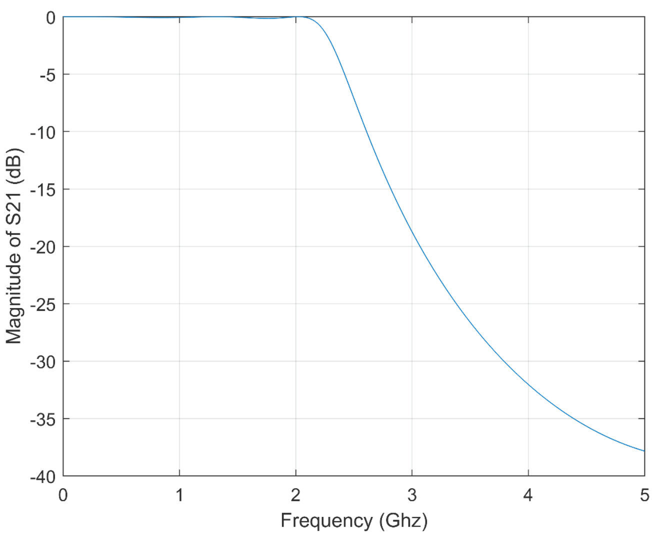


**Figure 10** *$S_{21}$ simulation results*

### 4.2- 8 Step Microstrip Filter Design

The microstrip structure in figure 11 was obtained depending on the criteria and cost functions in Table 2. The change of cost and function evaluation of the algorithm according to iteration while obtaining these results is shown in Figure 12. Among the results obtained, the result values with the lowest cost value are shown in Table 4. The $S_{11}$ and $S_{21}$ graphics obtained using the results in Table 4 are shown in Figure 13 and Figure 14, respectively.

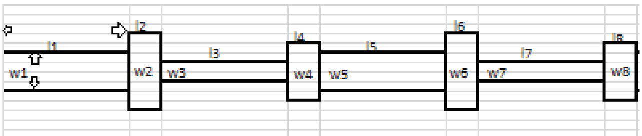


**Figure 11** *Schematic view of ultra-wideband 8-element microstrip filter*

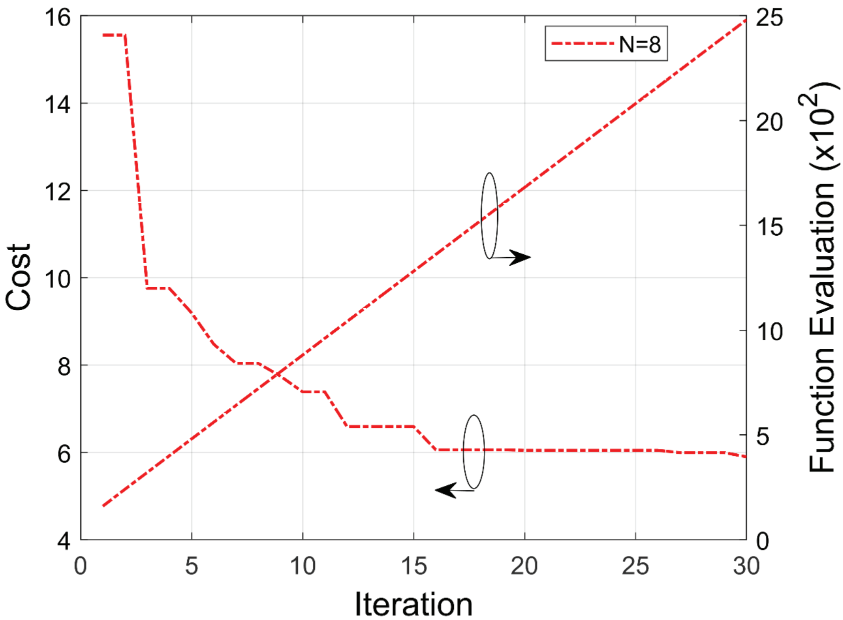


**Figure 12** *Cost-iteration performance of the GA*

**Table 4** *Dimensions of the stepped impedance low pass filter (N=8)*

| **Section** | **$Z_i$=$Z_L$ or $Z_H$ (Ω)** | **$\beta l_i$ (degree)** | **$w_i$ (mm)** | **$l_i$ (mm)** |
|---|---|---|---|---|
| **1** | 20 | 27.6363 | 11.1056 | 4.9691 |
| **2** | 120 | 36.2592 | 0.4084 | 7.3359 |
| **3** | 20 | 47.1969 | 11.1056 | 8.4863 |
| **4** | 120 | 41.0390 | 0.4084 | 8.3030 |
| **5** | 20 | 46.0594 | 11.1056 | 8.2817 |
| **6** | 120 | 37.9663 | 0.4084 | 7.6813 |
| **7** | 20 | 29.0762 | 11.1056 | 5.2280 |
| **8** | 50 | 22.9183 | 3.0589 | 4.1859 |

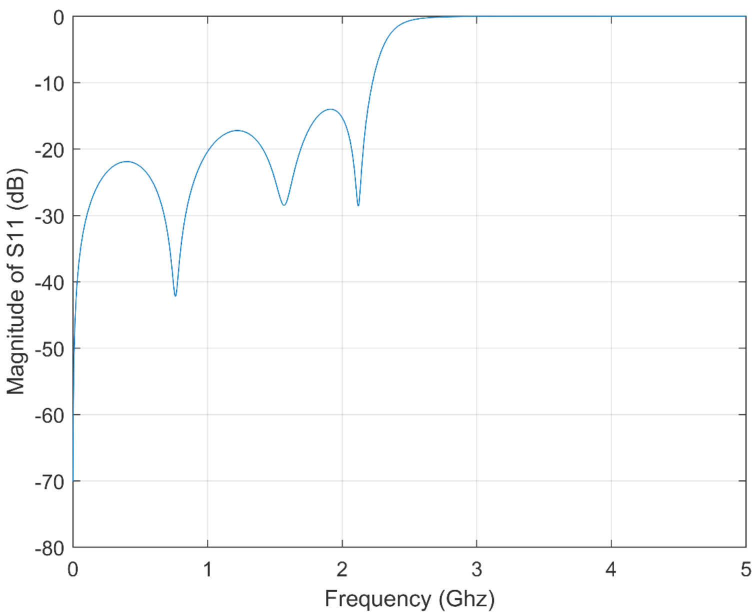


**Figure 13** *$S_{11}$ simulation results*

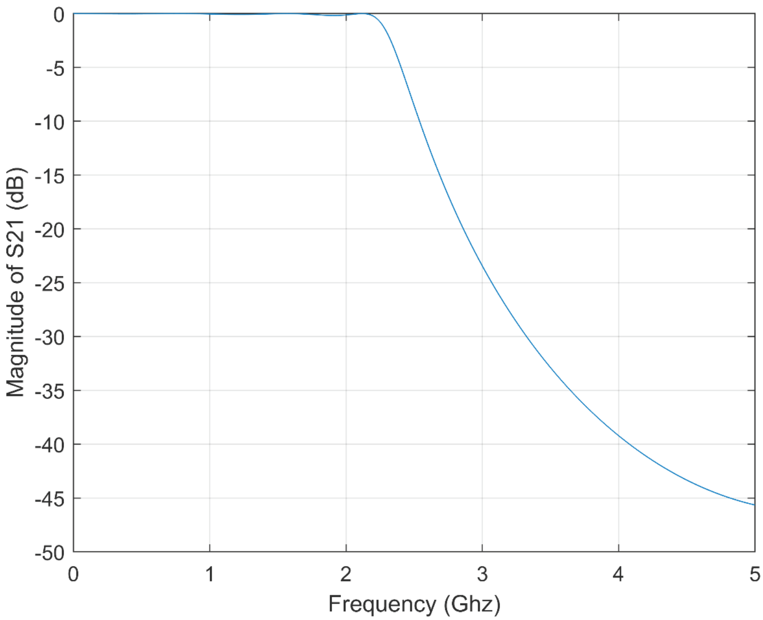


**Figure 14** *$S_{21}$ simulation results*

**4.3- 9 Step Microstrip Filter Design**

The microstrip structure in figure 15 was obtained depending on the criteria and cost functions in Table 2. The change of cost and function evaluation of the algorithm according to iteration while obtaining these results is shown in Figure 16. Among the results obtained, the result values with the lowest cost value are shown in Table 5. The $S_{11}$ and $S_{21}$ graphics obtained using the results in Table 5 are shown in Figure 17 and Figure 18, respectively.

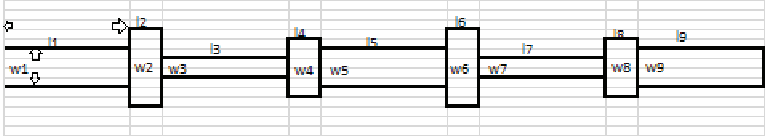


**Figure 15** *Schematic view of ultra-wideband 9-element microstrip filter*

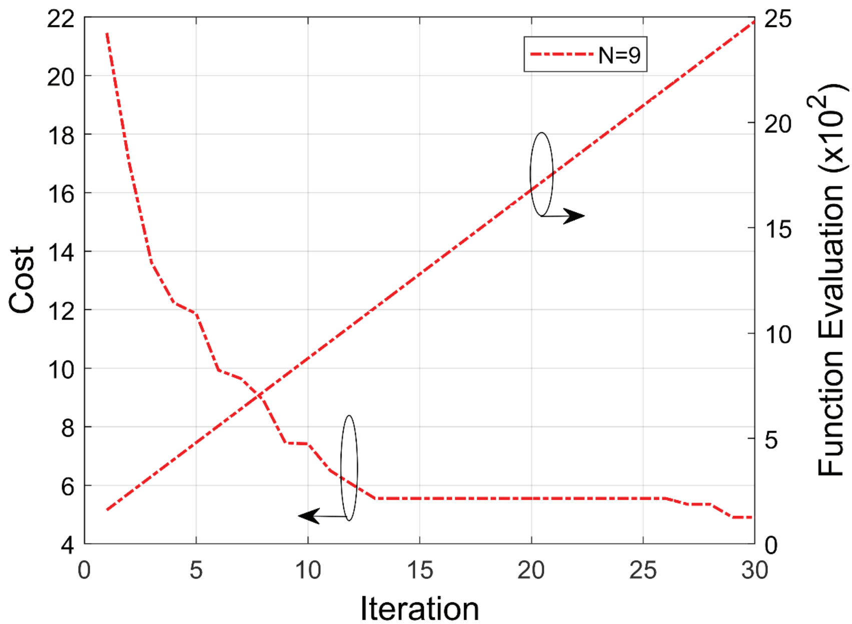


**Figure 16** *Cost-iteration performance of the GA*

**Table 5** *Dimensions of the stepped impedance low pass filter (N=9)*

| Section | $Z_i$=$Z_L$ or $Z_H$ (Ω) | $\beta l_i$ (degree) | $w_i$ (mm) | **$l_i$ (mm)** |
|---|---|---|---|---|
| **1** | 20 | 27.7869 | 11.1056 | 4.9962 |
| **2** | 120 | 36.7362 | 0.4084 | 7.4324 |
| **3** | 20 | 46.5267 | 11.1056 | 8.3658 |
| **4** | 120 | 43.5227 | 0.4084 | 8.8055 |
| **5** | 20 | 41.5009 | 11.1056 | 7.4621 |
| **6** | 120 | 47.9554 | 0.4084 | 9.7023 |
| **7** | 20 | 36.1751 | 11.1056 | 6.5045 |
| **8** | 120 | 24.7044 | 0.4084 | 4.9982 |
| **9** | 50 | 22.9183 | 3.0589 | 4.3606 |

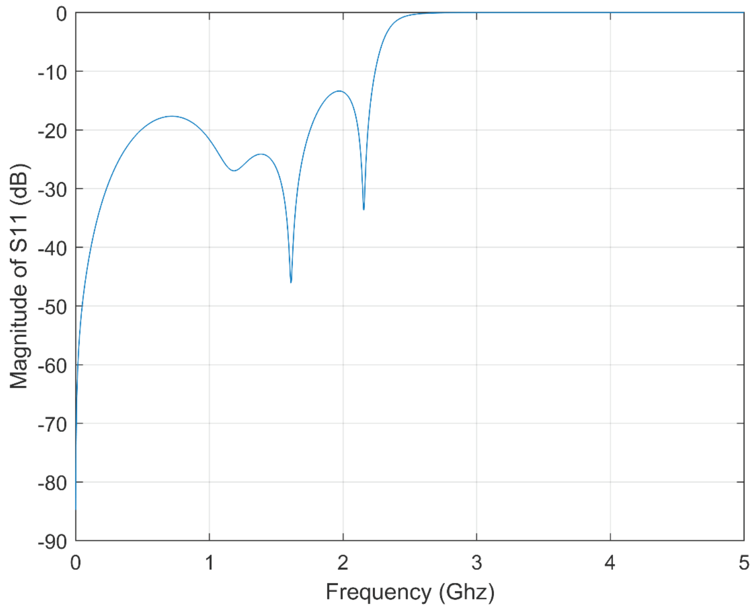


**Figure 17** *$S_{11}$ simulation results*

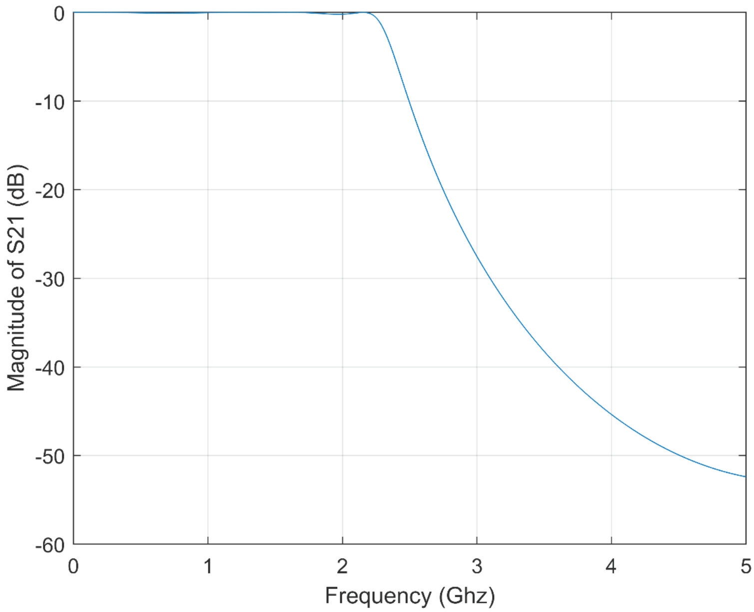


**Figure 18** *$S_{21}$ simulation results*

## 5- CONCLUSION

As a result of the studies and simulations, it has been seen that the genetic algorithm provides solutions with very low error margin in the desired solution intervals. It has been observed that the desired low-pass filter design can be optimized in the most appropriate way with the solutions obtained. In the design, 7,8 and 9 transmission lines and FR4 material were selected for low cost, low size and easy production.

In addition, GA has shown that its success in this design problem can be applied to many different microwave circuit problems other than microstrip filter design. In addition, as a result of the studies and simulations, the equations given in the desired solution intervals of the genetic algorithms have been provided with lines with low error margin. It has been seen that with these solutions, the desired microwave circuits can be optimized in the most appropriate way. In future studies, different types of filters will be compared with different meta-heuristic algorithms.

## REFERENCES

[1] Vaseghi, S.V. 2009. Advanced digital signal processing and noise reduction. Wiley, USA, 544 pp.

[2] Ertürk, S. 2009. Sayısal işaret işleme. Birsen Yayınevi, İstanbul, Türkiye, 293 pp.

[3] Winder, S. 2002. Analog and digital filter design. Newnes, USA, 450 pp.

[4] Haykin, S. 2013. Adaptive filter theory. Pearson, USA, 912 pp.

[5] Schlichthatle, D. 2000. Digital filters basics and design. Springer, Germany, 361 pp.

[6] Lacanette, K., 2010. A Basic introduction to filters-active, passive, and switched-capacitor. Texas Instruments, USA.

[7] Edwards, T. Steer, M. 2016. Foundations for Microstrip Circuit Design. John Wiley & Sons, 857, ABD.

[8] Pozar, D. M. 1998. Microwave Engineering. John Wiley & Sons, 732, ABD.

# Chapter 4

# THE ROLE OF HYDROGEN IN GLOBAL ENERGY, ENVIRONMENT, AND ECONOMIC SYSTEM

*Yavuz SÜMER*[1]
*Ceren KARAMAN*[2]

1 M.S, Sabancı University, Faculty of Engineering and Naturel Sciences, Department of Mechatronics, Istanbul, Turkey. Orcid: 0000-0003-1219-5899
2 Ph.D, Akdeniz University, Vocational School of Technical Sciences, Department of Electrical and Energy, Antalya, Turkey. Orcid: 0000-0001-9148-725, *cerenkaraman@akdeniz.edu.tr

## 1. Energy Demand

Civilizations have remained dependent on carbon fuels for thousands of years to survive and sustain their existence. Coal became the main source of machines with the industrial revolution in the 19th century (Fernihough and O' Rourke, 2014). The countries were in competition with each other in order to obtain the social and economic gains that emerged from the industrial revolution. The usage of excess coal to achieve these gains has adversely affected both human health and the natural environment. The great advances, developments, and discoveries have not only been in the field of engineering, but they have also been in natural sciences, including space science, atmospheric science, and meteorology, and have enabled us to see climate change understanding and greenhouse gas effects in our world (Giannakoudis et al., 2010). Nowadays, coal, oil, and natural gas still play an important role in global energy, and clean coal technologies such as carbon capture and storage are tried to being developed (Wennersten et al.,2015). Even if the technology in this research area has been developing, it is not clear that new technologies can limit the carbon footprint that comes with the use of carbon fuels (Don et al.,2012).

The increase of the world population, the irresponsible consumption of energy resources, and the increasing environmental problems have caused the consumption habits of energy and natural resources to change over time (Jha et al.,2017). Humanity has begun to take the place of renewable eco-friendly alternatives to remove the negative effects of fossil fuels on the environment and to sustain the rising energy demand. Fossil fuels, also known as mineral fuels, are natural sources of energy, such as coal, natural gas, and oil, which are made up of the remnants of millions of years of animals and plants. The fossil resources that meet most of the world's energy needs are diminishing cause serious environmental and air pollution (Bilgena et al., 2008). The consumption of fossil fuels causes people to encounter a tough problem by causing the earth's ozone layer adversely affected, the formation of acid rain, and global warming problems (Jeon et al.,2012). The most important problem of fossil fuels is that they are not renewable sources and have limited reserves (Dresselhaus and Thomas, 2001). Another point that must be taken into account here is the fact that in the second half of the next century, fossil fuels will be consumed by the irresponsible use of these fuels. Furthermore, not only the limited resources or greenhouse effect of petroleum but also the accidents during transportation or storage is a crucial problem for the environment. It is known that thousands of tons of crude oil leaked from gasoline tankers or mixed into the seas after the accident caused great damage, which is difficult or even insufficient to compensate (Nasrollahzadeh,2010). The effects of fossil resources will lead to greater harm to humanity, although the cost of energy generated from natural sources such as solar and wind, known as renewable and clean energy sources, is slightly more expensive than fossil fuels (Chu and Majumdar, 2012). For instance, the use of nuclear energy, which is claimed to have low environmental pollution, is spreading to many countries and, if it continues to increase, the risk of using it as a weapon arises; besides nuclear accidents, even more, important is nuclear waste causing big problems (Ewing et al., 1970).

The methods used to generate energy are very diverse, and the methods of generating more energy from renewable energy sources due to global warming are a special interest of nowadays. The scientists are acknowledged to be the state-of-art technology of the hydrogen energy system that can meet the increasing energy demand of the world without polluting the environment (Yürüm, 2001). There is no harmful chemical production or gas emission that increases the environmental pollution and greenhouse effect except water vapor during hydrogen energy production. In addition, hydrogen energy does not have any known negative effects on the environment and human health.

In addition to fossil resources such as coal and natural gas, hydrogen, which is also obtained from water and biomass, is also considered as an energy carrier rather than an energy source (Yürüm, 2001). In contrast to the other fuels, there is no greenhouse emission gases including $CO_2$, $SO_x$, $NO_x$, etc. occurred as a result of burning of hydrogen. This chapter mainly focuses on hydrogen energy solutions to provide better sustainability and discusses opportunities and challenges from various dimensions, including economic, global energy and environmental issues (Shahbaz et al.,2020).

## 2. Fossil Fuels and Environmental Concerns

The atmosphere, which surrounds the earth and is stabilized by gravity, absorbs solar radiation and heats the surface. Thus the atmosphere protects the life on Earth by reducing the temperature extremes between day and night during day and night change (Fischer et al.,2012). The air we breathe contains approximately 78.1% nitrogen, 20.9% oxygen, 0.9% argon, 0.04% carbon, small amounts of other gases so called trace gases, and also the greenhouse gases (Coyle et al.,2014). Greenhouse gases in the Earth's atmosphere such as water vapor, carbon dioxide, methane, nitrous oxide can absorb and diffuse radiation in the thermal infrared range of the light. The solar radiation passing through the atmosphere is reflected back into the atmosphere and some of these waves return to the space and some are absorbed by the gas layer surrounding the Earth. The mixture and density in this gas layer affects the climatic conditions and these conditions may cause climate change (Hegerl et al., 2019).

Climate change emerges as one of the greatest concerns of both environments and humanity. Since the beginning of the 18th century industrialization, the burning of fossil fuels and the destruction of industrial wastes by nature, as well as the destruction of forests that are absorbing carbon dioxide, have changed the types and quantities of gases in the atmosphere. As a result, the absorption capacity of the heat energy has increased to a large extent and the increased atmosphere allows the scenario to be unstoppable in the future (Poizot and Dolhem, 2011). The mysteries of the greenhouse effect began to be solved by Joseph Fourier in the 19th century. Assuming that the Earth was heated only by incoming solar rays, it was calculated that the Earth would normally be colder. As he searched for this temperature difference, he decided that the atmosphere acted as an insulator and thus retained the amount of heat from the sun (Ayres,2016). At the beginning of the 20th century, scientist Svante Arrhenius explored whether the average temperature of the earth was affected by the presence of heat-absorbing gases in the atmosphere (Abatzoglou et al.,2007).

Within the same time, Arrhenius continued to investigate the effect of doubling the amount of atmospheric carbon dioxide on the global climate and was awarded worthy of the 1903 Nobel Prize for Chemistry. Carbon dioxide emissions mainly occur as a result of combustion of hydrocarbon fuels such as coal, petroleum and natural gas (Anderson et al.,2016).

## 2.1. Coal

Coal, which is among the most valuable natural resources of the world, has been providing people's energy for hundreds of years. Coal is one of the most plentiful and most common fossil fuels used in the world, making up more than four quarters of the world's primary energy claim. Coal mainly consists of carbon, hydrogen, oxygen, nitrogen, aluminum, silicon, iron, sulfur and calcium elements (White and Lee, 1980). Moreover, coal includes more than seventy of the naturally found elements and almost 120 inorganic compounds.  Thanks to its globally proven reserves of 1,139 trillion tons, it continues to be one of the world's most important energy sources, especially for energy generation. Most of the coal-producing countries are only producing for their domestic markets and providing the balance they need to meet national demands. Despite environmental concerns, it is expected to continue to be the second largest source of energy in the world in the coming years. Figure 1. depicts the world coal proved reserves distribution in 1999, 20009 and 2019. It can be clearly seen that due to its geological structure Asia Pasific and North America are the leader of the coal reserves around the world.

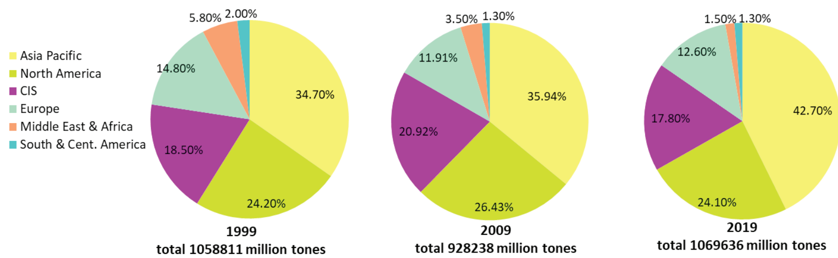


**Figure 1.** *World coal proved reserves' distribution in 1999,2009 and 2019 ("BP Statistical Review of World Energy", 2020)*

Coal, which also played a vital role in the development of the industry, has become one of the world's largest energy sources with the industrial revolution. Steam engines and rapidly expanding railway networks, and the machines that produce the necessary parts for them demand coal that provides principal power. However, main disadvantage of the coal used in this period is that it does not deal with alternatives and does not deal with efficiency as much because coal was abundant, except for pollution, excessive production of waste and toxic flue gas production as much as carbon dioxide. Abundant use of coal sources instead of clean energy wasn't taken into account as agenda due to profit increase.

Despite the development of cleaner coal technology today, long-term damage cannot be recovered. When the coal deposits which consists medium and high sulfur content and the ambient layers of the rock in the ground are deteriorated by mining, acid drainage occurs so that air and water are mixed with sulfides.  Sulfur oxides formed as a consequence of the burning of high sulfur coal falls into the earth as acid rain. The ash and flue gases, which are the products of the burning of the coal, have hazardous effects on the nature and the quality of the ground waters (Wrigley, 2013).

## 2.2. Crude oil and natural gas

Petroleum, which is found in natural formations underground, consists of deposits of organics such as algae and hydrocarbons. Within half a century from its founding, the oil has initiated to replace coal as the primary global energy source. The automobile industry's development and widespread gasoline consumption accelerated the process. Today refined petroleum is divided into a number of final products such as petrol, paraffin, asphalt and chemical reagents used to produce plastics (Veil et al.,2004). Figure 2 represents the Organization of the Petroleum Exporting Countries (OPEC) share of the world's proven crude oil reserves in 2018.

According to the estimates, 79.40 % of the crude oil reserves are in the Organization of the Petroleum Exporting Countries (OPEC) member countries.

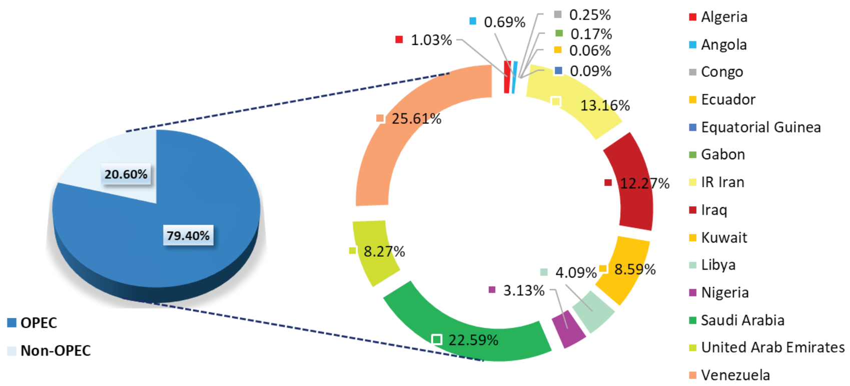


**Figure 2.** *The world's proven crude oil reserves are in OPEC member countries ("OPEC Annual Statistical Bulletin", 2019)*

Natural gas is also encountered in deep underground natural rock formations or other hydrocarbon reservoirs in coal deposits Where natural gas is abundant, gas can also be transported as liquid gasoline or as a jet fuel by applying chemical reactions, as well as being transported as a gas using the natural gas pipeline network. Before using natural gas as fuel, it must be treated to remove foreign substances, including water, to meet the needs at the end of which the process produces by-products such as ethane, propane, butanes, pentanes and higher molecular weight hydrocarbons, hydrogen sulphide carbon dioxide, water vapor (Olah et al.,2011). When the natural gas dissolved in the crude oil comes out to the ground, it separates from the solution due to the pressure difference between the ground and the surface heavy hydrocarbons such as pentane, heptane in gas form condense at surface conditions and turn into natural gas. Five Middle Eastern countries, including Saudi Arabia, Iran, Iraq, Kuwait and the United Arab Emirates, are members of the Organization of Petroleum Exporting Countries (OPEC), accounting for seventy per cent of oil reserves in 2009 and currently account for 65 per cent of the oil reserves (Overton et al.,2016).

Natural gas reserves in the world are 198.8 trillion cubic meters in 2016. Russia, which has the world's largest reserves of natural gas in 2009, has reduced natural gas reserve from about 34 trillion cubic meters to 38 trillion cubic meters in 2019. Iran has gained leadership in the world's proven natural gas reserves ranking with 32 trillion metric tons of natural gas reserves in 2016. Other important reserves are respectively 24.7 in

Qatar, 8.71 in the US, 8.43 trillion cubic meters in Saudi Arabia ("BP Statistical Review of World Energy", 2020).

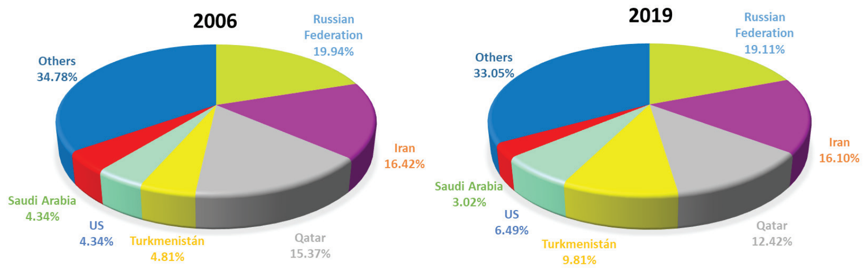


**Figure 3.** *World's natural gas reserves in 2009 and 2019 ("BP Statistical Review of World Energy", 2020)*

## 3. Global Energy

Energy is at the core of environmental and economic development, and energy provisions and authority depend on cautious and accurate application to deal with these complications. Indeed, it has been playing an active role in the last century, especially in the level of economic growth, prosperity and globalization. The limited availability of resources, the factors of world safety and increasing environmental concerns have increased demand for renewable and clean energy sources as an alternative to traditional fossil fuels (Acker and Kammen,1996). Taking into account the current energy demand, this chapter will review the not only the energy sources, but also efficiency studies and policies to reduce emissions and meet energy demand. The interaction of energy, environment and climate policy in the energy markets of the major countries of the world has great importance on this subject.

It has been known clearly that all-inclusive energy and environmental issues have caused great difficulties in the most developed regions of the world, that they have taken a global perspective on energy and environmental politics. The Industrial Revolution, and the oil crisis in the 1970s, reveal the relationship between historical energy and economic growth. Furthermore, the economic crisis that began in 2007, excessive uncertainty in oil and natural gas, and unexpected price changes triggered the use of nuclear energy for electricity generation and the need for many renewable energy technologies. When the new energy systems are adopted and accommodated, it has great inactivity due to its expenditure and intricacy, so restructuring of new fuels and technologies is getting harder. It is necessary to concentrate on sustainable energy sources by taking advantage of having more data and possibilities than in the past in order to get rid of the indistinctness periods where similar examples are observed in the history and to continue economic development (Petrova,2014).

The opulence and the economic situation of the vast majority of developed countries in the world is highly variable compared to emerging countries and emerging economies. As a result of the convenience of the developing economy, the quality of life of citizens of some countries has increased and has benefited well from health and social services; but many countries have been avoiding attempts to keep up with rising demands due to rapid population growth. While individuals are taxed beyond design boundaries for clean air and water, waste, transport-related operations, energy and other services; assumptions and customary initiatives may be insufficient to overcome the predicted population growth trends, and harmful air quality, electricity cuts may be characterized as undesirable side effects. By approaching systematically instead of traditional approaches, resources can be optimized, productivity can be improved, a higher quality of life can be presented in convenient enforcement (Lee, 2011). Figure 4 represents the global share of total energy supply by source in 1973 and in 2018. It can be clearly seen that whereas in 1973 the world's energy needs were derived from fossil fuels at almost 86 %, in 2018 it decreased to 81%. There has been a slight increase in other alternative fuels since the material and environmental constraints imposed by the Earth's atmospheric release of greenhouse gases resulting from the burning of these fossil fuels, in addition to the uncertainty of the reserves and price fluctuations have led us to new solutions.

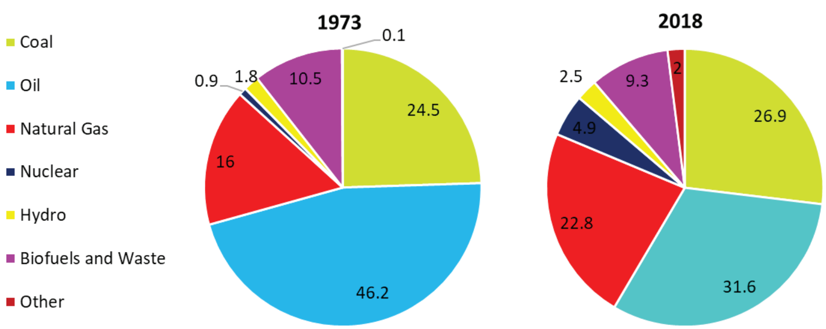


**Figure 4.** *The global share of total energy supply by source in 1973 and in 2018 ("IEA Key World Energy Statistics", 2020)*

The International Energy Agency (IEA) has been collecting and analyzing all energy data in order to observe major energy-intensive facilities and find appropriate solutions for the countries. The IEA uses these data to formulate scenarios and develop proposals for policy to accurately estimate future energy demand, energy consumption, and alternative energy sources. In this context, the estimated regional share of $CO_2$ emissions of some countries including the Middle East, Bunkers, Organisation for Economic Co-operation and Development (OECD) countries, China, Non-OECD Americans, Non-OECD Asia, Africa, and Non-OECD Europe and Eurasia have been presented in Figure 5. The interpretation of the data allows us to predict the global energy situation and to pursue the strategic energy policies of the countries. From an environmental point of view, the measurement of emissions from the burning of fossil fuels and potential emission threats arise as a result of the research conducted over the last 30 years ("IEA Key World Energy Statistics", 2020).

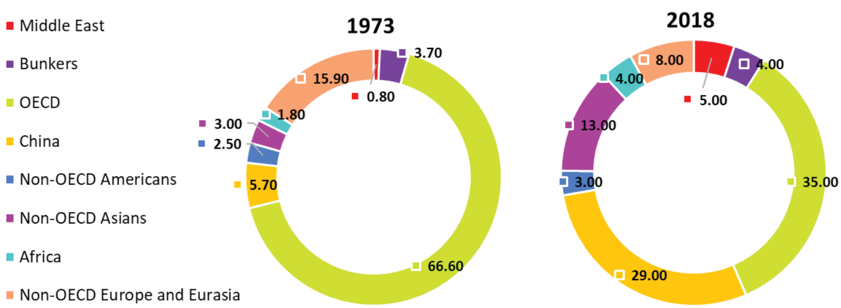


**Figure 5.** *The regional share of $CO_2$ emissions in 1973 and 2018 ("IEA Key World Energy Statistics", 2020)*

The communal attention of the adverse effects of greenhouse gas emissions has increased markedly and the low-carbon energy potential has been recognized. The link between energy and climate trends should be developed with a focus on long-term strategic actions. Resolving the interaction of energy and climate for growing countries is complicated in a rapidly globalizing world. Economic competition and environmental and social influences, which are among the great superpowers, are important in this context. The impact of China, Russia, Brazil and India, as well as the United States and the European Union's energy and climate policy, which are some of the fastest growing economies of the world, can be easily understood from the global perspective of carbon emissions. Future economies in the world will be defined by the sustainable balance of energy demand, the environmental impact of resources and the provision of economic growth. The policy necessary to achieve global peace and prosperity to be successful in a perspective focused on globalization should be as coordinated and conscious as possible; not with national efforts (Rice et al.,2020).

According to the International Energy Agency (IEA)'s statement in 2012, the total global primary energy supply (TPES) was 13,371 Mtoe, electricity generation 22,668 TWh and consumption 8979 Mtoe. As a consequence of population growth and the consumption will lead to increase in these amounts fiercely. Estimated data for 2035 according to The New Policies Scenario the total global primary energy supply is expected to show an increase, reaching 18,700 Mtoe in 2035. Even if there are new policies that limit $CO_2$ emissions, this amount is expected to be 450 ppm. Moreover, it can be predicted that global total energy use of renewable energy consumption will increase by about 15 per cent by 2035. Even though some programs have been applied for the transition to renewable energy sources from Fossil fuels for a cleaner life area in our world; fossil fuels will be used for a while unless there is a clear change in policy, large-scale capital investment in alternative technology ("IEA Key World Energy Statistics", 2020). Figure 6 shows the global annual average change in energy production by energy resources.

In another respect, it is expected that the prices of fossil fuels will increase due to the loss of accessibility due to the consumption of easily accessible fossil fuels and the increasing political uncertainty of countries with world fossil fuels. Apart from economic issues, as shown in Figure 5, almost all of the greenhouse gas, which leads serious concerns about the environment and human health, is the result of the use of fossil fuels. Therefore, it should be noted that the clean energy systems that will ultimately respond to the world's increasingly increasing demands without environmental harm and fossil fuel dependence can provide significant social, environmental, and economic benefits.

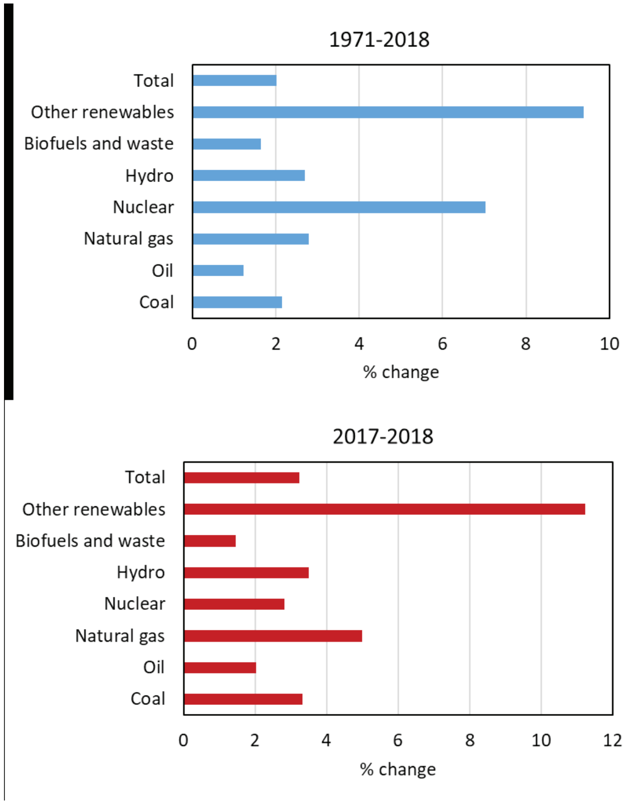


**Figure 6**. *Global annual average change in energy production by energy resources, 1971-2018 ("IEA Key World Energy Statistics", 2020)*

## 4. Clean Energy

A sustainable energy system must have no adverse impacts on the environment and humanity, and provide energy for the current and future population with no consumption of natural resources. In this context, the clean energy systems have gained considerable attention due to their outstanding features such as reducing emissions by using renewable and clean sources, increasing system efficiency by reducing emissions and waste by energy recovery, lower energy input requirements. Renewable energy sources can reduce greenhouse gas emissions associated with fossil fuel burning and overcome environmental issues. Hence, in the case of using renewable energy sources in an effective way, it will be possible to reduce the adverse impacts of the energy sector on the environment through safe and sustainable procurement and can lead to social and economic development. Renewable energy is defined as the energy generated from natural processes benefiting from renewable sources. Mainly, these sources of energy can be obtained directly or indirectly from the sun, hydroelectric, wind, biomass, geothermal (Delucchi and Jacobson,2011).

The sunlight, which plays a direct role in the growth of plants, forms organic matter and is called biomass. Biomass can be used to produce electricity, transportation fuels or chemicals, and this use is expressed as bioenergy. Biomass can be used directly in addition; it can be converted into liquid fuel such as biofuels. For example, wood and wood service waste can be used for direct heating purposes and waste materials, agricultural products are converted to liquid biofuels as fuel or are burned to produce electricity in plants or convert biogas in storage areas. Biomass can be found in plenty with countless feed storage and recycling technologies, and aboriginal fuel production and transit technologies can be considered as developing countries, but greenhouse gases, especially methane and carbon emissions, emerge during biofuel production (De Moel et al.,2010).

Geothermal energy, a renewable source of energy that is not directly fed from the sun, in principle uses the Earth's interior temperature for various uses, including electricity generation and heating and cooling of buildings, by opening deep shaft and force to move hot groundwater or steam to the surface. Geothermal energy sources despite being ample and clean; costly start-up and overhaul costs due to abrasion, risk of hydrogen sulphide release, settlement changes caused by opening deep wells and pollution of waterways are major disadvantages (De Moel et al.,2010).

Hydropower is one of the oldest and historical energy sources producing mechanical and electric energy. Hydropower began to be used for the rotation of the wheels to help grind grain thousands of years ago, then the grain factories with the discovery of electricity equipped with this energy. The volume of the water flow and the change in height that occurs when the water flows from one point to another indicates the amount of energy contained in the moving water. The transformation of the energy generated by this flowing water into electric energy is defined as hydroelectric power. In spite of the fact that hydro energy is abundant, clean,safe, has a fairly constant production rate ,and requires cheaper maintenance costs and less maintenance; the need for high investment costs, the threat of torrents in the immediate vicinity, the impact of local water and land changes on the environment, the risk of drought and the constant water resources are factors to be considered (Hepbasli,2008).

Solar energy is used to provide heat, light, electricity for home and industry. Since solar energy systems do not emit air pollutants or carbon dioxide, they have less environmental harm than other renewable alternatives. Because the amount of sunlight changes depending on geographical conditions, time of day, weather and weather conditions, the amount of solar energy is not constant, and there are also storage and reserve problems (Kabir et al.,2018).

Wind is a renewable source of energy, and relative to other sources of energy, using wind to produce energy has less environmental impact than many other sources of energy. Wind turbines do not create wastes that pollute air or water. Modern wind turbines are big machines, and the blades of the turbine are making noise and can cause populations to kill birds. It is a separate problem that certain zones can be established (De Moel et al.,2010).

## 5. Alternative Energy Fuel: Hydrogen

Energy fuels should ideally be able to transport easily and safely everywhere, and that energy loss is expected to be minimal during transport. It should also be a clean, inexhaustible and safe source, free of carbon, and able to minimize damage to the environment. It is very important to be able to easily convert to other types of energy in addition to the criteria for generating energy with high efficiency. It must have a wide range of usage and finally be economical. It can be considered that there is not a fuel that can fulfill all these conditions. However, there is a fuel that meets these requirements. Hydrogen is regarded as a fuel not only in the coming century but also in the next 5 billion years, which is estimated to be the sun's life, including all these qualities as fuel (Kabir et al.,2018).

Various feed-stocks are available for hydrogen production. These include fossil resources such as natural gas and coal, and resources such as biomass and water, which are members of renewable energy sources. Many technologies can be used for hydrogen energy applications, including chemical, biological, electrolytic, photolytic and thermochemical. Each technology is at a different stage of development and each offers unique opportunities, advantages and challenges. The local presence of raw material, the progress of technology, market applications and requests, policy issues and costs will affect the choice and timing of various options for hydrogen production (De Moel et al.,2010).

- *Easy Transportation*

Hydrogen gas can be transported easily and safely through pipes similar to natural gas or air gas everywhere. It is possible to use the underground pipe distribution network for natural gas in hydrogen with little change in the future. Apart from pipelines, hydrogen can be transported as pressurized gas or liquefied by tubing and transported by tankers. Today, industrial pipelines use commercial hydrogen pipelines ranging from one kilometer to several hundreds in length to distribute large amounts of hydrogen in a gaseous state. For example, in March 2009, Air Products expanded the US Gulf Coast pipeline network in Louisiana by 60 km. It is predicted that the hydrogen network is 1,600 km in Europe and 1,100 km in North America (Liang et al.,2012).

❖ *Carbon Free and Inexhaustible*

Large supply of hydrogen production at competitive costs and without too much carbon emissions will provide significant advantages when we compare the use of hydrogen to other secondary fuels. In addition to being able to burn cleaner in combustion engines, hydrogen is more suitable for use of hydrogen fuel cells than competing fuels. The fuel cell can affect the energy system and hydrogen can become a destructive technology that will replace the oil and carbon-released fuel cycles. Hydrogen and electrical integrity is a fascinating issue of great importance in fuel cell vehicles and automobile electrification, and is what automobile manufacturers are demanding extensively. The low-cost and durable fuel cell allows the in-car service of the vehicle to serve more effectively than alternatives, providing mobile and high-power electricity. The replacement of mechanical and hydraulic subsystems with electrical energy allows for increased productivity and the creation of new designs. Since the fuel cell does not have a moving part, it is quite quiet compared to the internal combustion engine and is almost 2.5 times more efficient. In addition to the high efficiency of hydrogen engines, Hydrogen-fueled engines have another advantage over gasoline engines in that they only produce water vapor as waste product. It should be borne in mind that very small amounts of petroleum products used to lubricate the rollers may be present between carbon monoxide and hydrocarbons and waste oxides in high-temperature nitrogen oxides. However, since these harmful gases are so low that they can be ignored relative to vehicles using petroleum products, it is possible to assume that hydrogen engines are entirely environmentally friendly (Dunn,2002).

❖ *Safety*

The high market domination of hydrogen-using devices to meet energy needs can expose the society to unusual hazards. These threats, from the first days of the transition to the hydrogen economy, present a challenge, such as the need to improve hydrogen security competence and the need to protect human life and property. At the point of emerging hydrogen technology, hydrogen fuel is much safer than accidents caused by the widespread use of nuclear fuels such as natural gas, oil, coal and uranium. When certain processes are followed in the use of hydrogen and a certain discipline is observed, the danger is considerably reduced. Today, fuel used in vehicles or in the plane is accidentally burned, resulting in excessive temperature and smoke, and as a result, many people are facing danger. In the case of using hydrogen as fuel, the hydrogen flame, which combines with the oxygen in the air when the hydrogen burns and does not emit another gas from the water vapor, emits very little heat at the same time, so there is no danger if it is not directly contacted with flame (Bose and Malbrunot, 2007). Hydrogen may burn or burst in the presence of oxygen or air when it is ignited, so hydrogen should be used with caution as other fuels. In the Table 1. the combustion properties of hydrogen are illustrated.

**Table 1.** *Hydrogen properties in terms of safety (Bose and Malbrunot,2007).*

| | |
|---|---|
| Flammability range in air (vol %) | 4 – 75 |
| Minimum ignition energy (at stochiometry) | 0.02 MJ |
| Auto-ignition temperature in air | 858 K |
| Adiabatic flame temperature of hydrogen at 300 K | 2 318 K |
| Detonation limits (vol %) | 13-65 |
| Detonation overpressure at stochiometry | 1.47 MPa |
| Diffusion constant in air | 0.61 $cm^2$ /s |
| Flame velocity in air | 260cm/s |
| Detonation velocity in air | 2 km/s |
| Stochiometric composition in air (vol %) | 29.53 |

If enough hydrogen is present, an explosion can occur and a ruthless energy release occurs. As a result, a flame field and a violent pressure wave can occur in different scenarios. The sparkle frequently occurs when the hydrogen concentration in the air is 4 to 18% or 59 to 75%. In this case, while the flame travels at a speed less than the sound speed, it causes an increase in the fresh gas pressure trapped by the effect of the burn. Detonation usually occurs when the hydrogen concentration is between 18% and 59%. During the explosion, the flame moves at supersonic speed with excessive pressure, creating a shock wave. Due to the fact that hydrogen is flammable and explosive, it requires great care in use and storage, and the leak is a serious risk. Hydrogen, one of the lightest and smallest molecules, tends to leak independently of the storage system it contains, such as compressed gas, liquid hydrogen containers. In confined spaces, small leaks quickly disperse and do not create a flammable and dangerous density. On the other hand, a large leak in enclosed spaces brings with it a serious risk. These risks can be reduced through safe procedures with suitable aeration, leak detectors (Bose and Malbrunot,2007).

Approximately 41 million short term hydrogen are produced annually in industrial plants worldwide. The experience gained from this industry practice has resulted in a positive comparison of professionally administered hydrogen safety records compared to similar industrial processes, and the result is that hydrogen can be produced and used by trained professionals with acceptable safety under controlled conditions. For this reason, safety considerations may arise if hydrogen consumers are not used in a particular instruction or rules of industrial procedures.

- *High efficient*

Hydrogen is a fuel with high energy content. When 1 kg of hydrogen is combined with oxygen during combustion, it produces 120 MJ of energy while generating water. It is necessary to use 2.5 kg of natural gas or approximately 4 kg of coal to acquire a similar amount of energy. However, hydrogen is a very light gas and has the lowest energy content per volume unit even though it has the highest energy content per unit mass compared to other fuels. To generate the same amount of energy from a certain volume of natural gas, 2.5 times more volume of hydrogen is required in ambient conditions. As a result, hydrogen requires large volumes in storage (Bose and Malbrunot,2007).

- *Storage*

In the twenty-first century, hydrogen is the most abundant element in the hydrogen environment, which can be an important energy carrier compared to electricity and is the main source of life for stars and galaxies. Although the idea of using solar energy, which is the power of nature as an alternative for many people to save energy in the world, the real problem is how to store this free energy as well as how to collect it. The basic purpose here is to generate electricity from solar energy in comparison to other energy cycles. However, as generated electricity is arduous to store in large amounts it should be consumed immediately. It is possible to transform hydrogen to electricity in a fuel cell and additionally to some amount of heat and water as a final production by electrochemical combination with oxygen of air. Hydrogen with a storable property solves this problem (Karaman et al.,2019).

- *Widespread application*

Hydrogen is used in many fields as chemical raw material in the industry especially fertilizer production, dyes, medicine and plastics construction. Moreover, hydrogen also operates in the treatment of oils and methanol produce and also as a source of welding. Besides it acts as a powerful fuel for space shuttles and other rockets, in form of liquid hydrogen in conjunction with liquid oxygen in space exploration. Until now, metallic hydrogen, which is the focus of laboratory work, can be used as an extremely energetic fuel if it can be produced in the required industrial quantities and stable at high and ambient temperatures, and also as a zero resistance electrical conductor in any electrical and electronic technology (Karaman et al.,2021).

❖ *Wide range of production techniques*

Hydrogen can be produced commercially with considerable choice, nevertheless most of these methods involve the removal of "hydro" from hydrocarbons. The most commonly used and smallest costly process is steam reforming. The most commonly used and smallest costly process is steam reforming. It is a process where natural gas reacts with steam and let out hydrogen. In places where electricity is cheap and pure water is abundant, it is possible to use an electrolysis method which is called as separation of hydrogen and oxygen in the water by passing electric current through it. Hydrogen storage can be carried out in the form of a high pressure gas, in microscopic carbon fibers, and as a component in specific alloys familiar as hydride called chemical hydride (Karaman et al.,2021).

The ability to produce hydrogen from a wide variety of primary sources offers a great advantage as it reduces the chance of creating a hydrogen cartridge similar to OPEC. Today, even if hydrogen is produced mostly from fossil fuels, it will be produced in the future from hydrogen clean water and clean solar energy, biomass and biofuels, even cleaner modifications of conceivably nuclear energy. As it can be done from non-renewable and renewable sources, a particular country, state, region or economy can be brought in gradually to the general energy network with the most appropriate and least congestion system. Particularly in desert areas, the sun's condensed heat is the study of the division of water molecules into hydrogen and oxygen by direct solar energy. On the other hand, the water can be electrolyzed according to the electricity generated from the geothermal sources in some regions (Dunn,2002).

## 5.1. Future of hydrogen

Basically, the most basic lines of the future hydrogen economy can be as follows. In many varieties as primary clean energy likely solar energy and a more environmentally improved version of nuclear energy separate hydrogen and oxygen as a byproduct from water and may use it as a hydrogen fuel for electricity generation. At the same time, the thermochemical breakdown effect of heat generated by solar energy and nuclear power plants on water molecules is still under advancement. Even strange methods such as the production of hydrogen in the field of genetic engineering from algae, cellulose and similar biological steps are being developed.

Hydrogen can be used as an energy storage appliance in exhausted natural gas fields, hydrogen bonded alloys, i.e. hydride, as a very cold liquid, in activated carbon materials, and also as a superior hydrogen carrier in non-nuclear fuels such as methanol. Hydrogen can be an inevitable storage task to remove the fluctuations and vacillation of solar energy and other unstable energy sources during the day and year.

The gas form of hydrogen can carry energy stingily by pipelines over prolonged distances, perhaps even more efficiently as electricity; the consumer can actuate fuel cells or other power generating machines to provide electricity and water. The chemical fuel version of hydrogen is much more likely to be used in energy-using vehicles than electrical power. it is very tough to design an aircraft with electric motors, whereas hydrogen is seen as an up-and-coming fuel for aeronautics.

Global hydrogen economy appears to have reached a certain level towards the end of the twentieth century and pure hydrogen is expected to be the worldwide energy vehicle in the middle of the twenty-first century. The fuel cells used directly with hydrogen, and indirectly with methanol and carbon-based fuels, are also playing an increasingly important role in producing electricity. Many variety methods that can be applied to hydrogen energy generation can be shaped according to the state of the sources as mentioned before. For instance, water can be converted into hydrogen and oxygen by electrolysis, and although it is quite exciting to produce electricity and water by hydrogen-re-combining with oxygen, it may be necessary to compete with conventional fossil fuels for a certain time in the future. Although there are some opinions on the use of nuclear energy as an inexpensive source of energy for decomposing atomic molecules in the production of hydrogen, the impact of the fire in space, caused by incredible energy that warms the stars and galaxies, will be quite different on the earth in the populated areas. Three Mile Island (1979) and Chernobyl (1986) accidents have shown that nuclear energy can lead to very dangerous results. This long-range project, extended until 2020, is described as a growth and re-development of Project Sunshine, the national alternative energy project launched in 1974, and it is clear that hydrogen can influence the energy planning and direct the future of a country (Bose and Malbrunot,2007).

## 6. Conclusion

This chapter has summarized the global energy, environment and economic system in the world and explores the status and importance of hydrogen in this area. Hydrogen has many advantages as an energy carrier, and if the benefits of hydrogen are so great, it can reasonably be questioned why there have not been prominent attempts at this energy system many years ago. There is no unique and simple answer to this problem, however there are a lot of complicated responses consisting of many factors related to each other. In the past, the necessity of using hydrogen had not been fully recognized since, oil, coal and natural gas reserves in the world were sufficient, the worries about the environment are small and people who are concerned about climate changes had remained a minority. Despite the fact that hydrogen has a significant advantage as emission free fuel over conventional fuels, this alone was not enough to accept an alternative fuel in the worldwide, even with its eco-friendly identity, because fossil fuels was several times cheaper than hydrogen. Liquid state of hydrogen, which is now used as a cold fuel that powers the space shuttle, was just a laboratory interest. From a technological perspective, hydrogen production, application and storage were at a very complicated, difficult and inadequate level.

Majority opinion on the need to reduce carbon emissions, the desire to increase the air quality around the world that people live in, laws encouraging the use of zero emission vehicles, advances in fuel cell technology, the formation of policies for the use of local resources in energy production, the necessity of storage of discontinuous renewable energy sources such as sun and wind, increasing concern about depletion of fossil fuel resources, the importance of the safety of energy resources and similar developments from past to today offer an opportunity for hydrogen. As a result, hydrogen is an important cornerstone of the energy future.

## References

Abatzoglou, J., DiMento, J. F., Doughman, P., & Nespor, S. (2007). A primer on global climate change and its likely impacts. *Climate change: what it means for us, our children, and our grandchildren*, 11-44.

Acker, R. H., & Kammen, D. M. (1996). The quiet (energy) revolution: analysing the dissemination of photovoltaic power systems in Kenya. *Energy policy*, *24*(1), 81-111.

Anderson, T. R., Hawkins, E., & Jones, P. D. (2016). CO2, the greenhouse effect and global warming: from the pioneering work of Arrhenius and Callendar to today's Earth System Models. *Endeavour*, *40*(3), 178-187.

Ayres, R. (2016). The Cosmos, The Sun and The Earth. In *Energy, Complexity and Wealth Maximization* (pp. 55-119). Springer, Cham.

Bilgen, S., Keleş, S., Kaygusuz, A., Sarı, A., & Kaygusuz, K. (2008). Global warming and renewable energy sources for sustainable development: a case study in Turkey. *Renewable and sustainable energy reviews*, *12*(2), 372-396.

Bose, T., & Malbrunot, P. (2007). *Hydrogen: facing the energy challenges of the 21st century*. John Libbey Eurotext.

BP Statistical Review of World Energy. (2020) Retrived From

https://www.bp.com/content/dam/bp/business-sites/en/global/corporate/pdfs/energy-economics/statistical-review/bp-stats-review-2020-full-report.pdf (Accessed on 27 April, 2021)

Chu, S., & Majumdar, A. (2012). Opportunities and challenges for a sustainable energy future. *nature*, *488*(7411), 294-303.

Coyle, E., Grimson, W., Basu, B., & Murphy, M. (2014). Reflections on Energy, Greenhouse Gases, and Carbonaceous Fules.

De Moel, M., Bach, P. M., Bouazza, A., Singh, R. M., & Sun, J. O. (2010). Technological advances and applications of geothermal energy pile foundations and their feasibility in Australia. *Renewable and Sustainable Energy Reviews*, *14*(9), 2683-2696.

Delucchi, M. A., & Jacobson, M. Z. (2011). Providing all global energy with wind, water, and solar power, Part II: Reliability, system and transmission costs, and policies. *Energy policy*, *39*(3), 1170-1190.

Don, A., Osborne, B., Hastings, A., Skiba, U., Carter, M. S., Drewer, J., ... & Zenone, T. (2012). Land-use change to bioenergy production in E urope: implications for the greenhouse gas balance and soil carbon. *Gcb Bioenergy*, *4*(4), 372-391.

Dresselhaus, M. S., & Thomas, I. L. (2001). Alternative energy technologies. *Nature*, *414*(6861), 332-337.

Dunn, S. (2002). Hydrogen futures: toward a sustainable energy system. *International journal of hydrogen energy*, *27*(3), 235-264.

Ewing, R. C., Weber, W. J., & Clinard Jr, F. W. (1995). Radiation effects in nuclear waste forms for high-level radioactive waste. *Progress in nuclear energy*, *29*(2), 63-127.

Fernihough, A., & O'Rourke, K. H. (2021). Coal and the European industrial revolution. *The Economic Journal*, *131*(635), 1135-1149.

Fischer, E. M., Oleson, K. W., & Lawrence, D. M. (2012). Contrasting urban and rural heat stress responses to climate change. *Geophysical research letters*, *39*(3).

Giannakoudis, G., Papadopoulos, A. I., Seferlis, P., & Voutetakis, S. (2010). Optimum design and operation under uncertainty of power systems using renewable energy sources and hydrogen storage. *International journal of hydrogen energy*, *35*(3), 872-891.

Hegerl, G. C., Brönnimann, S., Cowan, T., Friedman, A. R., Hawkins, E., Iles, C., ... & Undorf, S. (2019). Causes of climate change over the historical record. *Environmental Research Letters*, *14*(12), 123006.

Hepbasli, A. (2008). A key review on exergetic analysis and assessment of renewable energy resources for a sustainable future. *Renewable and sustainable energy reviews*, *12*(3), 593-661.

IEA Key World Energy Statistics (2020) Retrieved from

https://www.iea.org/reports/key-world-energy-statistics-2020 (Accessed on April 27, 2021).

Jeon, J., Yoon, S., Park, T., Cho, J. J., Kang, S., Han, Y. K., & Lee, H. (2012). Tuning glycolide as an SEI-forming additive for thermally robust Li-ion batteries. *Journal of Materials Chemistry*, *22*(39), 21003-21008.

Jha, S. K., Bilalovic, J., Jha, A., Patel, N., & Zhang, H. (2017). Renewable energy: Present research and future scope of Artificial Intelligence. *Renewable and Sustainable Energy Reviews*, *77*, 297-317.

Kabir, E., Kumar, P., Kumar, S., Adelodun, A. A., & Kim, K. H. (2018). Solar energy: Potential and future prospects. *Renewable and Sustainable Energy Reviews*, *82*, 894-900.

Karaman, C., Karaman, O., Atar, N., & Yola, M. L. (2021). Tailoring of Cobalt Phosphide Anchored Nitrogen and Sulfur Co-doped Three Dimensional Graphene Hybrid: Boosted Electrocatalytic Performance Towards Hydrogen Evolution Reaction. *Electrochimica Acta*, 138262.

Karaman, O., & Karaman, C. (2019). Three Dimensıonal (3D) Graphene Networks: Synthesis Methods. Afşin Güngör, Bekir Can Lütfüoğlu, Azim Doğuş Tuncer, Onur Karaman (Ed.), In *Energy And Envıronmental Studies For The Near Future,* (pp. 89-100) Ankara: Akademisyen Kitabevi .

Lee, H. P. (2011). *The impact of the hedge fund economy on social structure: Housing in Greenwich, Connecticut*. Southern Connecticut State University.

Liang, F. Y., Ryvak, M., Sayeed, S., & Zhao, N. (2012). The role of natural gas as a primary fuel in the near future, including comparisons of acquisition, transmission and waste handling costs of as with competitive alternatives. *Chemistry Central Journal*, *6*(1), 1-24.

Nasrollahzadeh, A. (2010). Caspian Sea and its ecological challenges. *Caspian Journal of Environmental Sciences*, *8*(1), 97-104.

Olah, G. A., Prakash, G. S., & Goeppert, A. (2011). Anthropogenic chemical carbon cycle for a sustainable future. *Journal of the American Chemical Society*, *133*(33), 12881-12898.

OPEC Annual Statistical Bulletin (2019) Retrieved from

https://www.opec.org/opec_web/en/data_graphs/330.htm (Accessed on April 27, 2021).

Overton, E. B., Wade, T. L., Radović, J. R., Meyer, B. M., Miles, M. S., & Larter, S. R. (2016). Chemical composition of Macondo and other crude oils and compositional alterations during oil spills. *Oceanography*, *29*(3), 50-63.

Petrova, E. (2014). Innovation in the pharmaceutical industry: the process of drug discovery and development. In *Innovation and marketing in the pharmaceutical industry* (pp. 19-81). Springer, New York, NY.

Poizot, P., & Dolhem, F. (2011). Clean energy new deal for a sustainable world: from non-CO 2 generating energy sources to greener electrochemical storage devices. *Energy & Environmental Science*, *4*(6), 2003-2019.

Rice, J. L., Cohen, D. A., Long, J., & Jurjevich, J. R. (2020). Contradictions of the climate-friendly city: new perspectives on eco-gentrification and housing justice. *International Journal of Urban and Regional Research*, *44*(1), 145-165.

Shahbaz, M., Al-Ansari, T., Aslam, M., Khan, Z., Inayat, A., Athar, M., ... & McKay, G. (2020). A state of the art review on biomass processing and conversion technologies to produce hydrogen and its recovery via membrane separation. *International Journal of Hydrogen Energy*.

Veil, J. A., Puder, M. G., Elcock, D., & Redweik Jr, R. J. (2004). *A white paper describing produced water from production of crude oil, natural gas, and coal bed methane* (No. ANL/EA/RP-112631). Argonne National Lab., IL (US).

Wennersten, R., Sun, Q., & Li, H. (2015). The future potential for Carbon Capture and Storage in climate change mitigation–an overview from perspectives of technology, economy and risk. *Journal of Cleaner Production*, *103*, 724-736.

White, C. M., & Lee, M. L. (1980). Identification and geochemical significance of some aromatic components of coal. *Geochimica et Cosmochimica Acta*, *44*(11), 1825-1832.

Wrigley, E. A. (2013). Energy and the English industrial revolution. *Philosophical Transactions of the Royal Society A: Mathematical, Physical and Engineering Sciences*, *371*(1986), 20110568.

Yürüm, Y. (2001). Advances in Hydrogen Energy Edited by Catherine E. Grégorie Padró and Francis Lau. Kluwer Academic/Plenum Publishers: New York; 2000, 192 pp. ISBN 0-306-46429-2.

# Chapter 5

# EXAMINING THE STRUCTURAL PROPERTIES OF QUINCE SEEDS/MUCILAGE AND RESEARCHING USABILITY IN DIFFERENT APPLICATIONS OF FOOD INDUSTRY

***Bilge ÇELİK[1]***
***Nil ACARALI[2]***

1 Yildiz Technical University, Department of Chemical Engineering, Davutpasa Campus, 34210, Esenler-Istanbul, Turkey, celikbilgee@gmail.com (https://orcid.org/0000-0003-0696-6976)
2 nilbaran@gmail.com (https://orcid.org/0000-0003-4618-1540)

# 1. INTRODUCTION

## 1.1. Quince

Quince (Cydonia oblonga) is a known fruit belonging to the Rosaceae family, grown in temperate and subtropical regions of West Asia origin as 10-12 cm in diameter. It can be found asymmetrically in different sizes. In addition, it has a distinctive odor and it is in the range of 100-280 grams. 90.6% of the quince fruit is the pulp part, 4.4% is the shell part and 5% is the core part. While its immature form has a greenish color, its maturing form gradually begins to turn yellow and its fully mature form is yellow in color. In Figure 1, there are figures of quince fruit [1].

*Figure 1. Quince fruit and tree [2]*

The hard and white-yellow pulp of the quince is easily oxidized and darkened when it comes into contact with the air. In addition, the fact that the quince is generally acidic and slightly sweet. It has a bitter taste due to its hard structure and high amount of tannins, negatively affects the fresh (raw) consumption of the fruit [2]. Quince, which is less preferred than other fruits, has high nutritional value. Because of this feature, it has an important place in terms of human health. The components and percentages of the quince fruit are shown in Table 1 [3]. Quince is used as a preservative and flavoring agent in marmalade, liquor, confectionery, jelly, etc. [4].

*Table 1. Quince fruit ingredients and quantities [3]*

| **Composition** | **Values** |
|---|---|
| Moisture (%) | 84.6 |
| Total soluble solids (°B) | 14.2 |
| Total sugars (%) | 9.0 |
| Titratable acidity (%) | 1.2 |

| | |
|---|---|
| Crude fibre (%) | 1.6 |
| Tannins (%) | 0.8 |
| Pectin (%) | 1.8 |
| Minerals (mg/100 g) | |
| Potassium | 248 |
| Phosphorous | 26 |
| Calcium | 18 |
| Sodium | 8.0 |

### 1.2. Quince Production in the World and Turkey

The homeland of Quince, which is grown in all countries in the world except Australia, is North-West Iran, North Caucasus, Caspian Sea coasts and North Anatolia. The wilds extend as far as Turkistan in the east, as well as in the South regions of Europe and North Africa in the west. Quince grows wild in these places [5].

The most important quince producing countries in the world are Turkey, China, Uzbekistan, Morocco and Iran. Turkey has a significant place for quince export, production and planting [6]. Turkey ranks first in quince production in the world with a production of 174,038 tons. In Turkey, besides the fresh consumption of quince, it has spread throughout the country due to its use in different ways such as jam, compote and marmalade as well as being used as rootstock for soft stone fruit types [7].

According to the data of Turkish Statistical Institute, 112900 tons of quince fruits were produced in 2015, 126400 tons in 2016 and 174038 tons in 2017 in our country. The provinces of Istanbul, Sakarya and Bursa are at the top in quince production, and in Erzurum 380 tons in 2015, 272 tons in 2016 and 389 tons in 2017 [8].

### 1.3. Quince Seed

There are three factors to determine the quality of quince seed. One of them is the gum structure that constitutes 20% by weight of the seed. Others are the color of the mucilage obtained as a result of the extraction with water and the condition that the surface does not interact with the dirt, dust, insects etc. in the core. In order for the seed to be used in special applications, it must first be purified from harmful substances [9]. Organic acids, phenolic compounds, free amino acids make up a significant majority for quince seeds (Table 2) [10].

| Phenolic compounds | Value (mg/kg) |
|---|---|
| 3/4/5-O-caffeoylquinic acid | 12.4; 1.70; 24.6 |
| 6-C-glucosyl-8-C-pentosyl chrysoeriol<br>(pentosyl) (glucosyl) | 7.70<br>8.00 |
| 3,5-O-dicaffeoylquinic acid | 4.40 |
| Stellarin-2 | 20.5 |
| Lucenin-2; Vicenin-2 | 5.20; 14.2 |
| 3-O-caffeoylquinic acid | 12.4 |

*Table 2. Phenolic content for guince seed [10]*

The analysis results in studies showed that the oxalic acid contained in the quince shell and pulp was not included in the kernel. Table 3 shows the organic acids in the quince seeds and their composition rates [10].

*Table 3. Organic acids for quince seed [10]*

| Organic acids | Value (mg/kg) |
|---|---|
| Citric acid | 93.2 |
| Ascorbic acid | 81.6 |
| Malic quinic acids | 281.8 |
| Shikimic acid | 1.40 |
| Fumaric acid | 1.80 |

A sample consists of L-aspartic acid, L-tyrosine, L-histidine etc. compounds and L-asparagine, L-glutamic acid make up most of the total amino acids [11]. The molecular structure of Vicenan-2, which is a type of phenolic acid found in the quince seed structure and is abundant (Figure 2).

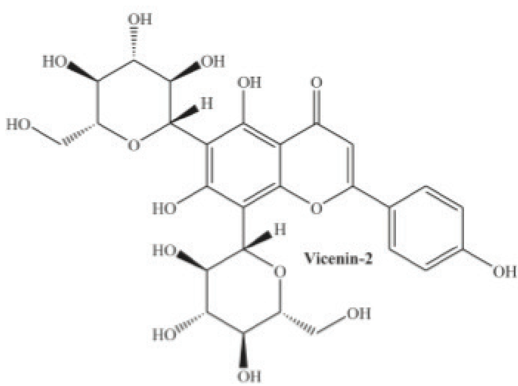


*Figure 2.Chemical structure for Vicenin-2 molecule [11]*

### 1.4. Quince Seed Mucilage

Chemically mucilages form slick, aqueous colloidal dispersions that are optically active and can be hydrolyzed and fermented. Mucilages are usually found in small percentages in almost all classes of plants, especially in the root, shell, seed, flower and cell wall of the plant. Although the exact role of mucilage in the plant is not known, it can be said that it has important functional functions as helping water storage, reducing diffusion in aquatic plants, seed dispersal and stabilizer [12].

Quince seed mucilage, which has become widespread as a natural substrate in studies conducted by engineers, is a complex substance that contains water-soluble polysaccharides with different structures. At the same time, it continues to attract the attention of both engineers and botanists with its unique properties and natural biomass resource that can be found in many different parts of the world. Studies show that mucilage can be obtained by extracting quince seeds with ethanol in the presence of distilled water [13]. Figure 3 shows the quince seed and mucilage [2].

Quince seed extract is a carbohydrate-containing liquid obtained using the quince fruit's core. Its structure mainly contains components such as water, cellulose nanofibrils and hemicelluloses such as glucoronoxylates, which have strong moisturizing properties. The extract has many features such as strong water absorption and slippery structure due to the hydration of the carbohydrate in the quince seed used. The physicochemical structure of the extract is very important. At this point, there are cellulose nanofibrils stored on the epidermal layer of the core [1].

*Figure 3. Quince seed mucilage [2]*

The extract obtained as a result of the extraction of quince seeds contains mucilage content. Mucilage shows water soluble properties. Because of this feature, mucilage is used as a gelling agent, thickener and stabilizer in various foods. Thanks to the added mucilage, the shelf life of foods can be extended, quality increased, textural resistance and so on. Studies conducted within the scope of quince seeds and mucilage in recent years have attracted attention in terms of the usability of these substances as additives in different foods [2]. In previous studies, it was reported that quince seed mucilage, as an edible coating, has an effect for extending the shelf life with the products quality in the food industry [14].

There are many different methods to separate mucilage from quince seeds in studies. Quince seeds are mostly kept in water for a certain period of time and mucilage is transferred to water. Filtering process is carried out with the help of a filter cloth to separate mucilage from its seeds. Mucilage yield is closely related to its viscosity and purity. Factors affecting yield include:

- Extraction temperature
- Extraction time
- Isolation techniques [15]

### 1.4.1. Uses of Quince Seed Mucilage

Quince seed mucilage, which has application areas in medicine and pharmacy, water treatment, cosmetics industry in health sector, is used in additive and packaging applications for food industry [16].

#### 1.4.1.1. Quince Seed Mucilage as a Food Additive

Food products are often packaged using biopolymer-based films due to their potential to act as barriers to oxygen and mechanical properties [15].

Demir (2019) investigated the physical and chemical characteristics for ice cream containing a certain amount of quince seed extract, salep and guar gum and the effect of these added additives on the storage time of ice cream. Considering the test results, it was thought that quince seed extract powder could be a natural stabilizer that can replace the industry-focused stabilizers used in ice cream production [1].

Gürbüz (2016) conducted on its use as a stabilizer in foods. It was aimed the chemical, physical and sensory properties of yoghurts containing different amounts of quince seed gel powder during the storage period. The results showed that the quince seed gel powder used as a stabilizer in yogurt improves the sensory properties, viscosity, cohesiveness and antimicrobial properties of yoğurt [17].

Yousefi et al. (2017) explored how various properties (water holding capacity, antioxidant activity, hardness, fat oxidation) of hamburgers change during the storage period by adding quince seed mucilage in different proportions in low-fat hamburger production. As a result of the analysis, it was revealed that the quince seed mucilage strengthens the structural formulation of hamburger and significantly reduced the negative effects due to its potential fat-changing feature [18].

Farahmandfar et al. (2017) analyzed the structural, physical and superficial characteristics of whipped cream by adding quince seed gum and different gum types into low-fat whipped cream. It was concluded that with the increase in gum concentrations, the viscosity and volume of the whipped cream increased and improved the product quality [19].

### 1.4.1.2. Quince Seed Mucilage as a Film Former

It is susceptible to rapid deterioration because of high respiration, perspiration, presence of harmful substances for vegetables and fruits. Thanks to edible coating technologies, it can reduce the respiration level of water, and the negative effects of textural properties can be minimized, thus it extends the shelf life of vegetables and fruits [20].

Mucilages obtained from different plants (Quince seed, Chia seed, Cassia seed, Balangu seed, Cress seed, Psyllium seed etc.) can be added to coatings and films to create a barrier according to the amount of oxygen and moisture in the ambient conditions [20].

Noshad et al. (2017) wanted to examine the effect of the renewable coating for food quality. They obtained a bioactive coating consisting of quince seed mucilage and green tea extract in order to reduce the transfer of excess fat intake to the product during frying. It has been investigated how this coating affects the physicochemical properties of fried shrimp. It has been determined that the edible coating obtained as a result of the study contains less oxidation products on the shrimp and reduced the hardness of the product with high moisture content [21].

Jouki et al. (2014) searched the changes in properties of rainbow trout fillet under certain storage conditions of films made with thyme oil and quince seed mucilage. It was determined that fillets with thyme oil and quince seed mucilage showed better physicochemical properties than control samples. A more efficient reduction in color and oxidation losses occurred owing to the films [22].

Another research conducted within the scope of edible film technology was to create edible film containing mucilage by Shahbazi et al. (2020) with extending the shelf life of strawberries. In the study, quince seed mucilage and okra seed mucilage were used together. When the results of the analysis were examined, it was seen that that mucilage-based films could be considered as promising materials in the food industry [23].

Shekarabi et al. (2014) purposed to improve the functional properties of renewable films containing nanokil and quince seed mucilage, which was a nano strengthening agent. Firstly different concentrations of nanoclays were prepared. The effects of edible films obtained from nanoclay-based quince seed mucilage on tensile properties, oxygen permeability, water vapor and glass transition temperature were evaluated. Nanoclay added quince seed mucilages reduced water vapor and oxygen permeability. It was concluded that films based on quince seed mucilage containing nanoclay could be used in preservative form in foods [15, 24].

Jouki et al. (2013) conducted and aimed to obtain a new biodegradable edible film from mucilage. By determining the chemical, mechanical and thermal characteristics for films produced, it was aimed to be effective against antioxidants and positive results were obtained in antibacterial and antioxidant tests [25].

In a recent study, whey protein isolate and sunflower oil emulsions were prepared using different concentrations of xanthan gum and quince seed mucilage. Quince seed mucilage reduced the low shear viscosity and shear thinning ability of the emulsions, enabling the emulsions to become stable in a long time. Based on the positive results obtained, it was proven that quince seed mucilage was a better emulsifying and stabilizing agent [15].

Jouki et al. (2013) determined to investigate the usability of quince seed mucilage in edible film preparation. Physical, mechanical thermal, etc. properties were examined to analyze the muscilage structure. When the analyzes were evaluated, an increase in water vapor and oxygen permeability of mucilage films prepared by adding glycerol in different concentrations, a decrease in surface hydrophobicity and a smooth surface were observed. In the light of the results obtained, it was concluded that mucilage as an antioxidant edible film could potentially be used in the packaging of various food products [26].

In the encapsulation-based study conducted by Dokoohaki et al. (2019), it was aimed to produce a milk dessert containing probiotics. For this purpose, quince seed permeation was used as a coating material in the microencapsulation of Lactobacillus rhamnosus bacteria. Shell thickness of quince seed mucilage was one of the most effective parameters determining the micromechanical properties of microcapsules. When the tests and analyzes were evaluated, it was concluded that the nutritional value of the dessert increased and had better quality as a result of the use of quince seed mucilage and alliginate beads and microencapsulation of probiotic bacteria [27].

Another study was done on Doogh, a type of milk drink commonly consumed daily in Iran. Pirsa et al. (2018) investigated how quince seed mucilage and guar gum affect the chareacteristics of Doogh. In the study, amounts of mucilage and guar gum to the product were determined by the response surface method, which was an optimization method. Storage time, acidity, viscosity, pH, etc. properties were tested and optimum results were evaluated. Considering the viscosity results, it could be said that the Doogh drink produced by adding 0.1% (w/w) quince seed mucilage and 0.2% (w/w) guar gum was the most optimum condition [28].

A different study was about nanocomposite films used in food. Firstly, quince seed mucilage was extracted by Bayzavi et al. (2020) and a composite film was prepared by adding different proportions of nanocrystalline cellulose. Then, the structural properties of the film such as water solubility, thickness and moisture content were analyzed. When the results are examined, it was hoped that by means of the additives added, the mechanical properties of the films were improved and a good interaction between quince seed mucilage and nanocrystalline cellulose was established, and it was seen that the study would shed light on the applications in the field of packaging for food industry [29].

# REFERENCES


[1] Demir, Ş. (2019). The Effect of Quince Seed Extract on Ice Cream Production, Pamukkale University, Institute of Science and Technology, MSc. Thesis, Pamukkale.

[2] Kozlu, A. (2020). Use of Quince Seed Mucilage as Edible Coating for Some Fruits and Determination of Quality Characteristics During Storage, Ege University, Institute of Science and Technology, MSc. Thesis, İzmir.

[3] Sharma, R., Joshi, V.K. and Rana, J.C. (2011). Nutritional Composition and Processed Products of Quince (Cydonia oblonga Mill.), Indian Journal of Natural Products and Resources, 2, 354-357.

[4] Patel, N.C., Shah, V.N., Mahajan, A.N. and Shah, D.A. (2011). Isolation of Mucilage from Cydonia vulgaris Pers. Seeds and its Evaluation as Superdisintegrant, Journal of Applied Pharmaceutical Science, 1, 110-114.

[5] Aygün, A. (2018). Quince Production Potential in Turkey, Garden 47-International Agriculture Congress, 2, 45-49.

[6] Şirikçi, B.S. (2016). Economic Structure and Marketing Problems of Quince Cultivation in Turkey, Süleymen Demirel University, Institute of Science and Technology, MSc. Thesis, Isparta.

[7] Uzun, A., Çil, A., Yaman, M. and Coşkun, Ö.F. (2020). Genetic Diversity and Some Fruit Characteristics of Quince Genotypes Collected from Kayseri Region, Turkish Journal of Agriculture-Food Science and Technology, 8, 318-323.

[8] Zor, M. and Şengül, M. (2020). Some Physicochemical Properties and Antioxidant Activity of Quince Jam Stored in Different Packages and Temperatures with Quince (Cydonia oblonga Miller) Fruit, Atatürk University Journal of Agricultural Faculty, 51, 97-108.

[9] Bemiller, J.N., Whistler, R.L., Barkalow, D.G. and Chen, C.C. (1993). Aloe, Chia, Flaxseed, Okra, Psyllium Seed, Quince Seed, and Tamarind Gums (Chapter 9), Industrial Gums, Third Edition, 228-243.

[10] Silva, B.M., Andrade, P.B., Ferreres, F., Seabra, R.M., Beatriz, M., Oliveira, P.P. and Ferreira, M.A. (2014). Composition of Quince (Cydonia oblonga Miller) Seeds: Phenolics, Organic Acids and Free Amino Acids, Natural Product Research, 19, 275-281.

[11] Ashraf, M.U., Muhammad, G., Hussain, M.A. and Bukhari, S.N.A. (2016). Cydonia Oblonga M., A Medicinal Plant Rich in Phytonutrients for Pharmaceuticals, Frontiers in Pharmacology, 7, 1-20.

[12] Arslan, A. (2018). Gastroprotective Effect Of Musilage Obtained from Cydonia Oblonga (L) Ayva (Rosaceae) Seeds, İstanbul University, Institute of Health Science, MSc. Thesis, İstanbul.

[13] Hosseinzadeh, H. and Mohammadi, S. (2015). Quince Seed Mucilage Magnetic Nanocomposites as Novel Bioadsorbents for Efficient Removal of Cationic Dyes from Aqueous Solutions, Carbohydrate Polymers, 3, 1-32.

[14] Shahbazi, Y. and Moosavy, M.H. (2019). Quince Seed Mucilage Supplemented with Titanium Dioxide and Silicon Dioxide Nanoparticles, Nanomedicine Research Journal, 3, 157-163.

[15] Hussain, M.A., Muhammad, G., Haseeb, M.T. and Tahir, M.N. (2019). Quince Seed Mucilage: A Stimuli Responsive/Smart Biopolymer (Chapter 5), Functional Biopolymers, Polymers and Polymeric Composites: A Reference Series, 127-148.

[16] Karaca, B. (2020). Development of Quince Seed Mucilage/Decellularized Bonederived Bi-Layered Bioscaffolds for Periodontal Tissue Regeneration, Çanakkale Onsekiz Mart University, Institute of Science and Technology, MSc. Thesis, Çanakkale.

[17] Gürbüz, Z. (2016). Use of Quince Seed Gel Powder as the Stabilizer in Yogurt Production, Atatürk University, Institute of Science and Technology, MSc. Thesis, Erzurum.

[18] Yousefi, N., Zeynali, F. and Alizadeh, M. (2017). Optimization of Low-Fat Meat Hamburger Formulation Containing Quince Seed Gum Using Response Surface Methodology, Journal of Food Science and Technology, 55, 598–604.

[19] Farahmandfar, R., Asnaashari, M., Salahi, M.R. and Rad, T.K. (2017). Effects of Basil Seed Gum, Cress Seed Gum and Quince Seed Gum on the Physical, Textural and Rheological Properties of Whipped Cream, International Journal of Biological Macromolecules, 98, 820, 828.

[20] Beikzadeh, S., Khezerlou, A., Jafari, S.M., Pilevar, Z. and Mortazavian, A.M. (2020). Seed Mucilages as the Functional Ingredients for Biodegradable Films and Edible Coatings in the Food Industry, Advances in Colloid and Interface Science, 280, 2-8.

[21] Noshad, M., Nasehi, B. and Anvar, A. (2017). Evaluating the Effect of Active Edible Coating of Quince Seed Mucilage and Green Tea Extract on the Quality of Fried Shrimps: Physicochemical and Sensory Properties, Nutrition and Food Sciences Research, 4, 31-36.

[22] Jouki, M., Mortazavi, S.A., Yazdi, F.T., Koocheki, A. and Khazaei, N. (2014). Use of Quince Seed Mucilage Edible Films Containing Natural Preservatives to Enhance Physico-Chemical Quality of Rainbow Trout Fillets During Cold Storage, Food Science and Human Wellness, 3, 65-72.

[23] Shahbazi, Y., Shavisi, N. and Karami, N. (2020). Development of Edible Bioactive Coating Based on Mucilages for Increasing the Shelf Life of Strawberries, Journal of Food Measurement and Characterization, 15, 394-405.

[24] Shekarabi, A.S., Oromiehie, A.R., Vaziri, A., Ardjmand, M. and Safekordi, A.A. (2014). Investigation of the Effect of Nanoclay on the Properties of Quince Seed Mucilage Edible Films, Food Science and Nutrition, 2, 1-7.

[25] Jouki, M., Mortazavi, S.A., Yazdi, F.T. and Koocheki, A. (2013). Characterization of Antioxidant-Antibacterial Quince Seed Mucilage Films Containing Thyme Essential Oil, Carbohydrate Polymers, 99, 537-546.

[26] Jouki, M., Yazdi, F.T., Mortazavi, S.A. and Koocheki, A. (2013). Physical, Barrier and Antioxidant Properties of A Novel Plasticized Edible Film from Quince Seed Mucilage, International Journal of Biological Macromolecules, 62, 500-507.

[27] Dokoohaki, Z.N., Sekhavatizadeh, S.S. and Hosseinzadeh, S. (2019). Dairy Dessert Containing Microencapsulated Lactobacillus Rhamnosus (ATCC 53103) With Quince Seed Mucilage as A Coating Material, LWT-Food Science and Technology, 115, 1-8.

[28] Pirsa, S., Dalili, R.and Yazdani, I. (2018). Effects of QuinceSeed Mucilage and Guar Gum on the Physicochemicaland Sensory Properties of Doogh, Journal of Agricultural Science and Technology, 20, 485-494.

[29] Bayzavi, T., Ansari, S. and Danesh, N. (2020). Preparation of Composite Films From Quince Seed Mucilage and Nanocrystalline Cellulose and Studying Their Properties, Journal of Food Technology and Nutrition, 17, 93-108.

# Chapter 6

# PHOTO-BIOREACTORS FOR VALUE-ADDED PRODUCTS FROM MICROALGAE

*Melih ONAY*[1]

1 [1]Department of Environmental Engineering, Van Yuzuncu Yil University, 65080, Van, Turkey, e-mail: melihonay@yyu.edu.tr, Melih Onay Orcid ID: 0000-0002-9378-0856

## 1. INTRODUCTION

Microalgae are single or multi-celled organisms. Recently, they have been used frequently due to their rapid breeding and high yields for industry. Microalgae can be applied for food, energy and environmental studies. Microalgae, like all living organisms, contain lipid, protein and carbohydrates in their cells. These products can be converted into bio-diesel, bio-ethanol and bio-methanol (Chowdhury & Loganathan, 2019). In addition to this, they can produce some pigments such as chlorophylls, carotenoids and phycobiliproteins. These products can be used for food industry as additive materials. Also, some molecules such as astaxanthin, lutein, and fucoxanthin can be produced by microalgae and they can be taken as supplement products. To obtain these products, microalgae must be cultured. At their cultivation, environmental conditions are important. Temperature, salt concentrations, pH, light intensity and medium concentrations can affect the cultivation conditions. Although microalgae are not being in very high amounts, they can grow under extreme conditions such as high temperature and pH. In addition to this, some types of microalgae can be cultured at high growth rates under very salty conditions (Hu et al., 2018; Chowdhury & Loganathan, 2019).

Microalgae can be used for bioenergy production. Bio-diesel is one of the most popular bio-fuel. It occurs with transesterification reaction. This reaction consists of triglycerides and a suitable alcohol by means of enzymatic or chemical catalysts. Triglyceride production from microalgae can be maintained with various organic solvents such as hexane, chloroform, ethyl acetate or acetone (Chyuan et al., 2021; Goh et al., 2019). For biofuel production, microalgal biomass may be wet or dried biomass. The extraction procedures may differ. The most used extraction methods are organic solvent, ionic liquid, supercritical fluid and expeller press. For bio-diesel production, pre-treatment procedures can be applied on microalgal biomasses. Physical, chemical, mechanical and enzymatic procedures are the most applied methods. These methods enable metabolic contents to be expelled fast (Suparmaniam et al., 2019). In the literature, *Chlorella pyrenoidosa* was studied for biodiesel yield. Spent coffee ground and *Chlorella pyrenoidosa* were mixed. Lipid content of *Chlorella pyrenoidosa* was 23.6%. Optimization studies were tried by mixing spent coffee ground and microalgae at the same rate. Optimum conditions were 198 $^{o}$C, 132 min and 6 mL of solvent. Biodiesel yield of *Chlorella pyrenoidosa* was 20.15 % (Abomohra et al., 2021). In another study, *Coelastrum sp.* was grown in urea stress conditions. *Coelastrum sp.* had lipid percentage of 41% under the stress condition without urea (Bhuyar et al., 2021). *Chlorosarcinopsis sp. MAS04* was cultivated in wastewater. Sewage wastewater was combined with zinc oxide nanoparticles for lipid and bio-diesel production. In primary treated wastewater with zinc oxide, lipid content was 1.9 times higher (36%) compared to control medium (Vasistha et al., 2021). *Desmodesmus sp.* EJ8-10 was studied in anaerobically digested livestock wastewater. Lipid content of *Desmodesmus sp.* was 28%. Original piggery effluent wastewater had the lower lipid content with 22.3% (Li et al., 2021). Morais et al. studied *Phaeodactylum tricornutum* in different concentrations of glycerol, glucose and salt. The highest lipid content was 338.97 mg/L at 0.1 M glycerol, 15% of salinity and continuously illumination (Morais et al., 2021). The studies related with lipid production were given in **Table 1**.

**Table 1.** *Lipid production from microalgae*

| No | Microalgae species | Lipid percentage or content | References |
|---|---|---|---|
| 1 | Chlorella pyrenoidosa | 23.6% | Abomohra et al., 2021 |
| **2** | Coelastrum sp. | 41.0% | Bhuyar et al., 2021 |
| **3** | Chlorosarcinopsis sp. MAS04 | 36.0% | Vasistha et al., 2021 |
| **4** | *Desmodesmus sp.* EJ8-10 | 22.3% | Li et al., 2021 |
| **5** | Phaeodactylum tricornutum | 338.97 mg/L | Morais et al., 2021 |

Bio-ethanol is one of the main types of bio-fuels. It was first produced from plant sources. Then, it was produced from plant wastes. Bio-ethanol can be obtained from any source of sugar. Sugars are isolated from plants or microalgae. Next, sugars are separated into their monomers. It is also converted to bio-ethanol through fermentation. Acidic, basic and enzymatic pretreatment methods are used to obtain higher yields of sugar similar to biodiesel. The amount of sugars in microalgae can be increased by changing environmental conditions. Also, saccharification and fermentation procedures can affect bio-ethanol content in microalgae (Phwan et al., 2018). In the literature, *Anabaena variabilis* was studied for carbohydrate and bio-ethanol production. Three different factors such as pH, sulfate and carbonate were used to increase production. Bio-ethanol content increased 2.6 times at pH 8.9, approximately 169 mg/L of sulfate and 64 mg/L of carbonate (Deb et al., 2021). *Chlorella sorokiniana* NITTS3 was carried out to analyze effects of ultrasonic pre-treatment. For fermentation, *Saccharomyces cerevisiae* NITTS1 was used and the highest bio-ethanol content was 52.1 g/L at pH:4, 30 $^{o}$C and 200 rpm. As can be seen from these results, ultrasound waves can be used for bioethanol production (Dhandayuthapani et al., 2021). In another study, acidic, basic and enzymatic methods were applied on mixed microalgae samples. The combination of $H_2SO_4$ and $MgSO_4$ had the highest sugar concentration.

Also, enzymatic method showed the maximum yield with 0.46 g/g of sugar (Shokrkar et al., 2017). Kim et al studied freshwater and seawater *Porphyridium cruemtum* for bio-ethanol. Also, the separate hydrolysis and fermentation and simultaneous saccharification and fermentation were examined. The simultaneous saccharification and fermentation method is more suitable for freshwater and seawater *Porphyridium cruemtum*. Bio-ethanol productivities were 65.4% and 70.3% for seawater *Porphyridium cruemtum* and freshwater *Porphyridium cruemtum*, respectively (Kim et al., 2017). In another study, *Chlorella sp.* GD and *Chlorella vulgaris* ESP-31 produced bio-ethanol by means of microwave-assisted heating wet torrefaction. The maximum bio-ethanol yield was 7.61% and conversion percentage was 95.22% for *Chlorella vulgaris* ESP-31 (Yu et al., 2020). The studies about bio-ethanol production were given in **Table 2**.

**Table 2.** *Bio-ethanol production from microalgae*

| No | Microalgae species | Bio-ethanol content | References |
|---|---|---|---|
| 1 | Anabaena variabilis | 2.6 times ↑ | Deb et al., 2021 |
| **2** | *Chlorella sorokiniana* NITTS3 | 52.1 g/L | Dhandayuthapani et al., 2021 |
| **3** | Mixed microalgae | 0.46 g/g of sugar | Shokrkar et al., 2017 |
| **4** | Porphyridium cruemtum | 70.3% (productivity) | Kim et al., 2017 |
| **5** | *Chlorella sp.* GD | 7.61% | Yu et al., 2020 |
| **6** | Chlorella vulgaris ESP-31 | 95.22% (productivity) | Yu et al., 2020 |

Bio-gas production can be obtained via anaerobic digestion. It contains four steps such as hydrolysis, acidogenesis, acetogenesis, and methanogenesis. Main product is methane. Biogas can be produced by changing the methods that are valid in the production of other biofuels. However, modifications in the methanogenesis step provide a high increase in production yield (Zabed et al., 2020). Thermophilic biogas production from microalgae was carried out according to hydraulic retention times. Methane production was 0.41 $m^3$ $CH_4$ $kgVS^{-1}$. This value corresponds to 1.7 times more methane production (Reyes et al., 2021). In another study, *Tetradesmus obliquus* was grown in various wastewaters such as swine manure, cattle manure and domestic sewage. Methane concentration was 91% v/v $CH_4$ after purification in bio-digested swine manure (Miyawaki et al., 2021). *Chlorella sp.* and *Scenedesmus sp.* was cultivated in industrial winery wastewater. Microalgae were exposed to various enzyme cocktails such as cellulase, chitinase, protease, xylanase, poligalacturonase and pectinliase. High concentration of enzymes maintained higher methanol yield with 5.3 times for pre-treatment. Methanol yield was 27% (Avila et al., 2021). *Chlorella vulgaris* was studied for methane production in three organic loading rates with OLR 6, 9, 12 g COD/Ld. Methanol efficiencies (from 61 to 67% v/v $CH_4$) were very close for three of them (Llamas et al., 2020). Bio-gas production was given in **Table 3**.

**Table 3.** *Bio-gas production from microalgae*

| No | Microalgae species | Bio-gas content | References |
|---|---|---|---|
| 1 | Mixed microalgae | 1.7 times ↑ | Reyes et al., 2021 |
| **2** | Tetradesmus obliquus | 91% v/v $CH_4$ | Miyawaki et al., 2021 |
| **3** | *Chlorella sp.* and *Scenedesmus sp.* | 5.3 times ↑ | Avila et al., 2021 |
| **4** | Chlorella vulgaris | 67% v/v $CH_4$ | Llamas et al., 2020 |

Chlorophyll is another significant molecule obtained from microalgae. Chlorophyll can be located in microbial cells. The green algae such as Chlophyta include chlorophyll. Chlorophyll is a photosynthetic pigment and it can be used to monitor the growth of microalgae and it is a lipid soluble molecule. In addition to this, chlorophyll is used in the tracking of toxic substances in the environment. Also, chlorophyll is a colorant in food industry due to its high stability (Li et al., 2019). Fernandes et al. studied radical scavenger activity of chlorophyll molecules from *Phormidium autumnale* on peroxyl molecules which are free radical molecules. Chlorophyll content was 159.3 μg/g. This value was 200 times higher than the contribution of α-tocopherol on the peroxyl molecule (Fernandes et al., 2017). Islam et al. carried out *Chlorella sp.*, *Nannochloropsis sp.*, *Tetraselmis sp.* and *Chaetoceros sp.* for chlorophyll contents. Chlorophll a contents of *Chlorella sp.*, *Nannochloropsis sp.*, *Tetraselmis sp.* and *Chaetoceros sp.* in Conway medium were 0.48, 0.48, 2.68 and 1.30 μg/L, respectively. In addition, chlorophyll b contents of *Chlorella sp.*, *Nannochloropsis sp.*, *Tetraselmis sp.* and *Chaetoceros sp.*were 0.19, 0.05, 1.23 and 0.04 μg/L, respectively (Islam et al., 2021).

*Dunaliella salina* is halophile green micro-algae and they can be produced under very salty conditions. It includes high amounts of carotenoid. Carotenoids can be taken as extra supplements. They have anti-oxidant, anti-cancer and anti-inflammatory properties. While most of the carotenoids are produced synthetically, those produced from microalgae have started to take their place in the markets. Synthetically produced ones have very low antioxidant effect and microalgae are a very good source for this (Pourkarimi et al., 2020). *Chlorella vulgaris* and *Arthrospira platensis* were investigated in tofu wastewater. Maximum carotenoid content was 72.20 mg/L. Also, maximum biomass content was 1715 mg/L (Ajijah et al., 2020). In another study, *Coelastrum cf. pseudomicroporum*, was examined in urban wastewater. Maximum total carotenoid content was 0.47 mg/L (Úbeda et al., 2017).

Phycobiliproteins are another important molecule extracted from microalgae Phycobiliproteins are hydrophilic molecules. They include protein and chromophore groups. Phycobilins maintain chromophore. They are classified into two groups such as phycoerythrin and phycocyanin. Phycoerythrin has red color and its energy absorption band is between 540 and 570 nm. Phycoerythrin exists in red microalgae. On the other hand, phycocyanin has blue color and its energy absorption band is between 610 and 620 nm. These pigments can be used for food, pharmaceutical and cosmetics industries. They are colorant molecules and also have anti-oxidant, anti-inflammatory, neuro and hepato-protective features (Manirafasha et al., 2016). In the literature, *Haematococcus pluvialis* and *Porphyridium cruentum* were studied with ultra-high pressure extraction method. Then, phycoerythrin content was calculated with various methods such as convention, pressurized liquid extraction and ultra-high pressure extraction. While phycoerythrin content of convention method was 93 mg/g extract, phycoerythrin content of pressurized liquid extraction was 13.2 mg/g extract. Ultra-high pressure extraction method on phycoerythrin content was carried out under different pressures. Maximum phycoerythrin content of *Porphyridium cruentum* was 144 mg/g extract under 300 MPa. Phycoerythrin contents were 86.97 and 33.51 mg/g extract under 100 and 600 MPa, respectively (Bueno et al., 2020). Li et al. investigated phycoerythrin content from *Porphyridium purpureum* under various carbon/nitrogen ratios. Maximum phycoerythrin content was 196 mg/L under 2.5 of carbon/nitrogen ratio and 0.16 g/L $NaHCO_3$ (Li et al., 2020). *Arthrospira sp.* was studied for higher phycocyanin content with lower energy consumption. For this aim, *Arthrospira sp.* was extracted with ultra-sonication for 20 min and phosphate buffer. Maximum phycocyanin content was 44.24 mg/g (Gorgich et al., 2020). In literature, *Thermosynechococcus sp.* CL-1 was studied in various light intensities and wavelengths and strategies with nitrogen concentrations. The highest phycocyanin productivity was 281.4 mg/L/day under double-mixed color lighting at 250 µmole $m^{-2}$ $s^{-1}$ of light intensity (Hoi et al., 2021).

Astaxanthin is a kind of carotenoid. Their amount increases excessively when the environment is stressed in any way. Because of this, they are called as secondary carotenoids. They prevent reactive oxygen species production and play a role in antioxidant defense. Also, it can be used as color additive and feed in food industry (Lu et al., 2021). *Haematococcus pluvialis* and *Chromochloris zofingiensis* were cultivated in various concentrations of palm oil mill effluent. The highest astaxanthin concentration was 22.43 mg/L for 7.5% of palm oil mill effluent (Fernando et al., 2021). In another study, *Haematococcus pluvialis* was cultivated in potato juice wastewater. This wastewater maintained stress factors for microalgae. Acetate and potassium in acidification effluents provided the highest astaxanthin production with 27.9 mg/g (Pan et al., 2021).

Lutein is another pigment and has yellow color. It can be presented in microalgae intensively. Like other microalgal pigments, lutein contents can change with environmental conditions such as temperature, pH and light intensities. It shows antioxidant properties. Also, it is coloring agent for cosmetic products (Becerra et al., 2020). Lutein production from *Chlorella vulgaris* was obtained by means of multi-injection high performance counter-current chromatography with ultrasound-assisted extraction of microalgae. Lutein concentration in lower phase was 3.20 mg/g (Fábryová et al., 2019). Also, lutein concentration from *Chlorella pyrenoidosa* was carried out in the various concentrations of sodium bicarbonate. The maximum lutein concentration was 4.84 mg/g for 100 mM of sodium bicarbonate. This result showed that sodium bicarbonate increased lutein biosynthesis (Sampathkumar et al., 2019).

Fucoxanthin can be isolated from *Phaeodactylum tricornutum*. It can be used for antioxidant, photo-protection and feed. Fucoxanthin is located in skin and save skin with the prevention of photo-aging (Lourenço-Lopes et al., 2021). *Chrysotila carterae, Chaetoceros muelleri, Pheodactylum tricornutum, Tisochrysis lutea, Navicula sp.* and *Amphora sp.* were investigated for fucoxanthin production in various concentrations of salt. *Chaetoceros muelleri* had the highest fucoxanthin concentration with 2.92 mg/g in 45% of salinity. Also, fucoxanthin concentration of *Tisochrysis lutea* was 2.05 mg/g in 45% of salinity (Ishika et al., 2017). In the other study, *Mallomonas sp.* was isolated and fucoxanthin concentration was researched. Fucoxanthin content of *Mallomonas sp.* was 26.6 mg/g. Also, Phaeodactylum tricornutum UTEX L642 had high fucoxanthin content with 10.2 mg/g (Petrushkina et al., 2017). Pigment studies from microalgae were given in **Table 4**.

**Table 4.** *Pigment studies from microalgae*

| No | Microalgae species | Pigment content | References |
|---|---|---|---|
| 1 | *Phormidium autumnale* | 159.3 µg/g (Chlorophyll) | Fernandes et al., 2017 |
| 2 | *Tetraselmis sp.* | 2.68 µg/L (Chlorophyll) | Islam et al., 2021 |
| 3 | *Chlorella vulgaris* and *Arthrospira platensis* | 72.20 mg/L (Carotenoid) | Ajijah et al., 2020 |
| 4 | *Coelastrum cf. pseudomicroporum* | 0.47 mg/L (Carotenoid) | Úbeda et al., 2017 |
| 5 | *Porphyridium cruentum* | 144 mg/g (Phycoerythrin) | Bueno et al., 2020 |
| 6 | *Porphyridium purpureum* | 196 mg/L (Phycoerythrin) | Li et al., 2020 |
| 7 | *Arthrospira sp.* | 44.24 mg/g (Phycocyanin) | Gorgich et al., 2020 |
| 8 | *Thermosynechococcus sp.* CL-1 | 281.4 mg/L/day (Phycocyanin) | Hoi et al., 2021 |
| 9 | *Haematococcus pluvialis* and *Chromochloris zofingiensis* | 22.43 mg/L (Astaxanthin) | Fernando et al., 2021 |
| 10 | *Haematococcus pluvialis* | 27.9 mg/g (Astaxanthin) | (Pan et al., 2021) |
| 11 | *Chlorella vulgaris* | 3.20 mg/g (Lutein) | (Fábryová et al., 2019) |
| 12 | *Chlorella pyrenoidosa* | 4.84 mg/g (Lutein) | (Sampathkumar et al., 2019) |
| 13 | *Chaetoceros muelleri* | 2.92 mg/g (Fucoxanthin) | Ishika et al., 2017 |
| 14 | *Mallomonas sp.* | 26.6 mg/g (Fucoxanthin) | Petrushkina et al., 2017 |

## 2. THE FACTORS DETERMINING BIOMASS

Microalgal biomass can be determined according to light, temperature, pH, carbon source, nitrogen, phosphorus and dissolved oxygen amount. Light is essential for all autotrophic cells. Photosynthesis occurs due to this light (Junior et al., 2020). In photosynthesis, photosynthetically active radiation (PAR) is used and organic molecules are produced by converting solar energy into chemical energy. PAR only is active between 400 and 700 nm in photosynthesis. Compensation irradiance is important for microalgae. This shows photosynthesis point of microalgae. Under this point, microalgae make respiration. Photosynthesis stops. Above this point, photosynthesis productivity increases and it reaches saturation irradiance point. At this point, microalgae perform maximum photosynthesis (Barati et al., 2021). This point may change due to the nature of each microalga. Above saturation irradiance point, the growth rate of microalgae begins to slow and eventually the microalgae die. This point is called the photo-inhibition point (Kumar et al., 2021). The mixed microalgae culture including *Chlorella sp., Scenedesmus sp*. and *Cyanobacteria* was grown in urban wastewater and various intensities of light were applied on microalgae. While light intensity increased, biomass concentration of microalgae increased. The maximum biomass concentration was 227 mg/L at 100 µmol $s^{-1}$ $m^{-2}$. Biomass concentrations were 159 and 219 mg/L at 20 and 50 µmol $s^{-1}$ $m^{-2}$ of light intensities, respectively (Iasimone et al., 2018). *Chlorella vulgaris* was studied in different light intensities such as

3500, 5000, 7500 and 10000 lx. The highest biomass concentration was 4 g/L at 10.000 lx with continuous illumination (Bazdar et al., 2018).

Another important factor is temperature. Microalgae, like other microorganisms, generally grow under room conditions. While thermophilic microalgae show maximum growth at higher temperatures, there are microalgae that grow under cold conditions. In this case, it changes according to the nature of the microalgae, just like the effect of light. The relationship between microalgae and temperature can be understood with the Arrhenius model (Solimeno & García, 2017). *Leptolyngbya sp., Picochlorum sp., Tetraselmis sp., Dunaliella sp.* and *Synechococcus sp.* were isolated and they were carried out for growth rates under various temperature degrees such as 20 °C, 25 °C, 30 °C, 35 °C, 40 °C and 45 °C. Each strain showed different growth rates at different temperatures. *Leptolyngbya sp.*and *Picochlorum sp.* had maximum growth rate among five strains. Growth rates of *Leptolyngbya sp.*and *Picochlorum sp.* was 0.12 $h^{-1}$ at the 35 °C and 40 °C, respectively. *Tetraselmis sp.* had 0.08 $h^{-1}$ of growth rate at 35 °C (Barten et al., 2020). Chlorella was grown in wastewater and its seasonal changes were investigated. At their study, temperature was not controlled and microalgae showed different properties at the each season. Average temperatures in the reactor were 20.6 °C, 16.4 °C, 28.8 °C and 31.5 °C at autumn, winter, spring and summer, respectively. Biomass productivity:light irradiance ratio of microalgae were 0.41 gVSS/mol 0.33 gVSS/mol 0.42 gVSS/mol 0.22 gVSS/mol at the 20.6 °C, 16.4 °C, 28.8 °C and 31.5 °C, respectively (González-Camejo et al., 2019). This situation shows us that microalgae can produce different biomass at different temperatures.

Like temperature, pH affects microalgal biomass. The majority of microalgae produce maximum biomass between pH 6 and 8. However, it is known that the microalgae in the medium increase the pH of the medium by using nutrients. This situation causes the medium to be unsustainable and the microalgae to die after a while. This is the biggest disadvantage of batch cultures. Therefore, it is important to use continuous cultures in terms of sustainability. In continuous cultures, carbon dioxide is usually added to the medium and the pH of the environment is controlled by three compounds such as $CO_{2,}$ $HCO_3^-$ and $CO_3$. The effect of pH on microalgae can be determined with the Cardinal model just like the effect of temperature (Solimeno & García, 2017). Apart from microalgae growing at room temperature, it is found in microalgae that grow at low and high pH and have a high economic contribution. *Dunaliella salina* is a microalga that can grow at high pH and produce high amounts of carotenoids. *Chlorella sorokiniana sp.* was examined for its harvesting efficiency under different pH values. From pH 2 to pH 8, while harvesting efficiency decreased gradually, harvesting efficiency increased from pH 8 to pH 12 after flocculation. Harvesting efficiency increased from 34% to 62% (Taghavijeloudar et al., 2021). *Chlorella sorokiniana* DOE1412 was studied under various pH levels such as 5.8, 6, 7, 8 and 9. pH changed by means of the addition of $CO_2$. The highest biomass productivity was 0.140 g/L/day at pH 6 and the lowest biomass productivity was 0.071 g/L/day at the pH 9 (Qiu et al., 2017).

Another factor affecting biomass is the carbon source. The carbon source will vary depending on the type of microalgae. While autotroph microalgae generally use carbon dioxide, heterotroph ones can use glucose, sucrose or xylose. Mixotrophs, on the other hand, have the ability to use whatever carbon source they find in the environment. If microalgae cannot find these sources directly, they can use the compounds in the environment by converting them into them or breaking them down. As a general opinion, it has shown that microalgae can grow faster as long as they easily reach the carbon source. In addition, the nitrogen and phosphorus amounts in the medium affect the growth of microalgae. Microalgae growth is expected to increase as the amount of nitrogen increases. In proportion to this, it contributes to growth with the amount of phosphorus and nitrogen. But, fast growth is not always considered a positive indicator. For, fast-growing microalgae generally produce lower lipids and carbohydrates. Generally, as the amount of nitrogen decreases, the amount of lipid increases in microalgae. For this, it would be more correct to use productivity when calculating microalgae yield. Dissolved oxygen is another important parameter. The amount of dissolved oxygen is calculated by the temperature and ionic power of the environment. If the microalga is autotroph, the amount of oxygen will increase with photosynthesis and this will decrease the photosynthesis rate (Yin et al., 2020). This is actually end product inhibition. It is determined by the activity of the rubisco enzyme. Total organic carbon and inorganic carbon can affect biomass production. Gao et al. studied various ratios of inorganic (IC) and organic carbon (OC) such as 1:3, 2:1, 1:1, 1:2 and 1:3 and biomass production of *Chlorella vulgaris*. Also, some carbon sources such as bicarbonate, carbonate, acetic acid and glucose were used for this study. 1:3 ratio (IC: OC) was 0.363 $d^{-1}$ for bicarbonate and glucose mixture. 1:2 ratios had the lower specific growth rate with 0.293 $d^{-1}$ for bicarbonate and glucose mixture. The highest specific growth rate was 0.527 $d^{-1}$ for bicarbonate and acetic acid. Specific growth rate of carbonate and glucose mixture (3:1) was 0.102 $d^{-1}$ and this value was the lowest specific growth rate value. As can be seen from this result, *Chlorella vulgaris* can convert carbonate and glucose into biomass by using it lower specific growth rate (Gao et al., 2021). Different nitrogen sources produce different biomass in microalgae. *Chlorella vulgaris, Scenedesmus dimorphus* and mixed culture were cultured various nitrogen sources such as nitrate, ammonium, urea and mixed nitrogen. *Chlorella vulgaris* with nitrate had the highest biomass concentration with 3.122 g/L. The highest biomass concentration of *Scenedesmus dimorphus* was 3 g/L in nitrate and mixed nitrogen. Also, mixed algae had the highest biomass concentration with 3.523 g/L in mixed nitrogen sources (Zhu et al., 2019). The studies related with the factors affecting biomass from microalgae were given in **Table 5**.

**Table 5**. *The factors affecting biomass from microalgae*

| No | Microalgae species | Factors | Biomass content or Growth rate | References |
|---|---|---|---|---|
| 1 | *Chlorella sp., Scenedesmus sp.* and *Cyanobacteria* | Light | 219 mg/L | (Iasimone et al., 2018) |
| **2** | Chlorella vulgaris | Light | 4 g/L | (Bazdar et al., 2018) |
| **3** | *Leptolyngbya sp.*and *Picochlorum sp.* | Temperature | 0.12 $h^{-1}$ | (Barten et al., 2020) |
| **4** | Chlorella sp. | Temperature | 0.42 gVSS/mol | (González-Camejo et al., 2019) |
| **5** | Chlorella sorokiniana sp. | pH | 62% ↑ | (Taghavijeloudar et al., 2021) |
| **6** | *Chlorella sorokiniana* DOE1412 | pH | 0.071 g/L/day | (Qiu et al., 2017) |
| **7** | Chlorella vulgaris | Organic carbon and inorganic carbon | 0.527 $d^{-1}$ | (Gao et al., 2021) |
| **8** | *Chlorella vulgaris* and *Scenedesmus dimorphus* | Mixed nitrogen sources | 3.523 g/L | (Zhu et al., 2019) |

## 3. MICROALGAE CULTIVATION SYSTEMS

Microalgae can be cultured for a variety of purposes such as pigment, bio-fuel and feed production, wastewater treatment and carbon dioxide mitigation. Cultivation can be in the different systems. There is no suitable cultivation system for a species. The system suitable for one culture may not be for the other species. The aim here is to use whichever system that will produce the highest biomass, quality product and the shortest time for the product to be produced. If an autotroph algae species are to be grown, the system to be used should be in a way that the maximum use of light. So, a higher amount of microalgae can be produced. But, this alone will not be a sufficient criterion. Temperature, mixing speed, pH, and the behavior of the system in the stationary phase will determine the amount and quality of the product. Daylight can be used to determine the system, as well as an artificial light source. Cultivation systems can be classified into two groups such as open raceways and photo-bioreactors. Open raceways can be used for microalgae species that can grow very quickly. These are Chlorella and Scenedesmus species. Also, microalgae with well-defined optimization conditions can be cultured under extreme growth conditions, and commercially important microalgae can be cultured with this method. Spirulina and Dunaliella species can be given as examples of these microalgae. Photo-bioreactors are more often used to determine the characteristics of a species and understand its industrial suitability. These systems are more expensive and their control mechanisms are stronger. So, it is more difficult to adjust these systems. However, high amounts of biomass can be obtained after setting up the system. The larger the volume in the reactor system, the harder it is to adjust the optimization conditions (Yin et al., 2020).

## 3.1. OPEN RACEWAY SYSTEMS

Open raceway systems cost less compared to photo-bioreactors. Therefore, approximately 90 percent of the products produced in the industry are carried out in raceway systems. Biomass yield is low in raceway systems, but high amounts of biomass can be obtained due to their wide diameter. On the contrary, this situation causes a high amount of contamination in microalgae growth. In addition, since microalgae are grown outside, light and temperature change depending on weather conditions. In this case, it lowers the estimate of how much biomass can be obtained. Raceway ponds usually consist of two channels and mixing of microalgae is provided by paddlewheels. More paddlewheels and very large raceway systems are not recommended in the industry. These systems cause problems in providing the pressure and mixing speed required for the operation of the system. In this system, it is desirable that the water depth is low. If the open raceways are deep, it prevents the entry of light and the growth of microalgae is restricted. This leads to lower biomass production. Liquid velocities in open raceways are important. Higher fluid velocity leads to more energy consumption. This is not a very desirable situation. At very low fluid velocity, it causes the accumulation of microalgae and the formation of dead microalgae cells in more than one area. Adjusting the liquid velocity in open raceways is necessary for the system to produce high biomass. The amount of light is another important problem in this system. As the depth of the system increases, the amount of light entering will decrease and the biomass efficiency will decrease. To overcome this, systems with larger surface area and less depth are designed. Difficulty of the temperature controlling is the disadvantage of this system. Biomass yield decreases due to the inability to achieve this in very large systems (Fernández et al., 2020; Aliyu et al., 2021). Stephenson et al. studied raceway system and air lift tubular reactor for *Chlorella vulgaris*. Biomass concentration was 1.67 kg/m$^3$ in raceway system. On the other hand, biomass content was 8.3 kg/m$^3$ in air lift tubular reactor. These biomasses was converted to bio-diesel and evaluated for economic feasibility (Stephenson et al., 2010). *Nannochloropsis salina* was cultivated in open raceway pond. The maximum biomass concentration was 0.99 g/L after harvesting by means of electropreci-flocculation in 120 m$^2$ of open raceway pond (Mohan et al., 2021). *Chlorella vulgaris* was cultivated in open raceway ponds. Microalgae were grown under batch and semi-continuous system. The maximum biomass concentration was 0.42 g/L under semi-continuous system (Yadav et al., 2020).

## 3.2. CLOSED PHOTO-BIOREACTORS

### 3.2.1. FLAT PHOTO-BIOREACTORS

These reactors generally consist of two flat panels. The panels of the reactor are designed for maximum use of light. The width of the reactor is determined as small as possible. This allows the light to penetrate as deep as possible. Microalgae with maximum light yield a higher biomass yield. This type of reactor usually has one hole that supplies carbon dioxide to the system. This carbon dioxide allows the pH value to be adjusted. Also, another hole can give air to the system. In continuous systems, there is one exit hole to keep the flow of the medium constant. The disadvantage of these systems is the low biomass production. On the contrary, biomass yield is high. It is frequently used in the laboratory as temperature, pH, medium concentration and light can be controlled in the system. This system is also expensive to provide the strict rules of control mechanisms. High rate of biofilm can be formed. The larger the system, the higher the cost of biofuel will be. One of the advantages of this system is the low risk of contamination (Fernández et al., 2020; Aliyu et al., 2021). *Scenedesmus obliquus* was cultivated in urban wastewater at a flat panel reactor. At the different hydraulic retention times such as 0.5 d, 1.1 d, 1.7 d, 2.3 d, 2.8 d and 3.4 d, various biomass concentrations were obtained. The highest biomass concentration was 1,052 mg/L at 2.8 d of hydraulic retention time (Ruiz et al., 2013). *Geitlerinema sp.* was cultivated in flat-panel photo-bioreactors by means of centrate as nutrient. The highest biomass concentration was 47.7 g biomass m$^{-2}$ day$^{-1}$ dry weight at 20 % of centrate (Romero-Villegas et al., 2018). *Chlorella zofingiensis* was cultivated in wastewater in flat-photo bioreactor. The highest biomass concentration was 2.83 g/L for 120 μM of IAA (Onay, 2020).

### 3.2.2. TUBULAR PHOTO-BIOREACTORS

This system is carried out as closed. It is costly compared to the open raceway systems. But, high amounts of biomass can be obtained easily. More susceptible species that are not suitable for cultivation in open systems can be cultured in the tubular reactors. Contamination rate is low. The ability to control the system is more difficult compared to flat ones. However, they are better controlled than open raceway systems. The aim of tubular reactors is to design to allow maximum light penetration like flat reactors. Bubble tubular photo- bioreactors have been widely used in recent years. The bubbles prevent microalgae cells from forming biofilms and allow the air to be distributed evenly throughout the system. The size and width of the reactor and the amount of carbon dioxide and air given to the system are important in order to produce biomass at the desired level. This system can be used successfully when high rates of biomass are desired to be grown (Fernández et al., 2020; Aliyu et al., 2021). *Chlorella vulgaris* and *Tetradesmus obliquus* were cultivated in modified Organization for Economic Co-operation and Development culture medium at innovative tubular photo-bioreactor. The highest biomass productivities *Chlorella vulgaris* and *Tetradesmus obliquus* were 28 mg dw $L^{-1}$ $d^{-1}$and 29 mg dw $L^{-1}$ $d^{-1}$, respectively (Porto et al., 2021). *Arthrospira platensis* was grown in Guillard's f/2 culture medium at the Fibonacci-type tubular photo-bioreactor. The maximum specific growth rate was 0.8 $d^{-1}$ in Fibonacci-type tubular photo-bioreactor (Díaz et al., 2019). *Chlorella pyrenoidosa* were cultivated in the mixed food wastewater at a pilot-scale tubular photo-bioreactor. The maximum biomass concentration was 1.83 g/L (Tan et al., 2021).

### 3.2.3. COLUMN PHOTO-BIOREACTORS

It can be used easily in lab-scale studies. It is easy to control. Continuous systems can be operated. Temperature, pH, light and flow rate can be controlled automatically and it can be followed by computers. Bubble column photo-bioreactors give air in system and prevent the formation of biofilm. As the length and width of the reactor increase, the drawbacks related with the entrance of the light in system prevent the design (Aliyu et al., 2021). The studies about microalgae cultivation systems were given in **Table 6**.

**Table 6.** *Microalgae cultivation systems*

| No | Microalgae species | Reactor systems | Biomass Content | References |
|---|---|---|---|---|
| 1 | Chlorella vulgaris | Raceway system | 1.67 kg/m$^3$ | (Stephenson et al., 2010) |
| **2** | Chlorella vulgaris | Air lift tubular reactor | 8.3 kg/m$^3$ | (Stephenson et al., 2010) |
| **3** | Nannochloropsis salina | Open raceway pond | 0.99 g/L | (Mohan et al., 2021) |
| **4** | Chlorella vulgaris | Open raceway ponds | 0.42 g/L | (Yadav et al., 2020) |
| **5** | Scenedesmus obliquus | Flat panel reactor | 1,052 mg/L | (Ruiz et al., 2013) |
| **6** | Geitlerinema sp. | Flat-panel photo-bioreactors | 47.7 g biomass m$^{-2}$ day$^{-1}$ | (Romero-Villegas et al., 2018) |
| **7** | Chlorella zofingiensis | Flat-panel photo-bioreactors | 2.83 g/L | (Onay, 2020) |
| **8** | Chlorella vulgaris | Tubular photo-bioreactor | 28 mg dw L$^{-1}$ d$^{-1}$ | (Porto et al., 2021) |
| **9** | Tetradesmus obliquus | Tubular photo-bioreactor | 29 mg dw L$^{-1}$ d$^{-1}$ | (Porto et al., 2021) |
| **10** | Arthrospira platensis | Tubular photo-bioreactor | 0.8 d$^{-1}$ | (Díaz et al., 2019) |
| **11** | Chlorella pyrenoidosa | Tubular photo-bioreactor | 1.83 g/L | (Tan et al., 2021) |

## 4. PHOTO-BIOREACTOR DESIGN

Photo-bioreactor design is basically done in accordance with the laws of thermodynamics. Mass transfer, heat transfer, fluid dynamics and reactor's geometry gain importance in reactor design. The main purpose in reactor design is to obtain more microalgal mass. Normally reactor systems are classified into two classes as batch and continuous culture. Batch culture generally includes mixer and it is a closed system. On the other hand, continuous system is an open system and the substances entering and discarded the system are strictly controlled. The system can be maintained for a long time provided the appropriate conditions are provided. Since the parameter used in these systems is microalgae, the light reaching the system is important (Fernández et al., 2020). *Chlorella* PY-ZU1 was cultivated in a horizontal tubular photo-bioreactor. This reactor was designed for the enhancement of mass transfer. A $CO_2$ microbubbles dissolver was used to obtain higher biomass production. Mass transfer of reactor increased up to 80.9 %. In addition, biomass content increased up to

30% (Cheng et al., 2019). *Arthrospira platensis* was cultivated in Zarrouk medium at open raceway pond. Self-rotary propellers with clockwise/ counterclockwise blades were developed to enhance mass transfer. Mass transfer of reactor increased up to 49 %. In addition, biomass content increased up to 35% (Kumar et al., 2019). Cell migration and kinetic model were combined for the increase of the heat transfer coefficient in the tubular reactor. *Chlorella pyrenoidosa* was cultivated in their study. A CFD model was applied and heat transfer coefficient increased by 1.05 (Chen et al., 2020). A flat-plate photo-bioreactor was designed for the development of ultra-high density cultures. Perforated baffles were designed and it increased biomass content of *Poterioochromonas malhamensis*. Flashing-light effect increased biomass content. Computational fluid dynamics method was developed for this aim. Biomass concentration increased up to 270% (Hinterholz et al., 2019). *Chlorella vulgaris* was cultivated in basal medium at the raceway system. $CO_2$ spargers and paddlewheel were joined. While paddlewheel rotation speed increased from 13 to 30 rpm, *Chlorella vulgaris* biomass increased. Computational fluid dynamics methods were applied and $CO_2$ spargers enhanced flow velocity. The highest biomass content was 5.2 g/L (Kusmayadi et al., 2020).

### 4.1. LIGHT

The light effect is independent on fluid dynamics. It is impossible for the light to reach every point of the reactor equally. According to the type and volume of the reactor, the light reaching the reactor from multiple points is measured from different points. Then, the average of the light intensity at these points is expressed as the amount of light given to the reactor. In reactor design, it is expected to be designed in such a way that light reaches the maximum reactor. The carbon dioxide supplied to the reactor, temperature, nutrient and biofilm formation rate may be parameters that determine the amount of biomass in the reactors. Microalgae grown in the reactor grow in proportion to the reactor design. The amount of light and the speed of photosynthesis show a relationship according to the Michaelis-Menten equation as in enzymes. This is called the PI curve. P shows photosynthesis while I value reflects the effect of irradiance. This kinetic curve is used as an indicator of the growth of microalgae and biomass production within the reactor. In this curve, as the light intensity increases, the rate of photosynthesis also increases. However, when the light intensity is increased at some point, the rate of photosynthesis does not increase and this remains constant. This point is called $P_m$ and indicates that photosynthesis is at its maximum. This point is also the saturation point and it is named stationary point. If the light intensity is increased after this point, the photosynthesis rate decreases and the event we call photo-inhibition occurs. Since the photosynthesis rate shows the growth of microalgae and the amount of biomass, their proportion decreases and the reactor will no longer be a suitable environment for the growth of microalgae. While designing the reactor, designing the light to have a high $P_m$ value depending on the type of microalgae will ensure the formation of high biomass. By using air in the reactor design or adding a stirrer, the mixing increases the homogeneity of the medium. This prevents the formation of biofilms and enables the formation of higher amounts of biomass. By designing reactors that will ensure the homogeneous distribution of the air in the reactor, the reactor can provide optimum conditions (Fernández et al., 2020; Aliyu et al., 2021). *Chlorella vulgaris* was cultivated in basal medium at the raceway system. Light intensity and mixing effect were investigated for biomass production. The highest biomass content was 5.2 g/L (Kusmayadi et al., 2020). *Scenedesmus almeriensis* was cultivated in Mann and Myers medium. In this system, photosynthetic light integration was formed in raceway reactor. Light regime increased and cell adaptation was provided via local irradiance. Biomass productivity was 40 $g/m^2$ /day and this result was a very high biomass yield compared to the control (Barceló-Villalobos et al., 2019).

## 4.2. TEMPERATURE

One of the factors limiting the growth of microalgae in reactors is high temperature. The light source placed very close to the reactor generates high heat. High temperature leads to microalgae to die and continuity cannot be maintained within the reactor. In order to prevent this, design can be made by using metal parts in the design of the reactors. In addition, a design that runs cold water through reactors can overcome this problem. *Scenedesmus* and *Chlorella* species were used for bio-crude production from microalgae by means of the hydrothermal liquefaction. In the reactor, temperature reached 300 $^{o}C$ -340 $^{o}C$. System maintained the in-situ collection of solids through a double tube design. This system produced high amounts of bio-crude and was inexpensive (Wagner et al., 2017).

## 4.3. MIXING

Mixing is another important parameter for reactor design. Mixing is a basic component of mass transfer. The purpose of mixing is to ensure that the light and the cells in the culture medium meet at the maximum rate for reactor design. The mixing process can be done with a metal static mixer such as steel. In addition, a gas such as air can be supplied to the culture medium. In addition, by adding a system that provides carbon dioxide input to the reactors, rapid growth of microalgae in the reactor can be achieved. Designs continue to be developed for homogeneous distribution of carbon dioxide in the reactor. While designing the reactor, the above mentioned events should be improved with minimum energy need. If the design cost is more than the amount of biomass produced before the design, the design will not make sense. For a successful reactor design, it is necessary to combine kinetics and fluid dynamics information. Recently, model-based reactor design studies have been started. In future studies, reactor design with computer-based simulation programs will give even more successful results related with microalgal biomass production.

## 4.4. CARBON DIOXIDE

Carbon dioxide is necessary for photosynthesis. Inorganic or organic carbon can be used in reactors. This situation may vary according to the species of microalgae. Some microalgae use inorganic carbon while others use organic carbon. The carbon used has a connection with the light. When the light is not in the medium, carbon cannot be utilized. If carbon dioxide is to be supplied to the system from outside, the reactor should be designed in such a way that the carbon dioxide is used maximally by cells. In this way, mass transfer increases with carbon dioxide (Gao et al., 2021). *Tetraselmis chuii* was cultivated in artificial sea salt at the bubble column. The system was adjusted to deliver carbon dioxide automatically and the pH (7.56) was kept constant. Each batch consumed 0.124kwh/ liter and this system inexpensive for the production of high amount of microalgae. Microalgae density was 1200 cells/ µl/ $m^2$ ISA (Erbland et al., 2020).

## 4.5. OXYGEN

Also, the amount of oxygen is also important in reactor design. In fact, plenty of oxygen is released during photosynthesis. Therefore, the amount of oxygen in the reactors must be carefully adjusted. If the amount of oxygen is excessive, oxidative damage will occur in the cells. This causes the death of microalgae cells by reducing the biomass yield. Excessive oxygen pressure easily exits the system in open photo-bioreactors. However, in closed systems, this ratio must be maintained carefully to prevent cell death (Fernández et al., 2020).

## 4.6. pH

pH changes significantly affect microalgae growth. pH is tightly controlled in reactors. pH is controlled with carbon dioxide, bicarbonate and carbonate. As in blood, the buffer system that enables bicarbonate formation is also used in reactors. Since the pH in the medium increases over time, carbon dioxide is supplied to the system. The probe is used to measure the pH value of the system. The size and location of this probe depends entirely on the design of the reactor. The aim is to achieve the same pH value all over the system.

### 4.7. MEDIUM OR WATER CONCENTRATION

Amount of medium or water is important in open systems. For, the water evaporates after a certain period of time and leaves the system. While designing, the design should be made in such a way that the water evaporates as little as possible. Excessive evaporation of water from the system can also lead to undesirable different types of algae to grow and become dominant after a certain period of time. If microalgae are grown in wastewater, the system should be designed with this in mind (Aliyu et al., 2021). Wastewater will give a certain amount of turbidity to the system. It will also increase the risk of contamination. This is not the case with closed photo-bioreactors. In other words, there is no loss of medium or water from the system. In continuous systems, the medium is refreshed by adjusting the medium with a certain dilution factor. In open systems, an increase in salt concentration may occur due to evaporation if microalgae are salt water microalgae. An up-flow anaerobic sludge blanket reactor was designed to digest microalgae and wastewater. Total suspended solid content of microalgae was 3200 mg/L. This system needs further development to digest wastewater and microalgae (Gonçalves et al., 2020). The studies about the parameters in reactor design were given in **Table 7**.

**Table 7.** *The parameters in reactor design*

| No | Microalgae species | Reactor Systems | Parameters | References |
|---|---|---|---|---|
| 1 | *Chlorella* PY-ZU1 | Horizontal tubular photo-bioreactor | Mass transfer | (Cheng et al., 2019) |
| **2** | Arthrospira platensis | Open raceway pond | Mass transfer | (Kumar et al., 2019) |
| **3** | Chlorella pyrenoidosa | The raceway system | Heat transfer | (Chen et al., 2020) |
| **4** | Poterioochromonas malhamensis | Flat-plate photo-bioreactor | Fluid dynamics method | (Hinterholz et al., 2019) |
| **5** | Chlorella vulgaris | The raceway system | Fluid dynamics method and Light | (Kusmayadi et al., 2020) |
| **6** | Scenedesmus almeriensis | The raceway reactor | Light | (Barceló-Villalobos et al., 2019) |
| **7** | *Scenedesmus* sp. and *Chlorella sp.* | Hydrothermal liquefaction reactor | Temperature | (Wagner et al., 2017) |
| **8** | Tetraselmis chuii | The bubble column | Carbon dioxide and pH | (Erbland et al., 2020) |
| **9** | Mixed microalgae | Up-flow anaerobic sludge blanket reactor | Medium and wastewater | (Gonçalves et al., 2020) |

## 5. CONCLUSION

Photo-bioreactor design is one of the most important issues for high biomass production from microalgae. The design of the reactor is decisive because the production of high biomass affects the amount of end product from microalgae. Mass transfer, heat transfer, fluid dynamics and reactor's geometry determine the design of the reactor. In addition, optimum conditions of light, temperature, mixing, carbon dioxide, oxygen, pH and water must be combined with photo-bioreactor design for the maximum end product. The more successfully these conditions are obtained, the more successful it will be achieved its purpose in design.

## REFERENCES

Abomohra, A.E., Zheng, X., Wang, Q., Huang, J., Ebaid, R. (2021). Enhancement of biodiesel yield and characteristics through in-situ solvo-thermal co-transesterification of wet microalgae with spent coffee grounds. *Bioresour. Technol.* 323, 124640. doi:10.1016/j.biortech.2020.124640

Ajijah, N., Tjandra, B.C., Hamidah, U., Widyarani, Sintawardani, N. (2020). Utilization of tofu wastewater as a cultivation medium for *Chlorella vulgaris* and *Arthrospira platensis*. *Earth Env. Sci.* 483, 012027. doi:10.1088/1755-1315/483/1/012027

Aliyu, A., Lee, J.G.M., Harvey, A.P. (2021). Microalgae for biofuels via thermochemical conversion processes: A review of cultivation, harvesting and drying processes, and the associated opportunities for integrated production. *Bioresour. Technol. Reports.* 14, 100676. doi: 10.1016/j.biteb.2021.100676

Avila, R., Carrero, E., Vicent, T., Blánquez, P. (2021). Integration of enzymatic pretreatment and sludge co-digestion in biogas production from microalgae. *Waste Manag.* 124, 254-263. doi:10.1016/j.wasman.2021.01.042

Barati, B., Zeng, K., Baeyens, J., Wang, S., Addy, M., Gan, S., Abomohra, A.E. (2021). Recent progress in genetically modified microalgae for enhanced carbon dioxide sequestration. *Biomass and Bioenergy.* 145, 105927. doi:10.1016/j.biombioe.2020.105927

Barceló-Villalobos, M., Olmo, P.F., Guzmán, J.L., Fernández-sevilla, J.M. (2019). Evaluation of photosynthetic light integration by microalgae in a pilot-scale raceway reactor. *Bioresour. Technol.* 280, 404-411. doi:10.1016/j.biortech.2019.02.032

Barten, R.J.P., Wijffels, R.H., Barbosa, M.J. (2020). Bioprospecting and characterization of temperature tolerant microalgae from Bonaire. Algal Res. 50, 102008. doi:10.1016/j.algal.2020.102008

Bazdar, E., Roshandel, R., Yaghmaei, S., Mahdi, M. (2018). The effect of different light intensities and light/dark regimes on the performance of photosynthetic microalgae microbial fuel cell. *Bioresour. Technol.* 261, 350-360. doi:10.1016/j.biortech.2018.04.026

Becerra, M.O., Contreras, L.M., Lo, M.H., Díaz, J.M., Castillo, G., Alimentaria, T., Investigación, C. De, Ciatej, A.C., Zapopan, U., Arenero, C., Bajío, E. (2020). Lutein as a functional food ingredient: Stability and bioavailability. *J. Funct. Foods.* 66, 103771. doi:10.1016/j.jff.2019.103771

Bhuyar, P., Sundararaju, S., Hasbi, M., Rahim, A., Pragas, G., Govindan, N. (2021). Enhanced productivity of lipid extraction by urea stress conditions on marine microalgae *Coelastrum sp.* for improved biodiesel production. *Bioresour. Technol. Reports* 15, 100696. doi:10.1016/j.biteb.2021.100696

Bueno, M., Gallego, R., Chourio, A.M., Ibanez, E., Herrero, M., Saldana, M.D.A. (2020). Green ultra-high pressure extraction of bioactive compounds from *Haematococcus pluvialis* and *Porphyridium cruentum* microalgae. *Innov. Food Sci. Emerg. Technol.* 66, 1-10. doi:10.1016/j.ifset.2020.102532

Chen, H., Fu, Q., Liao, Q., Xiao, C., Huang, Y., Xia, A., Zhu, X. (2020). Modeling for thermal hydrolysis of microalgae slurry in tubular reactor : microalgae cell migration flow and heat transfer effects. *Appl. Therm. Eng.* 180, 115784. doi:10.1016/j.applthermaleng.2020.115784

Cheng, J., Xu, J., Ye, Q., Lai, X., Zhang, X., Zhou, J. (2019). Strengthening mass transfer of carbon dioxide microbubbles dissolver in a horizontal tubular photo-bioreactor for improving microalgae growth. *Bioresour. Technol.* 277, 11-17. doi:10.1016/j.biortech.2019.01.019

Chowdhury, H., Loganathan, B. (2019). Third-generation biofuels from microalgae: a review. *Curr. Opin. Green Sustain. Chem.* 20, 39-44. doi:10.1016/j.cogsc.2019.09.003

Chyuan, H., Wei, Y., Han, B., Goh, H., Yang, Y., Mofijur, M., Fattah, I.M.R., Tung, C., Alam, A., Voon, H., Silitonga, A.S., Mahlia, T.M.I. (2021). Recent advances in biodiesel production from agricultural products and microalgae using ionic liquids: Opportunities and challenges. *Energy Convers. Manag.* 228, 113647. doi:10.1016/j.enconman.2020.113647

Deb, D., Mallick, N., Bhadoria, P.B.S. (2021). Engineering culture medium for enhanced carbohydrate accumulation in *Anabaena variabilis* to stimulate production of bioethanol and other high-value co-products under cyanobacterial refinery approach. *Renew. Energy* 163, 1786-1801. doi:10.1016/j.renene.2020.10.086

Díaz, J.P., Inostroza, C., Fernández, F.G.A. (2019). Fibonacci-type tubular photobioreactor for the production of microalgae. *Process Biochem.* 86, 1-8. doi:10.1016/j.procbio.2019.08.008

Dhandayuthapani, K., Sarumathi, V., Selvakumar, P., Temesgen, T. (2021). Study on the ethanol production from hydrolysate derived by ultrasonic pretreated defatted biomass of *chlorella sorokiniana NITTS*3. Chem. Data Collect. 31, 100641. doi:10.1016/j.cdc.2020.100641

Erbland, P., Caron, S., Peterson, M., Alyokhin, A. (2020). Aquacultural Engineering Design and performance of a low-cost, automated, large-scale photobioreactor for microalgae production. *Aquac. Eng.* 90, 102103. doi:10.1016/j.aquaeng.2020.102103

Fábryová, T., Cheel, J., Kubá, D., Hrouzek, P., Long, D., Lenka, T. (2019). Purification of lutein from the green microalgae *Chlorella vulgaris* by integrated use of a new extraction protocol and a multi-injection high performance counter-current chromatography (HPCCC). *Algal Res.* 41, 101574. doi:10.1016/j.algal.2019.101574

Fernandes, A.S., Nogara, G.P., Menezes, C.R., Cichoski, A.J., Mercadante, A.Z., Jacob-lopes, E., Zepka, L.Q. (2017). Identification of chlorophyll molecules with peroxyl radical scavenger capacity in microalgae *Phormidium autumnale* using ultrasound-assisted extraction. *Food Res. Int.* 99, 1036-1041. doi:10.1016/j.foodres.2016.11.011

Fernández, F.G.A., Fernández-Sevilla, J.M., Moya, B.L., Grima, E.M. (2020). Microalgae production systems. In E. Jacob-Lopes, M.M. Maroneze, M.I. Queiroz, L.Q Zepka. *Handbook of Microalgae-Based Processes and Products. Fundamentals and Advances in Energy, Food, Feed, Fertilizer, and Bioactive Compounds* (pp.127-163). United Kingdom: Academic Press (Elsevier). https://doi.org/10.1016/B978-0-12-818536-0.00006-3

Fernando, J.S.R., Premaratne, M., Sineru, D.M., Dinalankara, D., Perera, G.L.N.J., Ariyadasa, T.U. (2021). Cultivation of microalgae in palm oil mill effluent (POME) for astaxanthin production and simultaneous phycoremediation. *J. Environ. Chem. Eng.* 9(4), 105375. doi:10.1016/j.jece.2021.105375

Gao, P., Guo, L., Zhao, Y., Jin, C., She, Z. (2021). Enhancing microalgae growth and product accumulation with carbon source regulation: New perspective for the coordination between photosynthesis and aerobic respiration. *Chemosphere*. 278, 130435. doi:10.1016/j.chemosphere.2021.130435

Goh, B.H.H., Ong, H.C., Cheah, M.Y., Chen, W.H., Yu, K.L., Mahlia, T.M.I. (2019). Sustainability of direct biodiesel synthesis from microalgae biomass: A critical review. *Renew. Sustain. Energy Rev.*107, 59-74. doi:10.1016/j.rser.2019.02.012

Gonçalves, R.F., Assis, T.I., Maciel, G.B., Borges, R.M., Cassini, S.T.A. (2020). Co-digestion of municipal wastewater and microalgae biomass in an upflow anaerobic sludge blanket reactor. *Algal Res.* 52. 102117. doi:10.1016/j.algal.2020.102117

González-Camejo, J., Aparicio, S., Ruano, M. V, Borrás, L., Barat, R., Ferrer, J. (2019). Effect of ambient temperature variations on an indigenous microalgae-nitrifying bacteria culture dominated by Chlorella. *Bioresour. Technol.* 290, 121788. doi:10.1016/j.biortech.2019.121788

Gorgich, M., Passos, M.L.C., Mata, T.M., Martins, A.A. (2020). Enhancing extraction and purification of phycocyanin from *Arthrospira sp*. with lower energy consumption. *Energy Reports.* 6, 312-318. doi:10.1016/j.egyr.2020.11.151

Hinterholtz, C.L., Trigueros, D.E.G., Módenes A.N., Borba, C.E., Scheufele, F.B., Schuelter, A.R., Kroumov, A.D. (2019). Computational fluid dynamics applied for the improvement of a flat-plate photobioreactor towards high-density microalgae cultures. *Biochem. Eng. J.* 151, 107257. doi:10.1016/j.bej.2019.107257

Hoi, S.K., Winayu, B.N.R., Hsueh, H.T., Chu, H. (2021). Light factors and nitrogen availability to enhance biomass and C-phycocyanin productivity of *Thermosynechococcus sp*. CL-1. *Biochem. Eng. J.* 167, 107899. doi:10.1016/j.bej.2020.107899

Hu, J., Nagarajan, D., Zhang, Q., Chang, J., Lee, D. (2018). Heterotrophic cultivation of microalgae for pigment production: A review. *Biotechnol. Adv.* 36, 54-67. doi:10.1016/j.biotechadv.2017.09.009

Iasimone, F., Panico, A., Felice, V. De, Fantasma, F., Iorizzi, M., Pirozzi, F. (2018). Effect of light intensity and nutrients supply on microalgae cultivated in urban wastewater: Biomass production, lipids accumulation and settle ability characteristics. *J. Environ. Manage.* 223, 1078-1085. doi:10.1016/j.jenvman.2018.07.024

Ishika, T., Moheimani, N.R., Bahri, P.A., Laird, D.W., Blair, S., Parlevliet, D. (2017). Halo-adapted microalgae for fucoxanthin production: Effect of incremental increase in salinity. *Algal Res.* 28, 66-73. doi:10.1016/j.algal.2017.10.002

Islam, Z., Khatoon, H., Mahmud, T., Redwanur, M., Hasan, S., Mahmud, Y., Hossain, S., Sarker, J. (2021). Data on growth, productivity , pigments and proximate composition of indigenous marine microalgae isolated from Cox's Bazar Coast. *Data Br.* 35, 106860. doi:10.1016/j.dib.2021.106860

Junior, M.W.G., Gorgich, M., Corrêa, P.S., Martins, A.A., Mata, T.M., Caetano, N.S. (2020). Microalgae for biotechnological applications: Cultivation, harvesting and biomass processing. *Aquaculture.* 528, 735562. doi:10.1016/j.aquaculture.2020.735562

Kim, H.M., Oh, C.H., Bae, H.J. (2017). Comparison of red microalgae (*Porphyridium cruentum*) culture conditions for bioethanol production. *Bioresour. Technol.* 233, 44-50. doi:10.1016/j.biortech.2017.02.040

Kumar, S., Cheng, J., Guo, W., Ali, K.A., Song, Y. (2019). Self-rotary propellers with clockwise/counterclockwise blades create spiral flow fields to improve mass transfer and promote microalgae growth. *Bioresour. Technol.* 286, 121384. doi:10.1016/j.biortech.2019.121384

Kumar, V., Sharma, N., Kumar, K., Vlaskin, M.S., Nanda, M., Kumar, M., Kumar, S. (2021). Microalgae with a truncated light-harvesting antenna to maximize photosynthetic efficiency and biomass productivity: Recent advances and current challenges. *Process Biochem.* 104, 83-91. doi:10.1016/j.procbio.2021.03.006

Kusmayadi, A., Philippidis, G.P., Yen, H. (2020). Application of computational fluid dynamics to raceways combining paddlewheel and $CO_2$ spargers to enhance microalgae growth. *J. Biosci. Bioeng.* 129, 93-98. doi:10.1016/j.jbiosc.2019.06.013

Li, S., Zhao, S., Yan, S., Qiu, Y., Song, C., Li, Y., Kitamura, Y. (2019). Food processing wastewater purification by microalgae cultivation associated with high value-added compounds production. A review. Chinese *J. Chem. Eng.* 27, 2845-2856. doi:10.1016/j.cjche.2019.03.028

Li, S., Ji, L., Chen, C., Zhao, S., Sun, M., Gao, Z., Wu, H., Fan, J. (2020). Efficient accumulation of high-value bioactive substances by carbon to nitrogen ratio regulation in marine microalgae *Porphyridium purpureum*. *Bioresour. Technol.* 309, 123362. doi:10.1016/j.biortech.2020.123362

Li, G., Zhang, J., Li, H., Hu, R., Yao, X., Liu, Y. (2021). Chemosphere Towards high-quality biodiesel production from microalgae using original and anaerobically-digested livestock wastewater. *Chemosphere*. 273, 128578. doi:10.1016/j.chemosphere.2020.128578

Llamas, M., Magdalena, J.A., Tom, E., Gonz, C. (2020). Microalgae-based anaerobic fermentation as a promising technology for producing biogas and microbial oils. *Energy.* 206, 118184. doi:10.1016/j.energy.2020.118184

Lourenço-lopes, C., Fraga-corral, M., Jimenez-lopez, C., Carpena, M., Pereira, A.G. (2021). Biological action mechanisms of fucoxanthin extracted from algae for application in food and cosmetic industries nuclear Magnetic Resonance. *Trends Food Sci. Technol*. x, xxx-xxx, doi:10.1016/j.tifs.2021.03.012

Lu, Q., Li, H., Zou, Y., Liu, H., Yang, L. (2021). Astaxanthin as a microalgal metabolite for aquaculture : A review on the synthetic mechanisms, production techniques, and practical application. *Algal Res*. 54, 102178. doi:10.1016/j.algal.2020.102178

Manirafasha, E., Ndikubwimana, T., Zeng, X., Lu, Y., Jing, K. (2016). Phycobiliprotein: Potential microalgae derived pharmaceutical and biological reagent. *Biochem. Eng. J.* 109, 282-296. doi:10.1016/j.bej.2016.01.025

Miyawaki, B., Mariano, A.B., Vargas, J.V.C., Balmant, W. (2021). Microalgae derived biomass and bioenergy production enhancement through biogas purification and wastewater treatment. *Renew. Energy.* 163, 1153-1165. doi:10.1016/j.renene.2020.09.045

Mohan, N., Hanumantha, P., Baskara, A., Rengasamy, R., Chinnasamy, S. (2021). A sustainable process train for a marine microalga-mediated biomass production and $CO_2$ capture: A pilot-scale cultivation of *Nannochloropsis salina* in open raceway ponds and harvesting through electro preciflocculation. *Renew. Energy*. 173, 263-272. doi:10.1016/j.renene.2021.03.147

Morais, K.C.C., Conceio, D., Vargas, J.V.C., et al. (2021). Enhanced microalgae biomass and lipid output for increased biodiesel productivity. *Renew. Energy.* 163, 138-145. doi:10.1016/j.renene.2020.08.082

Onay, M. (2020). The effects of indole-3-acetic acid and hydrogen peroxide on *Chlorella zofingiensis* CCALA 944 for bio-butanol production. *Fuel*. 273, 117795. doi:10.1016/j.fuel.2020.117795

Pan, M., Zhu, X., Pan, G., Angelidak, I. (2021). Integrated valorization system for simultaneous high strength organic wastewater treatment and astaxanthin production from *Haematococcus pluvialis*. *Bioresour. Technol.* 326, 124761. doi:10.1016/j.biortech.2021.124761

Petrushkina, M., Gusev, E., Sorokin, B., Zotko, N., Mamaeva, A., Filimonova, A., Kulikovskiy, M., Maltsev, Y., Yampolsky, I., Guglya, E., Vinokurov, V., Namsaraev, Z., Kuzmin, D. (2017). Fucoxanthin production by heterokont microalgae. *Algal Res.* 24, 387-393. doi:10.1016/j.algal.2017.03.016

Phwan, C.K., Ong, H.C., Chen, W., Ling, T.C., Ng, E.P., Show, P.L. (2018). Overview: comparison of pretreatment technologies and fermentation processes of bioethanol from microalgae. *Energy Convers. Manag.* 173, 81-94. doi:10.1016/j.enconman.2018.07.054

Porto, B., Gonçalves, A.L., Esteves, A.F., Guelli, S.M.A., Souza, U. De, Pires, C.M. (2021). Assessing the potential of microalgae for nutrients removal from a landfill leachate using an innovative tubular photobioreactor. *Chem. Eng. J.* 413, 127546. doi:10.1016/j.cej.2020.127546

Pourkarimi, S., Hallajisani, A., Alizadehdakhel, A., Nouralishahi, A. (2020). Factors affecting production of beta-carotene from *Dunaliella salina* microalgae. *Biocatal. Agric. Biotechnol*. 29, 101771. doi:10.1016/j.bcab.2020.101771

Qiu, R., Gao, S., Lopez, P.A., Ogden, K.L. (2017). Effects of pH on cell growth, lipid production and $CO_2$ addition of microalgae *Chlorella sorokiniana*. *Algal Res.* 28, 192-199. doi:10.1016/j.algal.2017.11.004

Reyes, J.C., Buitron, G., Arcila, J.S., Gomez, M.O.L. (2021). Thermophilic biogas production from microalgae-bacteria aggregates: biogas yield, community variation and energy balance. *Chemosphere.* 275, 129898. doi:10.1016/j.chemosphere.2021.129898

Romero-Villegas, G.I., Fiamengo, M., Fernández, F.G.A., Grima, E.M. (2018). Utilization of centrate for the outdoor production of marine microalgae at pilot-scale in flat-panel photobioreactors. *J. Biotechnol*. 284, 102-114. doi:10.1016/j.jbiotec.2018.08.006

Ruiz, J., Álvarez-díaz, P.D., Arbib, Z., Garrido-pérez, C., Barragán, J., Perales, J.A. (2013). Performance of a flat panel reactor in the continuous culture of microalgae in urban wastewater: Prediction from a batch experiment. *Bioresour. Technol.* 127, 456-463. doi:10.1016/j.biortech.2012.09.103

Sampathkumar, S.J., Gothandam, K.M. (2019). Biocatalysis and Agricultural Biotechnology Sodium bicarbonate augmentation enhances lutein biosynthesis in green microalgae *Chlorella pyrenoidosa*. *Biocatal. Agric. Biotechnol.* 22, 101406. doi:10.1016/j.bcab.2019.101406

Shokrkar, H., Ebrahimi, S., Zamani, M. (2017). Bioethanol production from acidic and enzymatic hydrolysates of mixed microalgae culture. *Fuel.* 200, 380-386. doi:10.1016/j.fuel.2017.03.090

Solimeno, A., García, J. (2017). Science of the Total Environment Microalgae-bacteria models evolution: From microalgae steady-state to integrated microalgae-bacteria wastewater treatment models. A comparative review. *Sci. Total Environ.* 607–608, 1136-1150. doi:10.1016/j.scitotenv.2017.07.114

Stephenson, A.L., Kazamia, E., Dennis, J.S., Howe, C.J., Scott, S.A., Smith, A.G. (2010). Life-Cycle Assessment of Potential Algal Biodiesel Production in the United Kingdom: A Comparison of Raceways and Air-Lift Tubular Bioreactors. *Energy Fuels.* 24, 4062-4077. doi:10.1021/ef1003123

Suparmaniam, U., Kee, M., Uemura, Y., Wei, J., Teong, K., Hoong, S. (2019). Insights into the microalgae cultivation technology and harvesting process for biofuel production: A review. *Renew. Sustain. Energy Rev.* 115, 109361. doi:10.1016/j.rser.2019.109361

Taghavijeloudar, M., Kebria, D.Y., Yaqoubnejad, P. (2021). Simultaneous harvesting and extracellular polymeric substances extrusion of microalgae using surfactant: Promoting surfactant-assisted flocculation through pH adjustment. *Bioresour. Technol.* 319, 124224. doi:10.1016/j.biortech.2020.124224

Tan, X., Wan, X., Yang, L., Wang, X., Meng, J., Jiang, M., Pi, H. (2021). Nutrients recycling and biomass production from *Chlorella pyrenoidosa* culture using anaerobic food processing wastewater in a pilot-scale tubular photobioreactor. *Chemosphere.* 270, 129459. doi:10.1016/j.chemosphere.2020.129459

Úbeda, B., Gálvez, J.Á., Michel, M., Bartual, A. (2017). Microalgae cultivation in urban wastewater : *Coelastrum cf . pseudomicroporum* as a novel carotenoid source and a potential microalgae harvesting tool. *Bioresou*r. Technol. 228, 210-217. doi:10.1016/j.biortech.2016.12.095

Vasistha, S., Khanra, A., Rai, M.P. (2021). Influence of microalgae-ZnO nanoparticle association on sewage wastewater towards efficient nutrient removal and improved biodiesel application: An integrated approach. *J. Water Process Eng.* 39, 101711. doi:10.1016/j.jwpe.2020.101711

Wagner, J.L., Le, C.D., Ting, V.P., Chuck, C.J. (2017). Design and operation of an inexpensive, laboratory-scale, continuous hydrothermal liquefaction reactor for the conversion of microalgae produced during wastewater treatment. *Fuel Process. Technol.* 165, 102-111. doi:10.1016/j.fuproc.2017.05.006

Yadav, G., Dubey, B.K., Sen, R. (2020). A comparative life cycle assessment of microalgae production by $CO_2$ sequestration from fl ue gas in outdoor raceway ponds under batch and semi-continuous regime. J. Clean. Prod. 258, 120703. doi:10.1016/j.jclepro.2020.120703

Yin, Z., Zhu, L., Li, S., Hu, T., Chu, R., Mo, F., Hu, D., Liu, C., Li, B. (2020). A comprehensive review on cultivation and harvesting of microalgae for biodiesel production: Environmental pollution control and future directions. *Bioresour. Technol.* 301, 122804. doi:10.1016/j.biortech.2020.122804

Yu, K.L., Chen, W.H., Sheen, H.K., Chang, J.S., Lin, C.S., Ong, H.C., Show, P.L., Ng, E.P., Ling, T.C. (2020). Bioethanol production from acid pretreated microalgal hydrolysate using microwave-assisted heating wet torrefaction. *Fuel*. 279, 118435. doi:10.1016/j.fuel.2020.118435

Zabed, H.M., Akter, S., Yun, J., Zhang, G., Zhang, Y., Qi, X. (2020). Biogas from microalgae: Technologies, challenges and opportunities. *Renew. Sustain. Energy Rev.* 117, 109503. doi:10.1016/j.rser.2019.109503

Zhu, L., Li, S., Hu, T., Nugroho, Y.K., Yin, Z., Hu, D., Chu, R., Mo, F., Liu, C., Hiltunen, E. (2019). Effects of nitrogen source heterogeneity on nutrient removal and biodiesel production of mono and mix-cultured microalgae. *Energy Convers. Manag.* 201, 112144. doi:10.1016/j.enconman.2019.112144

# Chapter 7

## SEISMIC PERFORMANCE OF ADJACENT BUILDINGS IN SERIES CONSIDERING SOIL-STRUCTURE INTERACTION

*Elif Çağda KANDEMİR*[1]

1 Civil Engineering Department, Izmir Democracy University, Izmir, elifcagda.kandemir@idu.edu.tr

## Introduction

Adjacent buildings in series are often come across in the large cities of Turkey. Especially the main streets are enclosed by zero-gap adjacent buildings, though Turkish Building Earthquake Code stipulate seismic gap between them. New buildings are also being built in the exact place of the old building (see Figure 1).


Figure 1. Adjacent buildings in Izmir city

The most interesting scene after a devastating earthquake is, while a building collapses, neighboring one can still stand as seen in Figure 2. The difference in the dynamic behavior may be one of the causes of that collapse. There are many factors influencing seismic performance of a building, however, there are much more if the building is adjacent to any other building(s). Pounding force may increase or decrease seismic responses depending on mostly the place of the collision, the differences in the dynamic characteristics, the location of building in the corner or in the middle.


Figure 2. Collapsed buildings after (a) 2020 Samos (02.03.2020, www.dailysabah.com) and (b) 2015 Nepal earthquakes (20.03.2020, www.abc.net)

This phenomenon is studied by the researchers who are familiar with the earthquake engineering in terms of structural pounding. Moustafa and Mahmoud (2014) presented the increase in damage by the decrease in gap size between two adjacent buildings. Ghandil et al. (2017) investigated SSI effect on building separation distance and damage distribution along the building height of adjacent buildings. Madani et al. (2015) presented pounding behavior of buildings with three to twelve stories, changing separation gap and building heights. They concluded that the soil flexibility often had a considerable increasing effect on the resultant of pounding forces. Kazemi at al. (2020) proposed performance levels to evaluate pounding effects on the seismic responses of adjacent buildings. They obtained increased responses when buildings collided.

There are also papers considering soil effect on pounding behavior. Naserkhaki et al. (2012) suggested accounting for soil-structure interaction by showing that soil effect augmented displacement and story shears. They emerged that structure-soil-structure interaction (SSSI) effect worsens seismic responses of buildings during pounding. The study of Mahmoud et al. (2013) also showed the soil effect on the pounding responses of two adjacent three-story buildings. They concluded that considering soil effect reduces the peak displacements, impact forces and inelastic shearing forces, while increases peak accelerations of equal heigh buildings. Mahmoud et al. (2013) present soil-structure effect on pounding responses of adjacent three-story buildings. Earthquake responses of lighter building increase when considering soil-structure interaction effect.

While there are many studies on two adjacent buildings in the literature, there are very few studies about pounding of adjacent buildings in series. In the three adjacent buildings investigated by Anagnostopoulos (1988), responses tended to increase in the end buildings while tended to decrease in the middle building According to the study of Elwardandy et al. (2017), infill panels were required to be considered in the analysis of adjacent buildings in series since they had considerable effect in reducing or accelerating structural response. Jankowski et al. (2015) conducted an experimental study on three tower models. The results showed that rigid tower was affected more than flexible tower because they acted like stoppers for more flexible ones. Finite element models of three adjacent structures were analyzed through spatial varied ground motions in the work of Bybordiani and Arici (2019). Two studies of El-Khoriby et al. (2015, 2015) execute experimental and numerical studies on adjacent structures in a row. Shakya et al. (2008) also have work on reinforced concrete buildings in series in terms of pounding. Relevant works in the literature may have disagreements and conflicts with each other drifting away a common inference because each work has its own unique assumptions, structures, impact models and earthquake load.

In this study, a parametric study comprising pounding behavior of three ten-story adjacent buildings is presented considering soil-structure interaction (SSI). The number of the floors of center and corner buildings are diversified from one to ten in separate cases to simulate construction stages of a building. Using building models with different rigidity and different heights provides to achieve large-scale information about the behavior of the structures. In addition, seismic performance of the structures erected on different soil types are investigated. The structures are assumed to be located in Bayrakli district of Izmir city which has experienced severe damage due to strong earthquake in 30th October 2020. Furthermore, the selected earthquakes of 1999 Duzce and 1995 Kobe earthquakes are scaled according to the elastic design spectrum of Bayrakli defined in the Turkish Building Earthquake Code 2018. This study is of importance to be a comprehensive study which may be a reference for related works and offer an insight into the behavior of adjacent structures in the Bayrakli district.

## Numerical Models

Three adjacent buildings were assumed as shear-type structures including one horizontal translation along floor levels so that lumped mass and stiffness idealization is sufficient to present seismic performance of the structures. The number of floors is designated up to ten. The mass value of one floor is $1 \times 10^5$ kg for each building. The stiffness values for left, middle and right buildings are $6.8 \times 10^7$ N/m, $10 \times 10^8$ N/m and $9.2 \times 10^{11}$ N/m, respectively. Rayleigh damping is used to generate damping matrices for damping ratio of 5% for each building. In order to simulate construction stages, the number of floors was changed from one to ten for only one building in question, while others were kept constant at ten story.

The model for collision is selected as linear viscoelastic model constituted of linear spring and dashpot in parallel, i.e. Kelvin-Voigt model. The model parameters are as follows,

$$F_p(t) = k_p\delta(t) + c_p\dot{\delta}(t) \tag{1}$$

$$c_p = 2\xi_p\sqrt{k\frac{m_1 m_2}{m_1 + m_2}} \tag{2}$$

$$\xi_p = \frac{-\ln e}{\pi^2 + (\ln e)^2} \tag{3}$$

in which $F_p(t)$ is pounding force, $k_p$ and $c_p$ are stiffness and damping coefficients of impact model, respectively. $k_p$ is twenty times of the maximum system rigidity as assumed in the paper of Anagnostopoulos (1988). Damping ratio of impact model, $\xi_p$, is 0.14 when coefficient of restitution ($e$) is 0.65 for concrete surfaces as given by Azevedo and Bento (1996). The linear spring and dashpot are activated when the gap between structure is closed, thereby generating pounding force. The equation of motion of adjacent single degree-of-freedom (SDOF) buildings is given as,

$$[\boldsymbol{M}]\{\ddot{\boldsymbol{x}}\} + [\boldsymbol{C}]\{\dot{\boldsymbol{x}}\} + [\boldsymbol{K}]\{\boldsymbol{x}\} + \boldsymbol{F_p} = -[\boldsymbol{M}]\{\boldsymbol{r}\}\ddot{\boldsymbol{x}}_{\boldsymbol{g}} \tag{4}$$

where $[\boldsymbol{M}] = \boldsymbol{diag}[\boldsymbol{m_1}\ \boldsymbol{m_2}\ \boldsymbol{m}_3]$ is coupled mass matrix, $[\boldsymbol{C}] = \boldsymbol{diag}[\boldsymbol{c_1}\ \boldsymbol{c_2}\ \boldsymbol{c_3}]$ is coupled damping coefficient matrix and $[\boldsymbol{K}] = \boldsymbol{diag}[\boldsymbol{k_1}\ \boldsymbol{k_2}\ \boldsymbol{k_3}]$ is coupled stiffness matrix. System responses, i.e. acceleration, velocity and displacement vectors, are given as $\{\ddot{\boldsymbol{x}}\} = \{\ddot{\boldsymbol{x}}_1\ \ddot{\boldsymbol{x}}_2\ \ddot{\boldsymbol{x}}_3\}$ , $\{\dot{\boldsymbol{x}}\} = \{\dot{\boldsymbol{x}}_1\ \dot{\boldsymbol{x}}_2\ \dot{\boldsymbol{x}}_3\}$ and $\{\boldsymbol{x}\} = \{\boldsymbol{x_1}\ \boldsymbol{x_2}\ \boldsymbol{x_3}\}$ , respectively. Subscripts describe building numbers, i.e. building 1, 2 and 3. $\ddot{\boldsymbol{x}}_{\boldsymbol{g}}$ is ground acceleration. $\boldsymbol{r}$ is the influence coefficient matrix in the form of unit vector.

In the study, since the shape of foundation does not make any difference in the seismic behavior of the buildings with soil effect, the foundation herein is considered as rigid circular surface footing of radius $r$. The supporting soil beneath the foundation is a homogeneous, linearly elastic and isotropic halfspace, described by its shear modulus $G$, Poisson's ratio $\nu$, mass density $\rho$ and shear wave velocity $V_s$. Springs and dashpots have been employed in the model to account for the translational and rotational movements of the soil, i.e. sway-rocking model. The stiffness and damping coefficients which represent the soil are computed as follows (Cruz and Miranda, 2017; Gazetas, 2006),

$$K_h = 8Gr/(2 - \upsilon) \tag{5a}$$

$$C_h = 4.6\rho V_s r^2/(2 - \upsilon) \tag{5b}$$

$$K_\theta = 8Gr^3/(3 - 3\upsilon) \tag{6a}$$

$$C_\theta = 0.4\rho V_s r^4/(1 - \upsilon) \tag{6b}$$

where $K_h$ and $K_\theta$ are static translational and rotational stiffness coefficients, while $C_h$ and $C_\theta$ are damping coefficient along sliding and rocking, respectively.

The structural models presenting fixed-base and flexible-base buildings considering soil-structure interaction is configured in Figure 3. The soil is represented by horizontal and rotational springs and dashpots.

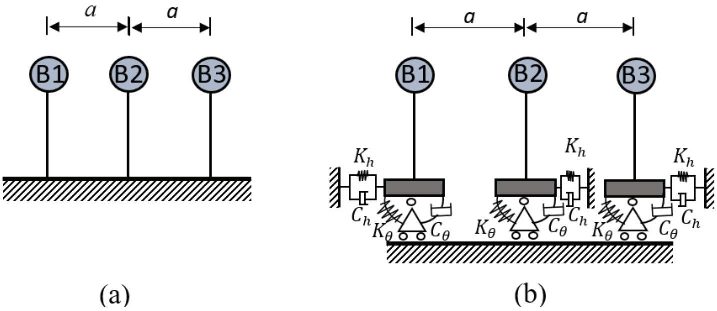


Figure 3. Structural models of buildings B1, B2 and B3 with: **(a)** fixed base **(b)** flexible base

Turkish Building Earthquake Code 2018 classifies six types of soil from hard soil (ZA) to soil with special treatment requirement (ZF). The mean shear wave velocities and calculated stiffness and damping coefficients are shown in Table 1. The soils except ZF are considered in this study. Soil shear modulus is given as $G = \rho {V_s}^2$. Poisson ratio, $\upsilon$, is 1/3 while mass density, $\rho$, is $2\,\mathrm{kNs^2/m^4}$. Radius of circular foundation, $r$, considered is 10 m.

Table 1. Stiffness and damping coefficients of soils given in TBEC 2018

| Parameter | Soil class | | | | |
|---|---|---|---|---|---|
| | ZA | ZB | ZC | ZD | ZE |
| Shear wave velocity, $V_s$ (m/s) | 1600 | 1130 | 560 | 270 | 170 |
| Horizontal stiffness coefficient, $K_h$ (kN/m) | $24.6 \times 10^7$ | $12.3 \times 10^7$ | $3.01 \times 10^7$ | $0.70 \times 10^7$ | $0.28 \times 10^7$ |
| Horizontal stiffness coefficient, $K_\theta$ (kN/m/rad) | $204.8 \times 10^8$ | $102 \times 10^8$ | $25.1 \times 10^8$ | $5.83 \times 10^8$ | $2.31 \times 10^8$ |
| Horizontal damping coefficient, $C_h$ (kNs/m) | $8.83 \times 10^5$ | $6.24 \times 10^5$ | $3.09 \times 10^5$ | $1.49 \times 10^5$ | $0.94 \times 10^5$ |
| Horizontal stiffness, $C_\theta$ (kNs/m/rad) | $1.92 \times 10^7$ | $1.36 \times 10^7$ | $6.72 \times 10^6$ | $3.24 \times 10^6$ | $2.04 \times 10^6$ |

## Ground Motions

Three ground motions with different characteristics of magnitude, peak ground acceleration and predominant period are chosen to conduct dynamic analyses. The acceleration data of earthquakes are scaled according to the earthquake design spectrum of Bayrakli district in Izmir city, which experienced buildings collapsed during the 2020 Samos earthquake. The acceleration record of 1995 Kobe and 1995 Duzce earthquakes are achieved and scaled by using the PEER ground motion database (https://ngawest2.berkeley.edu/). The 2020 Samos earthquake data is obtained from AFAD database (https://tadas.afad.gov.tr/list-event). Properties of selected ground motions are given in Table 2 in terms of station, peak ground acceleration (PGA), peak ground velocity (PGV), predominant frequency and magnitude.

Table 2. Properties of ground motions

| Earthquake | Station | PGA (g) | PGV (m/s) | PGA/PGV | Frequency (Hz) | Magnitude ($M_w$) |
|---|---|---|---|---|---|---|
| Samos, 2020 | Kusadasi | 0.183 | 0.225 | 0.813 | 5.315 | 6.6 |
| Duzce, 1999 | Bolu | 0.739 | 0.583 | 1.268 | 1.851 | 7.2 |
| Kobe, 1995 | JMA | 0.834 | 0.902 | 0.925 | 1.450 | 6.9 |

## Results and Discussion

The comparative results of the structural responses are given in this section. Due to limited space in the template, here only discussed comparative displacement time responses acceleration time responses, interstory drift ratios and wavelet scalogram of pounding forces for Duzce, İzmir and Kobe earthquakes.

Adjacent structures in series are of importance due to having considerable effect by neighboring structures during seismic motions. Center structures which are exposed to two-sided pounding may have advantageous since their responses are restricted by two neighboring structures. Anagnostopoulos has been stated that even zero-span buildings are more advantageous in that they are not exposed to collisions (Anagnostopoulos, 1988). Displacement time responses of center (B2) and right (B3) buildings due to Duzce earthquake are given in Figure 4. Standalone building B2 has larger displacement responses compared to the two-sided adjacent one. On the contrary, responses of the right corner building B3 has augmented when it is exposed to one-sided pounding. Acceleration responses as given in Figure 5 have the same behavior for two buildings: acceleration responses increased when they were adjacent to other buildings. However, the increment quantity is much more in the two-sided adjacent building, B2.

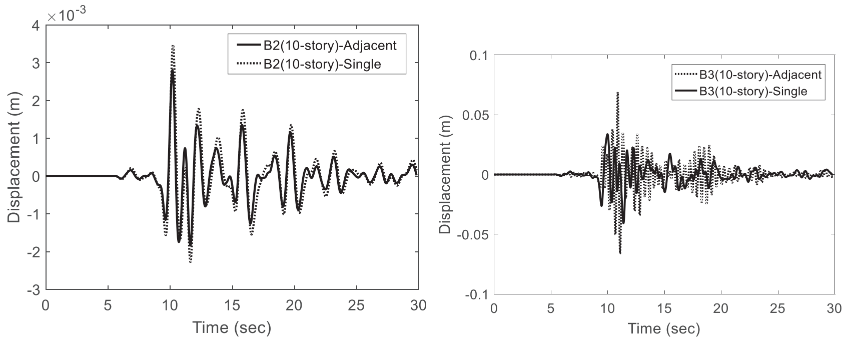


Figure 4. Displacement time responses under Duzce earthquake (a) 10-story center building (B2) (b) 10-story right corner building (B3)

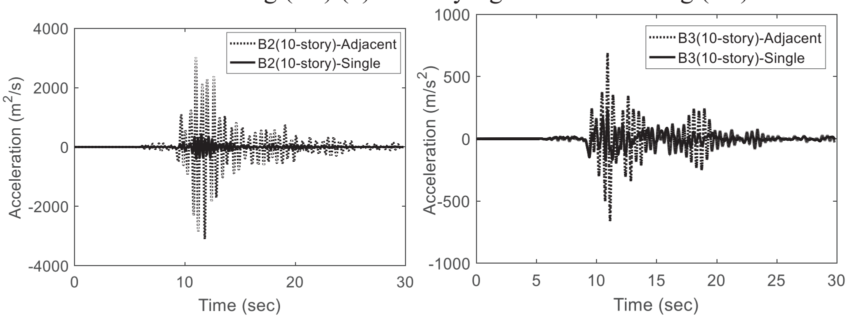


Figure 5. Acceleration time responses under Duzce earthquake (a) 10-story center building (B2) (b) 10-story right corner building (B3)

The interstory drift ratios (IDR) of B2 with 2-, 5- and 10- stories are given in Figure 6 due to fixed-base which neglect soil effect and flexible base considering different soil types. Results show that the system responses decrease when the soil gets softer under Duzce and Kobe earthquakes. The maximum drift ratio occurs when the building has 5 stories on the ZB soil. This is an unexpected result that may be stemmed from the periodical convergence of the soil and the building during Duzce and Kobe earthquakes. However, during Samos earthquake as the soil gets softer, the IDR responses increase for each building as expected.

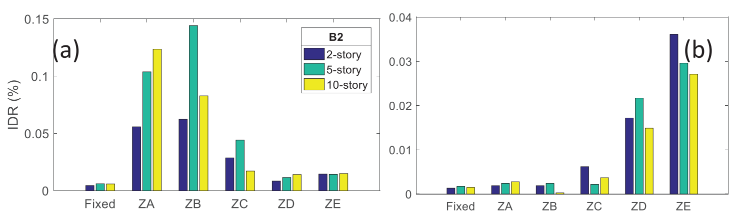

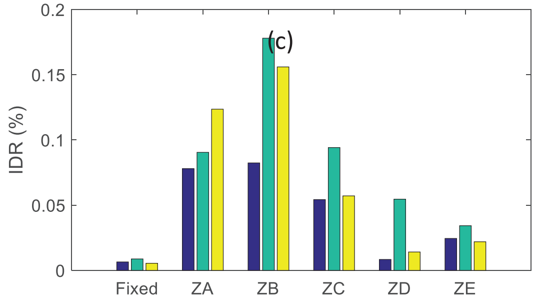


Figure 6. Soil effect on the IDR of center building (B2) with 2-, 5- and 10-stories under (a) Duzce, (b) Samos and (c) Kobe earthquakes

Wavelet transform is a suitable tool for a non-stationary signal since it decomposes the signal into basic functions of dilated and translated versions of the mother wavelet function, supplying frequency-time knowledge of the signal. Detailed information and mathematical background which are not given in this study can be found in related literature (Xing et al., 2012; Li et al., 2009). Pounding forces between the buildings were obtained by numerical integration method at the time when the buildings collided. In the time history of pounding forces, they are represented like impact forces changing abruptly for an infinitesimal time interval. Therefore, wavelet transform provides excellent insight into the pounding behavior. Morlet wavelet in Matlab environment is used in this study. Figure 7 shows the wavelet scalogram of pounding forces when 5-story center building with fixed-base collided left and right buildings. There is a slight difference between the graphs showing that there are more pounding incidents when B2 collide B3, which is stiffer than B1. Also red bulbs can be explained as representative of the severity of pounding force.

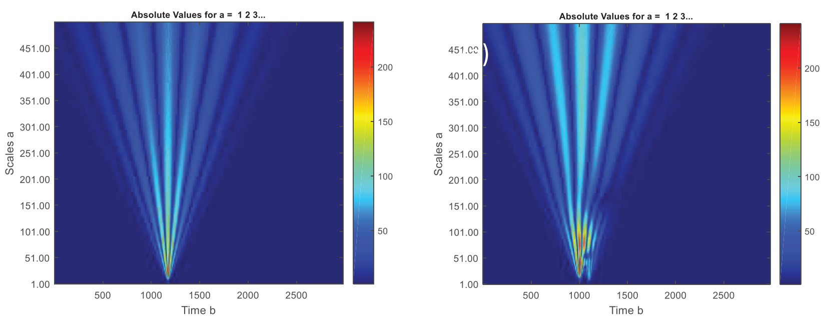


Figure 7. Wavelet scalograms of pounding forces between fixed-based 5-story center building with and (a) left corner building (b) right corner building under Kobe earthquake

It is clear that the severity and incidents of pounding increase when the soil effect is accounted for the 5-story center building on ZB soil as given in Figure 8 compared to Figure 7. Nevertheless, pounding occurs earlier. Slight difference between Figures 8 (a) and (b) is only the blue bulbs showed up when B2 collided to stiffer building.

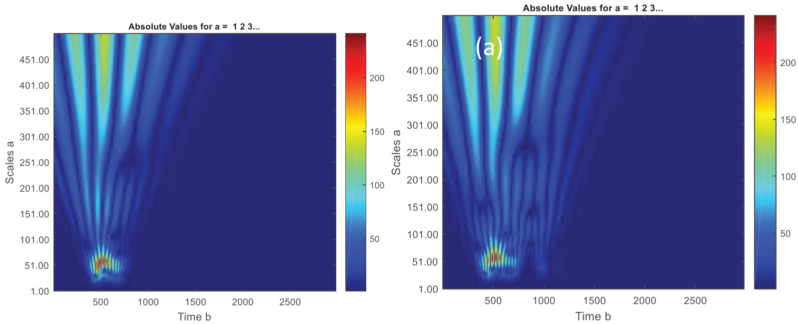


Figure 8. Wavelet scalograms of pounding forces between 5-story center building on ZB soil and
(a) left corner building (b) right corner building under Kobe earthquake

Soil effect to flexible structure may be advantageous in reducing seismic responses since considering soil adds damping to the system. For the most flexible building (B1) analyzed herein, soil contributed exactly the same. Figure 9 shows that the IDR responses are largest for fixed-base structure. As the soil gets softer, responses decreased under all earthquake loads.

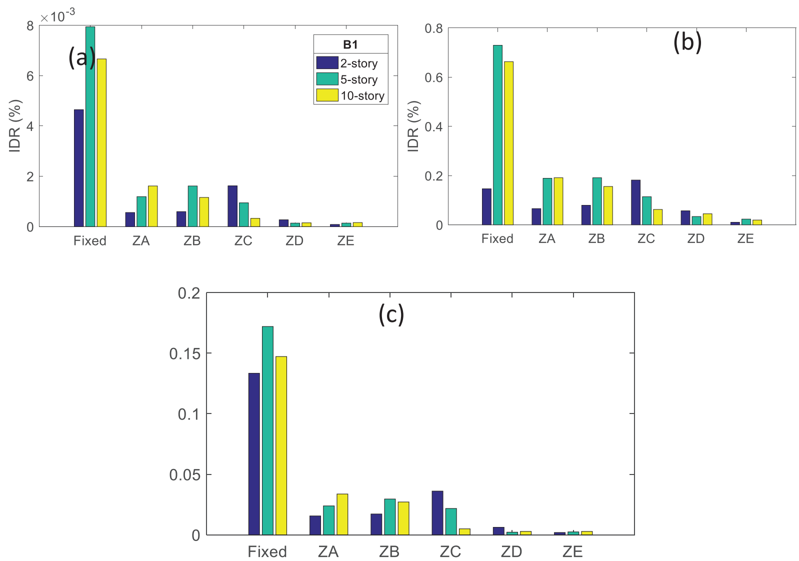


Figure 9. Soil effect on the IDR of left corner building (B1) with 2-, 5- and 10-stories under
(a) Duzce, (b) Samos and (c) Kobe earthquakes

Figure 10 illustrates wavelet scalogram for structure on ZE soil. Number of pounding incidents increased while severity was reduced.

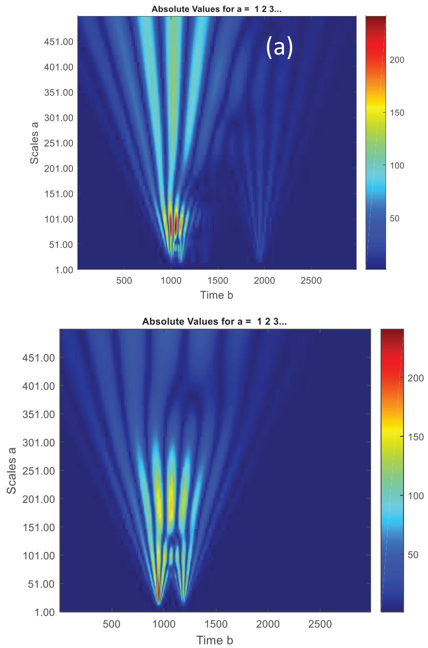


Figure 10. Wavelet scalogram of pounding forces of 5-story left building (B1) with (a) fixed-base (b) flexible base of ZB soil under Kobe earthquake

In Figure 11, there is a common increasing trend for the stiffer structure on the right corner (B3) under earthquake loads. On soft soil, IDR responses are larger, especially a clear jump is apparent for 10-story building.

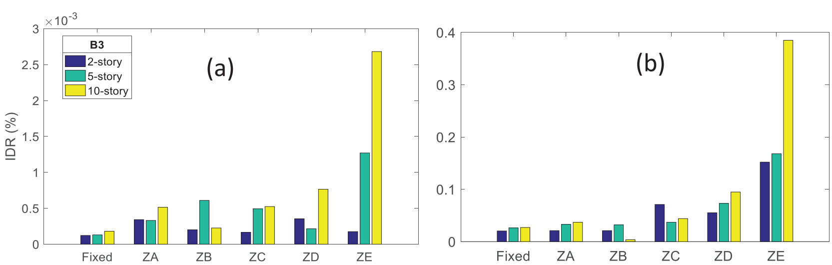

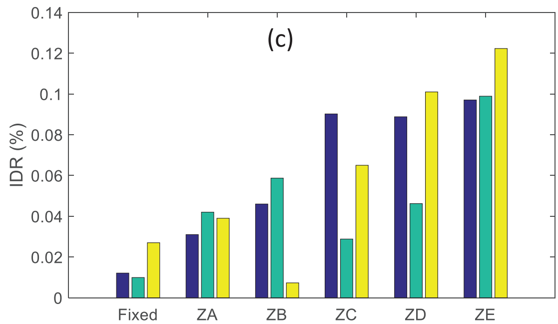


Figure 11. Soil effect on the IDR of right corner building (B3) with 2-, 5- and 10-stories under (a) Duzce, (b) Samos and (c) Kobe earthquakes

Figure 12 shows wavelet scalograms for B3 with flexible base of ZE soil. Larger number of collisions occurs when considering soil effect. This phenomenon is due to significant contribution of foundation moments to overall response of stiffer structural system.

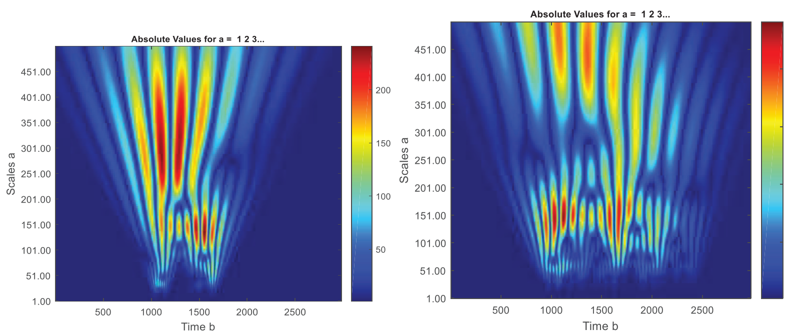


Figure 12. Wavelet scalogram of pounding forces of 5-story right building (B3) with (a) fixed-base (b) flexible base of ZE soil under Kobe earthquake

## Conclusion

In this paper, soil-structure interaction (SSI) is considered for pounding of adjacent buildings in series. The structural responses due to pounding has many parameters such as structural characteristics, position of the structure, impact model and earthquake loading. Ignoring soil beneath the structures can cause major errors in designing new buildings and predicting seismic responses of existing buildings. Evaluation of three adjacent buildings in series are assessed herein to discuss comparisons between the buildings with no SSI and SSI effect. All the results are summarized below.

1. Structural pounding has considerable effect on displacement responses if the building experiences one-sided pounding as in

the state of the right corner building, B3 which has high rigidity among others. Two-sided pounding can preserve the building B2 form freely moving resulting in the reduction of displacement responses.

2. Two-sided pounding effectively reduced the displacement responses of center building, while significantly augmented acceleration responses, which raises the probability of damage to the building even if the violent collision does not occur. Also, the pounding forces increase when SSI was considered. Impact to stiffer building (B3) produces severer forces. For center building, there is no special trend in behavior for different soil types.

3. The more flexible corner building in the left (B1) had maximum displacement responses for fixed base. As the soil gets softer, displacement responses were decreased, while pounding forces were increased. Soil flexibility is advantageous for flexible buildings since it increases damping in the structure.

4. Displacement responses had a clear increasing trend for the stiffer building in the right corner (B2) under all earthquakes as the soil get softer. Pounding incidents also extended with lower severity of forces compared to fixed-based building.

In summary, SSI amplifies seismic responses of all structures in all cases as a result of translational and rotational displacements of foundation level. Number and severity of pounding incidents highly depends on whether the pounding is one-sided or two-sided as well as the SSI is taken into account. In all cases, SSI have a considerable effect on the impact force because the ratio of their seismic response under SSI conditions with pounding to those without pounding is greater than that of the fixed-based condition. Buildings with SSI collide more often when the neighboring building is stiffer than when the neighboring building is more flexible, that is to say, incorporation of SSI prevents from large number of impacts of flexible structures. Stiffer corner buildings with SSI effect are more susceptible to impact. This phenomenon is due to significant contribution of foundation moments to overall response of stiffer structural system.

## References


AFAD Turkish Accelerometric Database and Analysis System, https://tadas.afad.gov.tr/list-event.

Anagnostopoulos SA. (1988). Pounding of buildings in series during earthquakes. *Earthquake Eng Struct Dynam 16*, 443–56.

Azevedo J., Bento R. (1996). Design criteria for buildings subjected to pounding. *Eleventh World Conference of Earthquake Engineering. Acapulco, Mexico, 23-28 June 1996*, Paper No. 1063.

Bybordiani M., Arici Y. (2019). Structure-soil-structure interaction of adjacent buildings subjected to seismic loading, Earthquake Engng Struct Dyn 48, 731–748.

Cruz C., Miranda E. (2017). Evaluation of soil-structure interaction effects on the damping ratios of buildings subjected to earthquakes, *Soil Dynamics and Earthquake Engineering 100,* 183-195.

El-Khoriby S., Seleemah A., Elwardany H., Jankowski R. (2015). Influence of earthquake–induced pounding on response of adjacent structures in series: experimental and numerical study. In: *Proceedings of international conference on advances in structural and geotechnical engineering, ICASGE'15, Hurgada, Egypt*, 6-9 April, 2015.

El-Khoriby S., Seleemah A., Jankowski R., Elwardany H. (2015). Experimental and numerical study on pounding of structures in series. *Adv Struct Eng, Springer,* ISBN: 978-81-322-2192-0.

Elwardany H., Seleemah A., Jankowski R. (2017). Seismic pounding behavior of multi-storey buildings in series considering the effect of infill panels, *Engineering Structures 144*, 139–150.

Gazetas G. (2006). Seismic design of foundations and soil–structure interaction, *In: First European Conference on Earthquake Engineering and Seismology*, Geneva, 3–8.

Ghandil M., Aldaikh H. (2017). Damage-based seismic planar pounding analysis of adjacent symmetric buildings considering inelastic structure–soil–structure interaction, *Earthquake Engng. Struct. Dyn. 46*, 1141–1159.

https://www.abc.net.au/news/2015-04-25/nepal-earthquake/6422026?nw=0 (05-03-2020)

https://www.dailysabah.com/turkey/unsafe-buildings-worsened-impact-of-izmir-earthquake-in-western-turkey/news?gallery_image=undefined#big (05-03-2020)

Jankowski R., Seleemah A., El-Khoriby S., Elwardany H. (2015). Experimental study on pounding between structures during damaging earthquakes. *Key Eng Mater 627*, 249–52.

Kazemi F., Miari M., Jankowski R. (2020). Investigating the effects of structural pounding on the seismic performance of adjacent RC and steel MRFs, *Bull. Earthquake Eng*, https://doi.org/10.1007/s10518-020-00985-y.

Li H., Yi T., Gu M., Huo L. (2009). Evaluation of earthquake-induced structural damages by wavelet transform, *Progress in Natural Science 19 (4)*, 461-470.

Madani B., Behnamfar F., Tajmir Riahi H. (2015). Dynamic response of structures subjected to pounding and structure–soil–structure interaction, *Soil Dyn. Earthq. Eng. 78*, 46–60.

Mahmoud S., Abd-Elhamed A., Jankowski R. (2013). Earthquake-induced pounding between equal height multi-storey buildings considering soil-structure interaction, *Bull. Earthquake Eng. 11*, 1021–1048.

Moustafa A., Mahmoud S. (2014). Damage assessment of adjacent buildings under earthquake loads, *Engineering Structures 61,* 153-165.

Naserkhaki S., Abdul Aziz F.N.A., Pourmohammad H. (2012). Earthquake induced pounding between adjacent buildings considering soil-structure interaction, *Earthq. Eng. Eng. Vib. 11*, 343-358.

PEER Ground Motion Database. https://ngawest2.berkeley.edu/

Shakya K., Wijeyewickrema A., Ohmachi T. Mid-column seismic pounding of reinforced concrete buildings in a row considering effects of soil, *The 14th World Conference on Earthquake Engineering*, October 12-17, 2008, Beijing, China

Turkish Building Earthquake Code TBEC 2018. Republic of Turkey Ministry of Interior Disaster and Emergency Management Authority, Ankara, Turkey, 2018.

Xing S., Halling M.W., Meng Q. (2012). Structural Pounding Detection by Using Wavelet Scalogram, Advances in Acoustics and Vibration 805141, 1687-6261.

# Chapter 8

## PUSH-PULL PARALLEL RESONANCE INVERTER AND APPLICATION EXAMPLES

*Serhat KÜÇÜKDERMENCİ*[1]

1 Balıkesir University Faculty of Engineering Department of Electrical and Electronics Engineering, kucukdermenci@balikesir.edu.tr

# 1. INTRODUCTION

Generally, an induction heating system consists of a power supply and a resonant circuit. Current can be supplied by a signal generator or a DC-AC converter connected to an amplifier. Soft switching is one of the most common and effective techniques for DC-AC inverters. This (Bellar et al., 1998) can be applied to different inverter topologies such as full bridge (Cano et al., 2011), half bridge (Mazon et al., 2017), push-pull (Namadmalan et al., 2010) etc. Push-pull inverters are one of the widely used topologies because they have simple control circuits, high efficiency, less affected by input voltage fluctuation and fewer switches (Green, 1993).

As shown in Figure 1, resonance circuits driven by inverter circuits are of two types, series and parallel. The resonant tank circuit basically consists of a capacitor, an inductor and a resistor. The series resonant circuit, in which the capacitor and the inductor are connected in series, act as a current source and the voltage is fed by the inverter through the capacitor. Due to the high capacitance of the capacitor, constant voltage is maintained in the circuit. The parallel resonant circuit in which the capacitor and inductor are parallel to each other acts as a voltage source and the current is fed by the inverter through the inductor. High inductance value maintains constant current in the circuit.

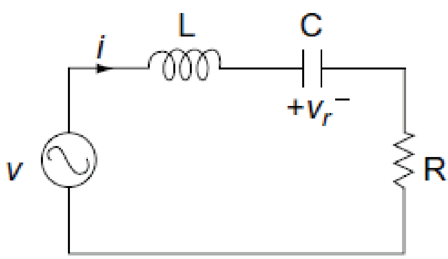


a) Series resonant circuit

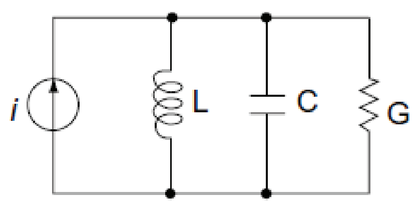


b) Parallel resonant circuit

**Figure 1.** Resonant circuits

The frequency at which the inductive reactance of the inductor and the capacitive reactance of the capacitor become equal is known as the resonance frequency and is shown in Equation 1. At the resonant frequency the impedance is minimal, so if the RLC tank circuit whose frequency is the same as the resonant tank frequency is fed with a voltage source, maximum current flows in the tank circuit. The resonant frequency of the inverter is the same for the serial and parallel tank circuit.

$$
\begin{aligned}
X_L &= X \\
j2\pi fL &= \frac{1}{j2\pi fC} \\
f &= \frac{1}{2\pi\sqrt{LC}}
\end{aligned}
\tag{1}
$$

If the relationship between the output current shown in Figure 2 and the source frequency is examined, it can be seen that there is maximum current and maximum energy at the resonance frequency.

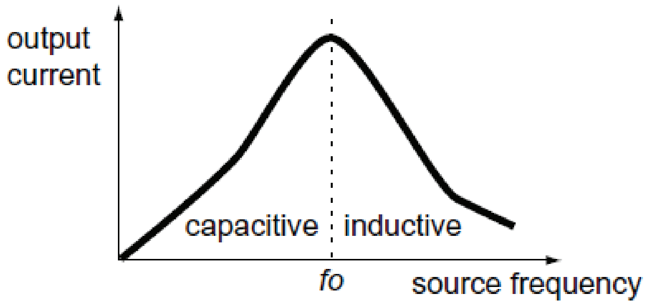


**Figure 2.** Output current-frequency graph.

The ratio of the reactive power of the system to its active power is known as the quality factor Q and is expressed by Equation 2.

$$Q = \frac{Z}{R} = \frac{2\pi fL}{R} = \frac{1}{2\pi fCR} \tag{2}$$

In the resonance state, when the capacitor is completely discharged ($V_C$ = 0V), the inductor is on and the inductor is fully energized. When the inductor is fully discharged ($I_L$ = 0A) the capacitor is fully charged. The current, voltage and energy states of the circuit elements are given in Equation 3. Practically every L-C circuit has a resistance. It oscillates between L and C until the energy in the resonant circuit is completely consumed by circuit losses. Energy here is expressed in joules. The Q factor is another expression of the losses in the resonant circuit.

$$I_C = C\frac{dv_c}{d_t}, V_L = L\frac{di_L}{d_t}, E_L = \frac{1}{2}L(I_L)^2, E_C = \frac{1}{2}C(V_c)^2 \tag{3}$$

The parallel resonant circuit gives the current amplification while the series resonance gives the voltage amplification. The Q factor is directly related to the current, if the value of Q is high, the current in the tank circuit is also high.

## 2. POWER CONVERTER TOPOLOGY

Electronic power systems are basically divided into four categories: DC-DC converters, AC-DC rectifiers, DC-AC inverters and AC-AC cyclo converters. With DC-DC converters, the magnitude of DC voltages is changed from input to output. An alternating voltage is converted to DC voltage with AC-DC rectifiers. With DC-AC converters, a DC voltage is converted into a time varying signal of a certain magnitude and frequency. With AC-AC cyclo converters, an AC voltage is converted into an AC voltage of different magnitude or frequency.

In induction heating systems, DC AC inverters are basically oscillator circuits. IGBTs are widely used in inverters with frequencies up to 100 kHz. Thanks to their fast-switching capabilities, MOSFETs can be used in the switching frequency range of 100-800 kHz. Oscillator structures used in inverters can be classified as self-oscillating and oscillating with control circuitry. Self-oscillating inverters continue their evolution as Royer oscillator, L-C MOS oscillators and Mazzilli oscillators.

### 2.1 Self-Oscillating Oscillators

The Royer oscillator, known for its self-resonating feature shown in Figure 3a, was described by George Royer in the 1950s. The third winding on the primary side of the transformer connected to the base of the transistors ensures that one transistor is open while the other is closed. The L-C MOS oscillator is a self-oscillating cross-linked oscillator as shown in Figure 3b. Here, MOSFETs are used as electronic switches instead of BJTs. Crossing the gates to opposite drains causes negative impedance in the drains.

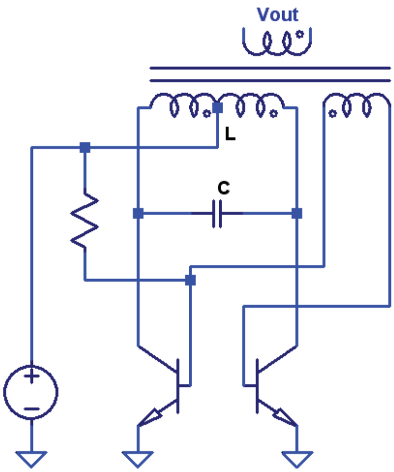


**Figure 3.** (a) Royer oscillator circuit

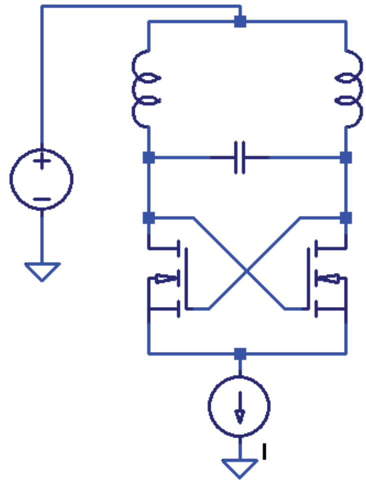


**Figure 3.** (b) L-C MOS oscillator circuit

Oscillator gain $g_m$ and oscillation condition are given in Equation 4. Here, $Q$ is the quality factor, $I_D$ drain current, $V_{GS}$ gate-source voltage and $Vt$ is the Mosfet threshold voltage.

$$g_m = \frac{I_D}{V_{GS} - V_t}, \frac{1}{g_m} \geq \frac{2\pi fL}{Q} \tag{2}$$

The Mazzilli oscillator designed by Vladimiro Mazzilli is a derivative of the Royer oscillator and the L-C MOS oscillator. L-C resonates by itself at the oscillation frequency. It is used in combination with a capacitor as a mid-end primary LC oscillator in this inverter. Using a mid-end transformer is usually done to increase the output at the secondary. A single inductor can usually be used in series with the supply before the current reaches the middle end. This is used as a choke to limit current spikes. The real thing that limits the current is the LC impedance. Choke coil only reduces current spikes. In Figure 4a, the middle-end Mazzilli inverter configuration and Figure 4b shows its improved version with auxiliary circuit elements.

In Figure 4a, when power is applied from + V, the current starts to flow to the drains of the MOSFETs from both sides of the primary. At the same time, the voltage at the gates of both mosfets starts to activate the gates. Due to the fabrication differences of the two circuit elements, one mosfet opens slightly faster than the other. In this case, more current can flow through the active mosfet. The extra current flowing on the opened mosfet side of the primary reduces the other mosfet gate current. This situation turns the other mosfet off (OFF). Thanks to the LC tank formed by a capacitor and primary, the voltage rises and falls sinusoidally.

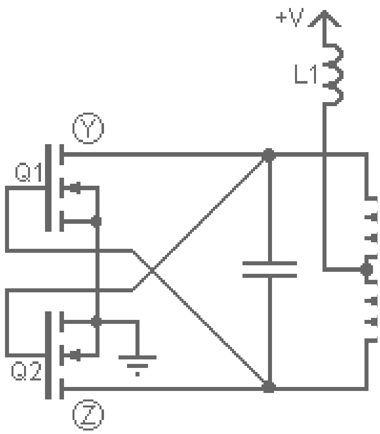


**Figure 4.** (a) Mazzilli oscillator basic circuit

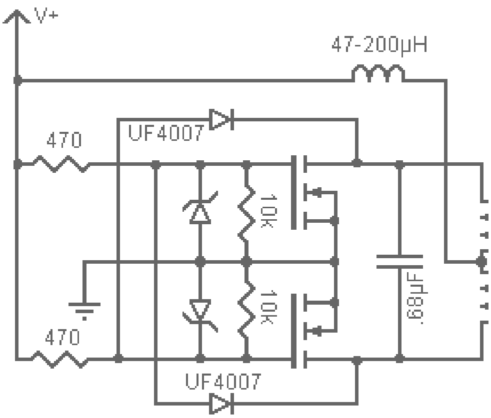


**Figure 4.** (b) Adding additional circuit elements to the oscillator

If the gate voltages are more than +/- 30V at the source voltage, the mosfets will be damaged and burn out. To prevent this, gate protection is provided by adding a few components as shown in Figure 4b. In the power supply, 470 ohm resistors that go serial to the gates limit the current charging the gates. Because too much gate current can cause damage. The latch-up is a process in which the mosfet gets locked. 10 kohm resistors connected in parallel to the gates pull the gates towards the ground voltage to prevent locking. Zener diodes connected to the gates prevent the gate voltage from exceeding 12, 15 or 18V depending on the zener structure used. Ultra-fast diodes (UF4007) cross between the drains draw the gates to ground voltage while the voltage at the cross leg of the LC tank is at the ground. Gates are charged with + V, discharged through ultra-fast diodes and LC tank. Connecting MOSFET gates to Vin with a suitable resistor overcomes the gate voltage limitation problem of the L-C MOS oscillator. These inverters use MOSFETs instead of Royer's BJTs because MOSFETs can switch faster.

## 2.2 Inverter Operating Modes

The operation of the converter circuit can be explained with four operating modes as shown in Figure 5:

In mode 1, as the drains of both switches approach zero, the cross-connection structure of the switches ensures that switch 2 is in the ON state and switch 1 is in the OFF state, as shown in Figure 5a. During this mode of operation, the capacitor is completely discharged. The total energy of the resonant circuit is in the form of peak current and stored in the inductor. Since there is no voltage in the coil, there is no output voltage or power transfer. The switch oscillation follows the tank oscillation, so no current flows through the switches.

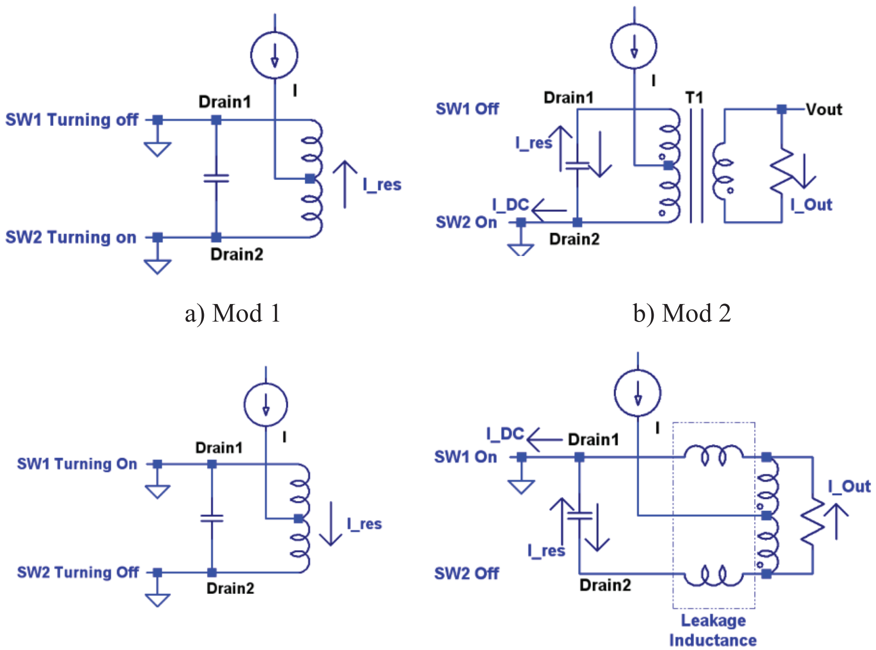


a) Mod 1 b) Mod 2

c) Mod 3 d) Mod 4

**Figure 5.** Inverter circuit operating modes

In mode 2, when switch 1 closing switch 2 is opened, the inductor current goes into resonance and the drain1 voltage rises and falls. Energy is transferred from the inductor to the capacitor and back to the inductor. During this process, the coil, which is also the resonance inductor, transfers the power to the load. The charge is reflected on the coil as shown in Figure 5b. The leakage inductances originating from the coil are shown in Figure 6.

In mode 3, when drain1 voltage is withdrawn to zero, switch 1 opens and switch 2 closes as shown in Figure 5c. Similar to Mode 1, the capacitor is completely discharged and the energy in the form of current is in the opposite direction in the inductor.

Mode 4 is the last mode of operation. Drain2 exhibits resonant rise and fall, similar to mode 2. Power is transferred back to the load as shown in Figure 5d. The polarity of the output voltage reverses similar to push-pull. When mode 4 is complete, the process starts over and mode 1 repeats.

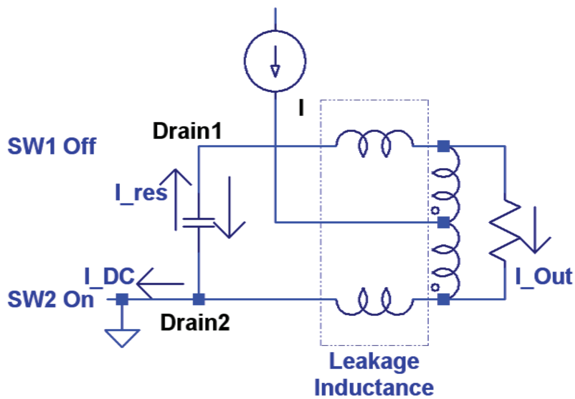


**Figure 6.** Leakage inductances from the coil

$V_{in}$ is split by coils at the node between the two drains. Drain voltages are represented by a half sine wave due to the parallel tank circuit. The full wave rectifier waveform is obtained at the load by the combination of half-wave voltage of each drain. Drain voltage peak value is mathematically expressed by Equation 3.

$$V_{in} = \frac{2}{T}\int_{0}^{\frac{T}{2}} V_{pk}\sin(2\pi/T)dt = \frac{V_{pk}}{\pi}, V_{pk} = \pi V_{in} \tag{3}$$

Here $V_{ind}$ is the inductor voltage, $T$ period and $V_{pk}$ is the drain peak voltage. The frequency at which the oscillator will operate is determined by the transformer primary winding and the inductance of the capacitor. The resonance frequency of the inverter is the same as that of the series and parallel tank circuit as shown in Equation 1.

## 2.3 Advantages and Disadvantages

## Advantages:

- This converter does not require a control unit due to its self-monitoring feature and the circuit setup is not considered complex compared to other oscillators.

- Zero-voltage switching (ZVS) means that in oscillators, the mosfets are turned on and off when there is zero volts on them. Switching losses are largely eliminated as mosfets turn on and off when they carry the least power. Therefore, MOSFETs heat up to a minimum and high efficiency is achieved in the circuit.

- High powers (> 1 kW) can be reached with well-chosen MOSFETs or IGBTs. Small metal sinks will suffice as switching losses are low in an inverter design at these watts.

- Sinusoidal output means less interference.

## Disadvantages:

- Feeding for Mosfet gates is provided from Vin via a resistor. Here the gate acts as a capacitance and the gate is charged with the R-C time constant. For low frequencies, the R-C time constant is not a problem. For high frequencies, it is necessary to generate a fast gate signal with the gate driver.

- High $V_{in}$ value creates a problem in gate. Usually, the gate driver circuit is powered by 12V and the LC circuit can operate at 24V or higher voltages. Solutions such as the use of two power supplies or limiting the gate voltage to a zener diode can be used to prevent this problem.

- When the voltage is high, the diodes responsible for closing the gates cannot fully do this and the oscillation stops when a mosfet remains open. This is actually a short circuit situation. Therefore, mosfets burn. The problem can be partially solved by placing a 0.5 ohm wire wound resistor in series with the filter inductor.

- When the gate signal is low, the switch will be in closed state. Thus, a case of latching of both of the MOSFET (Latch-up) occurs. Another reason for locking is rapid changes in load and attention should be paid to this situation.

- When the drain voltages drop, the current is drawn through the counter gate diode capacitance, which can disable the switch. Losses increase and no switching. To overcome this problem, the gate resistance value can be lowered.

As a result, these types of circuits have the advantages of requiring few circuit elements, having a simple structure that does not require a control unit, harmony between input voltage and resonant voltage, harmony between LC circuit and operating frequency. For the continuation of oscillation, the drain and gate signals should be kept at an appropriate level by establishing a balance between RLC.

## 3. APPLICATION EXAMPLES

It is seen that different variations of current-fed push-pull oscillators are used in many different areas such as wireless power transfer, x-ray generators, magnetic hyperthermia.

In a study (Yu et al., 2018) an improved autonomous current powered push-pull inverter was proposed (see Figure 7). The driver and DC voltages are separated and a configuration consisting of diode, transistor and resistors is used for the gate driver. The improved inverter reduces gate losses and switching losses, increasing the output power level and system efficiency. It has been shown that the improved inverter can increase the output power from 7.68 W to 8.74 W and the overall efficiency from 63.5% to 72.5% compared to the traditional inverter with a coil distance of 2 cm.

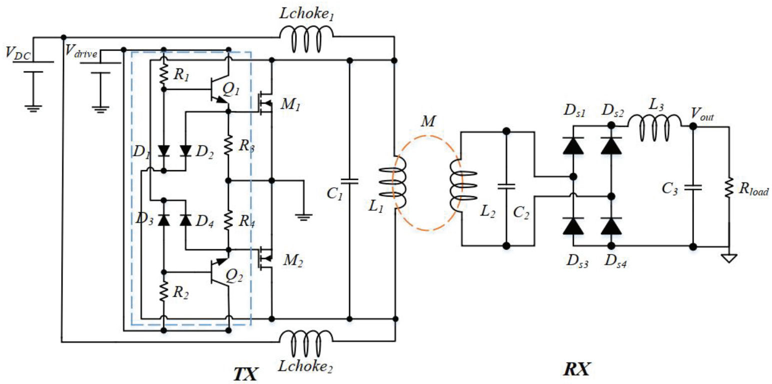


**Figure 7.** Diagram of the current-fed push-pull system.

In another study (Piernas Díaz, 2020) a variation of Mazzilli inverter was used for X-Ray production. As shown in Figure 8, thanks to the TPS2814P integrated circuit that accelerates the gate signal, the circuit can operate at 116kHz. If a driver IC such as the IR2110 is used, the undervoltage lock (UVLO) will turn off the integrated circuit if the supplied voltage is not high enough. Therefore, TPS2814P8 integrated circuit is used instead of IR2110 in the circuit because this gate driver is a bit faster and does not have UVLO feature.

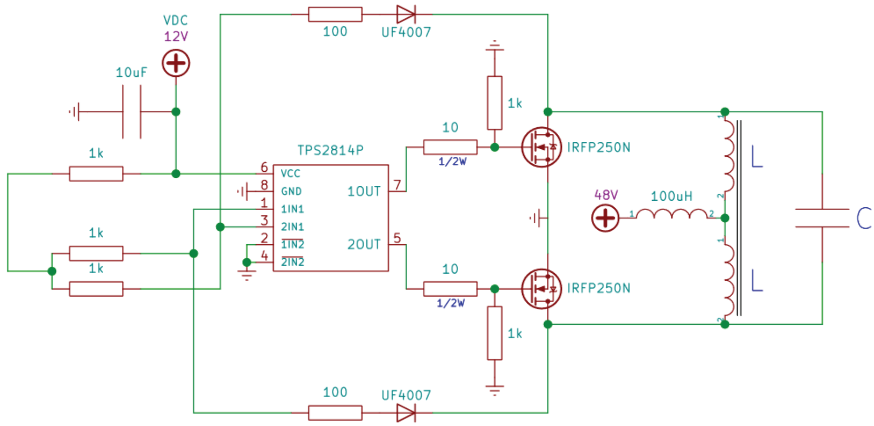


**Figure 8.** Modified ZVS circuit.

In an induction heating system designed for magnetic hyperthermia studies (Hadadian et al., 2019) under different experimental conditions, modifications were made in the gate drivers as shown in Figure 9. With the gate driver circuit arrangement consisting of transistors and resistors, resonance frequency variation is provided for different capacities and coil types. With 4 different types of inductors and 5 different capacitor banks, an output signal from 63 kHz to 530 kHz was observed at the output.

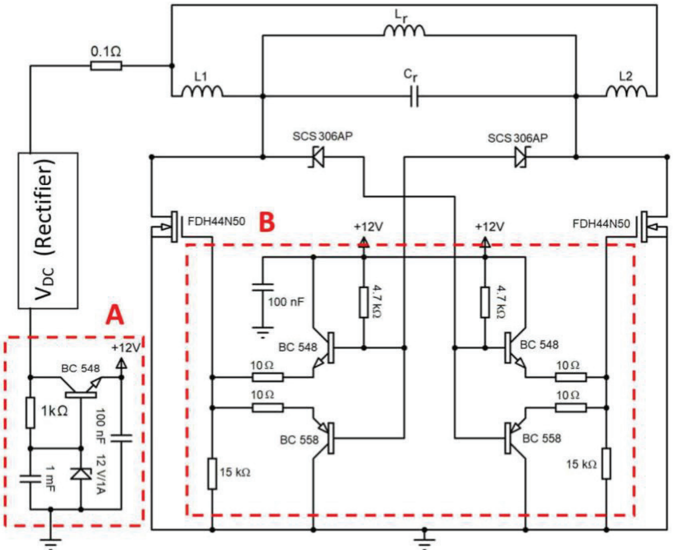


**Figure 9.** Regulation of the gate signal with the driver circuit.

## 4. CONCLUSION

Push-pull inverters can be used in a variety of applications such as wireless power supply (Bakula et al., 2015), flyback transformers (Zin et al., 2017), (Hapidin et al., 2017) ozone generation (Alonso et al., 2005) and induction heating (Namadmalan et al., 2010). Due to some of the disadvantages in this category of inverter and depending on each specific application, various modifications have been proposed. In a conventional Royer circuit, a high current rise after a transistor is open significantly increases transistor dissipation. This may exceed the safe operating area, causing the circuit to malfunction. Another example would be severe input voltage limitation in switches of cross-linked oscillators and high AC losses that can disrupt switches in the Mazzilli circuit. The Mazzilli circuit is a crosslinked oscillator and a derivative of the Royer oscillator. Different gate drivers may be proposed for cross-linked oscillator circuits for use in high voltage converters to overcome the aforementioned drawbacks.

## 5. REFERENCES

Alonso, J. M., Garcia, J., Calleja, A. J., Ribas, J., & Cardesin, J. (2005). Analysis, Design, and Experimentation of a High-Voltage Power Supply for Ozone Generation Based on Current-Fed Parallel-Resonant Push–Pull Inverter. *IEEE Transactions on Industry Applications*, *41*(5), 1364–1372. https://doi.org/10.1109/TIA.2005.853379

Bakula, M., Pelgrims, P., & Puers, R. (2015). A Wireless Powering and Communication System for Implantable Devices Based on a Royer Oscillator with Radio and Near-field Communication Links. *Procedia Engineering*, *120*, 306–309. https://doi.org/10.1016/j.proeng.2015.08.622

Bellar, M. D., Wu, T. S., Tchamdjou, A., Mahdavi, J., & Ehsani, M. (1998). A review of soft-switched DC-AC converters. *IEEE Transactions on Industry Applications*, *34*(4), 847–860. https://doi.org/10.1109/28.703992

Cano, M. E., Barrera, A., Estrada, J. C., Hernandez, A., & Cordova, T. (2011). An induction heater device for studies of magnetic hyperthermia and specific absorption ratio measurements. *Review of Scientific Instruments*, *82*(11), 114904. https://doi.org/10.1063/1.3658818

Green, A. W. (1993). Modelling a push—pull parallel resonant convertor using generalised state-space averaging. *IEE Proceedings B Electric Power Applications*, *140*(6), 350. https://doi.org/10.1049/ip-b.1993.0045

Hadadian, Y., Azimbagirad, M., Navas, E. A., & Pavan, T. Z. (2019). A versatile induction heating system for magnetic hyperthermia studies under different experimental conditions. *Review of Scientific Instruments*, *90*(7), 074701. https://doi.org/10.1063/1.5080348

Hapidin, D. A., Saleh, I., Munir, M. M., & Khairurrijal. (2017). Design and Development of a Series-configuration Mazzilli Zero Voltage Switching Flyback Converter as a High-voltage Power Supply for Needleless Electrospinning. *Procedia Engineering*, *170*, 509–515. https://doi.org/10.1016/j.proeng.2017.03.081

Mazon, E. E., Villa-Martínez, E., Hernández-Sámano, A., Córdova-Fraga, T., Ibarra-Sánchez, J. J., Calleja, H. A., Leyva Cruz, J. A., Barrera, A., Estrada, J. C., Paz, J. A., Quintero, L. H., & Cano, M. E. (2017). A high-resolution frequency variable experimental setup for studying ferrofluids used in magnetic hyperthermia. *Review of Scientific Instruments*, *88*(8), 084705. https://doi.org/10.1063/1.4998975

Namadmalan, A. R., Abdi, B., & Moghani, J. S. (2010). Current-fed parallel resonant push-pull inverter with coil flux control for induction heating applications. *2010 1st Power Electronic & Drive Systems & Technologies Conference (PEDSTC)*, 186–190. https://doi.org/10.1109/PEDSTC.2010.5471834

Piernas Díaz, F. (2020). *Design and Development of an X-Ray Machine*. http://hdl.handle.net/10481/62950

Yu, A., Zeng, X., Xiong, D., Tian, M., & Li, J. (2018). An Improved Autonomous Current-Fed Push-Pull Parallel-Resonant Inverter for Inductive Power Transfer System. *Energies*, *11*(10), 2653. https://doi.org/10.3390/en11102653

Zin, R. M., Soon, C. F., Sani, M. Z. A., Rizon, E. R., Tee, K. S., Ahmad, M. K., Ahmad, N., Jubadi, W. M., & Nayan, N. (2017). *Zero voltage switching driver and flyback transformer for generation of atmospheric pressure plasma jet*. 020023. https://doi.org/10.1063/1.5002041